

Ultra-photostable genetically targeted fluoromodules for live cell imaging

A Dissertation by
Saumya Saurabh

M.S. Indian Institute of Technology, Bombay 2008

Submitted to the faculty of the Department of Chemistry,
Carnegie Mellon University

in partial fulfilment of the requirements for the degree of

DOCTOR OF PHILOSOPHY

April 24, 2014

Epigraph

“And extracting one molecule’s signature [in spectral analysis] from the rest of the signatures is hard work, sort of like picking out the sound of your toddler’s voice in a roomful of screaming children during playtime. It’s hard, but you can do it.”

– Neil deGrasse Tyson

Death by black hole

Acknowledgements

A continuous flow of new ideas, excitement about the science and unrelenting support, especially in the face of obstacles are the key ingredients that go into Ph.D. research. I would like to sincerely thank my advisor, Dr. Marcel Bruchez, the fountainhead of ideas that went into my Ph.D., for his sheer enthusiasm and support that led to this work in his lab. He honed my scientific thought and experimental approach throughout this time. I aspire to have his relentlessness in science and brilliance throughout my scientific career. I would not have been able to perform this research without his guidance and support.

I thank Dr. Linda Peteanu, Dr. Bruce Armitage, Dr. Frederick Lanni and Dr. Alan Waggoner for being on my thesis committee and guiding my research through stimulating discussions and critical thoughts on experiments throughout the course of my Ph.D.

My sincerest thanks go to my lab members who have been very helpful throughout my research. Dr. Qi Yan, Dr. Cheryl Telmer, Dr. Dmytro Yuschenko, Dr. Suvrajit Maji, Yi Wang, Christopher Pratt, Matharishwan Naganbabu, Jianjun He, Dr. Xiaohong Tan, Dr. Anmol Grover, Dr. Brigitte Schmidt and Alexandra Carpenter. Without their help in, and outside the lab, the research work would not have seen fruition. Colleagues from the Molecular Biosensor and Imaging center also deserve my heartiest thanks for helping me find my way in the center since I started. Dr. Chris Szent-Gyorgyi, Dr. Byron Ballou, Dr. Haibing Teng, Dr. Lauren Ernst, Susan Andrecko, Yehuda Creeger and Allison Dempsey have all been very helpful in my research and a big thanks to all of them.

I also thank my collaborators who have enabled me to make forays into cell biology and inspired me to attack hypothesis driven problems. Heartfelt thanks Ming Zhang, Dr. Cheemeng Tan, Dr. Philip LeDuc, Dr. Russell Schwartz, Dr. Catherine Jackson Baty, Dr. Mads Breum Larsen and Kyle Justus.

I was very fortunate to get a chance to mentor three excellent undergraduate students: Victor R. Mann, Lauren E. Beck and Andrea Costello. I really appreciate their hard work and thank them for their efforts during my Ph.D.

My friends at CMU had a very important role in my life of pulling me up on bad days and enthusing in me the “never say die” spirit. Heartfelt thanks to Yash Puranik, Matthew A. DeNardo, Gino Gallo, Dr. Kiran Rafiq, Emily Daniels and Joanna Burdynska.

I would like to thank the Department of Chemistry, Dr. Bruce McWilliams and Mrs. Astrid McWilliams for awarding me with the fellowship in their name that has funded the last year of my research here at C.M.U.

Finally, I thank my Mother, Father and Sister who have endured endless pains to see me where I am and have been supportive of my decisions in life. They have been and will always be a great support and a source of inspiration for me, in all endeavors of my life.

Preface

The desire for an ever increasing number of fluorescent photons from fluorophores is an insatiable one in live cell imaging applications. Advances in microscopy techniques and semiconductor technology for detectors have provided us with sub-diffraction imaging methods that can resolve biological structures up to a few nanometers. Further, fluorophore photophysics and in particular, their dark states have been exploited towards the same gains in live cell imaging. Despite this, fluorescence remains several orders of magnitude behind some other methods in resolution. While optics limit the resolvable limits in fluorescence microscopy, the number of photons emitted per fluoromolecules decide the precision with which, a structure can be resolved.

“How to get more photons out of a fluoromolecule?” , is the underlying theme of this thesis. We start in chapter I with a brief review of genetically encoded technologies available for live cell imaging with a focus on fluorogen activating peptides. In chapter II, we dive straight into methods for improving the photostability of fluorogen activating peptides by exploiting their kinetics. Additionally, we also outline mechanisms behind the photostability of fluorogen activating peptides and how their photochemistry can be controlled at a single molecule level. In chapter III we introduce a method of targeting quantum dots using fluorogenic haptens, again with the intention of satisfying the photon output demanded by superresolution microscopy. Finally, in chapter IV we provide the bio-imaging community with very powerful, Photostability enhancing peptides (PEP) that bind Cy3 and Cy5. Together, the tools discussed throughout this thesis are catered towards live cell imaging with enhanced photostability.

Table of contents

Chapter I: Targeting dyes for biology

Introduction	1
Intrinsically fluorescent probes	6
Direct labeling	6
Indirect labeling	15
Fluorogenic probes	19
Covalent fluorogenic probes	20
Non-covalent fluorogenic probes	22
Conclusions and future outlook	25
Tables of probe properties	26
Bibliography	28

Chapter II: Fluorogens for photostable imaging

Introduction	36
Proposed Mechanism for the kinetic dependence of photostability	43
Photostability enhancement through encapsulation	45
The role of molecular oxygen and the triplet state	49
Photostability enhancement through exchange	52
Exchangers by rational design and screening	55
New directions to screen for exchangers using flow cytometry	59
Discussion	62
Materials and methods	63
Bibliography	71

Chapter III: Targeting Quantum dots using fluorogenic haptens

Introduction	77
Streptavidin QDs can be targeted to proteins through biotinylated haptens	81
Selectivity of targeting ensured through haptens targeted to cognate proteins	83
Simultaneous multiplexed single particle tracking using QDs	84
Intracellular targeting of QD-haptens	88
Discussion	93
Materials and methods	94
Bibliography	97

Chapter IV: Genetic targeting of cyanine dyes for photostable imaging

Introduction	105
Screening of Cy3 and Cy5 binding clones	110
Fluorescence spectroscopy of Cy3 and Cy5 binding yeast clones	112
Targeting other Cy3 and Cy5 derivatives	115
Mammalian cell studies using PEPCy3 and PEPCy5	118
Live cell single molecule imaging using PEPCy3 and PEPCy5	120
Photostability enhancement of Cy3 and Cy5 bound to PEPs	122
Discussion	127
Materials and methods	129
Bibliography	133

Chapter I: Targeting dyes for biology

Introduction

Measurements of the structure, function and interactions of proteins are crucial to our understanding of living systems. Biologists and chemists have developed a variety of methods to study these proteins both *in vitro* and *in vivo*. Among the methods to observe proteins, fluorescence spectroscopy has proven to be a unique tool in cell biology and biophysics, capable of revealing the dynamic nature of many processes. The prime requirement for observing a protein of interest (POI) using fluorescence spectroscopy is that the protein has to be labeled with a fluorescent probe. While *in vitro* labeling of biomolecules for biochemical methods is relatively straightforward as it relies on standard functional groups in purified proteins (typically cysteines) for covalent labeling, labeling POIs in living cells is a very formidable task. Labeling inside the cell requires balancing trade-offs between spatio-temporal control, specificity, selectivity and modularity (e.g. the ability to swap one dye for another). Developments in fluorescent probes and microscopy techniques over the last two decades have given us tools that address all these challenges, thus making fluorescent labels the tool of choice for live cell imaging.

Cellular structures range from nanometers to microns in size, yet conventional optical microscopy is limited by the diffraction of light to resolve structures separated by ~200 nm. The emergence of superresolution microscopy and probes suited for it has made possible the resolution of cellular structures considerably beyond this limit, and the localization of single molecules with a precision of 1 nm or better.^{1, 2} Protein interactions inside the cell occur across a wide range of time scales, anywhere from well under a second to hours or days. Typical fluorescent probes can emit up to 10^5 - 10^7 photons per

second to allow for fast imaging of protein locations in real time.^{3, 4} However, most probes emit only $\sim 10^5$ – 10^6 photons before photobleaching that limits the duration of such imaging. Finally, fluorescent probes come in a variety of colors, covering the spectrum from ultra-violet to infra-red and enabling specific multicolor labeling (multiplexing).⁵

A protein inside a cell is surrounded by numerous other biomolecules with identical chemical building blocks (amino acids) and standard functional groups (SH, NH₂) in its microenvironment. This poses one of the most daunting challenges in labeling proteins. The ability to orthogonally label multiple POIs with different colors has been made possible through the development of organic dyes and genetically encoded fluorescent protein (FP) technology.^{6, 7, 8} While organic dyes date back over 150 years, and for specific fluorescence detection more than 60 years, tagging with FPs has become the most widely used technology since the discovery and development of the green fluorescent protein (GFP).^{9, 10} These genetically encoded proteins allow one to express a FP fusion with any POI without secondary labeling using standard molecular biology techniques. This approach has transformed fluorescence microscopy from a static method, applied to fixed cells, to a dynamic real-time approach to visualize changes within living cells and organisms. The FP family has been developed further to cover a large spectral range, from 440 nm to 720 nm, that allows the simultaneous tagging of multiple POIs with different colors.^{11, 12}

FPs are typically ~25-30 kDa in size and thus can perturb the function of the POI. Secondly, most FP chromophores mature post-translationally, leading to a “lag time” before fluorescence can be observed from them. Finally, the photochemical properties of the FPs such as extinction coefficients (EC), quantum yields (QY) and photostability tend to be limiting factors in imaging, especially considering that many of the orange and red FPs show some photoconversion to alternate colors.¹³ Organic dyes on the other hand,

are small molecules that can be targeted to POIs for fluorescence detection. Labeling with organic dyes is triggered by addition of dye to the cells, allowing controlled sequencing with biological treatments (e.g. labeling before or after drug addition) for detection of distinct biological processes. The synthetic chemistry involved in making organic dyes is well understood, allowing significant rational design of organic dyes with desirable properties, for example photoactivation or photoconversion upon illumination with specific excitation wavelength or chemical sensing. This same synthetic control provides us with tunability of spectral and photochemical properties yielding a suite of organic fluorophores with a broader spectral range, higher molecular brightness (Quantum yield * Extinction coefficient) and photostability compared to FPs. Finally, different organic dyes can be tailored to bind specifically to functional groups or expressed tags on the POI through standard synthetic chemistry, providing the modularity that is needed to genetically target POIs in the cellular environment.

Traditionally, organic dyes have been targeted to POIs using antibodies. While this methodology has been useful in several *in vivo* and *in vitro* assays, it takes away the “small molecule” advantage from the dye. Covalent labeling approaches circumvent this disadvantage by employing specific functional groups on the proteins (NH₂, OH, SH) to target organic dyes with respective reactive functional groups. While the synthetic steps involved in this type of covalent labeling are well established, the non-specific labeling poses a challenge to the widespread utility of simple, direct bioconjugation, especially in cellular systems, where all proteins have the same available functional groups. In another approach, various cell surface receptor ligands have been covalently tagged with fluorescent dyes. Following the work of Farinas and Verkman to target cell permeable fluorescent ligands to receptors, several other ligands for cell surface receptors have been targeted successfully.¹⁴ In particular, covalently labeled fluorescent

conjugates of the epidermal growth factor (EGF) have been successfully employed in several studies of the epidermal growth factor receptor (EGFR).¹⁵ While antibody labeling, bioconjugation and affinity-directed labeling have several limitations as discussed above, they have in some way inspired chemists to develop hybrid chemical labeling approaches for targeting proteins.

An ideal fluorescent probe for labeling POIs for live cell imaging should have of course, excellent spectroscopic and photochemical properties. It should have a small size so that it does not perturb protein function. It should also have the modularity with respect to binding partners and flexibility with respect to location of the probe on or inside the cell. The labeling reaction should complete in a specific and selective fashion in the shortest possible time, and should not leave any background or non-specific products. The labeling reagents should not be cytotoxic. Finally, the approach should be free of washing to allow for monitoring POIs in real-time while the labeling reaction is going on (Figure 1A).

With the advent of bio-orthogonal chemistry, we have been able to incorporate chemical entities genetically or metabolically inside live cells. In the last 16 years, there has been a surge in the development of hybrid labeling approaches that utilize an organic molecule as a fluorescence reporter and a genetically encoded peptide tag as the bio-orthogonal targeting moiety. These approaches combine the synthetic control over the structure and function of the fluorescent reporter (dye) while maintaining the ease of labeling that is offered by genetic encoding. Since the discovery of the tetracysteine tags by Roger Tsien, the field has rapidly expanded and there are over two dozen tags that cover a wide range of bio-orthogonality and fluorescent properties.¹⁶ Since many technologies are unique in their modalities, classifying them based on the underlying chemistry is very useful for further discussions in this chapter (Figure 1B).

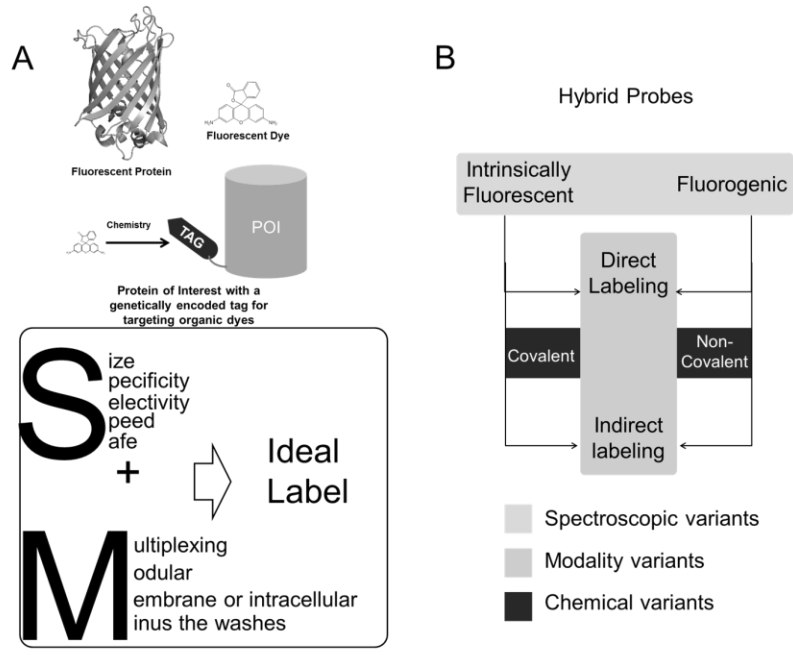


Figure 1. A. A hybrid approach combining the properties of fluorescent dyes and genetically encoded proteins for labeling proteins of interest. Also outlined are the qualities that are expected from an ideal label. B. Categorization of probes in our discussion based on the spectroscopy, modality and chemical variations.

Intrinsically Fluorescent probes

Because of the availability of fluorescent dye conjugates of a wide range of antibodies, antibody mediated labeling remains a very practical method to tag POIs on the surface of living cells as long as the bound antibodies do not perturb the protein's function. However, when the perturbation of protein function and structure is a concern, smaller tags need to be incorporated. Several approaches have been developed that utilize the chemistry of functional groups of a directly fused peptide tag to interact specifically and selectively with modified organic dye molecules. The final labeling can be as a result of a direct chemical reaction between the dye and the tag functional groups (direct labeling) as in the case of SNAP and CLIP tags or, alternatively as a result of a reaction mediated by an enzyme such as PPTase or BirA, or any external means such as light that leads to the dye binding the tag irreversibly. Finally, these interactions may be covalent or non-covalent depending on the chemistry used. Once a particular peptide tag has been engineered to perform a specific chemical reaction, any dye molecule with the cognate functional motif can be used to label the tagged POI, thus allowing for multiplexing as well as pulse chase measurements using the same tag with different dye molecules.

Direct labeling

The selectivity that arises from a specific functional group binding to a specific tag makes the direct labeling approach a very versatile tool for targeting POIs. The absence of any enzymes or catalysts in the reaction circumvents the limitations of enzyme catalysis such as narrow substrate range, sub-optimal efficiency of the reaction, compartment-specific labeling challenges and the limited stability of enzymes under reaction conditions. Most reactions that result in the formation of a specific covalent bond employ weak electrophiles that liberate non-fluorescent and non-reactive side-products that do not interfere with the measurements. Direct labeling techniques that

Covalent labels

SNAP-tag: SNAP-tag is a classic example of a bio-inspired labeling approach. Human DNA repair protein O⁶-alkylguanine-DNA alkyltransferase (hAGT) selectively and irreversibly transfers the alkyl residue from alkylated DNA or its substrate to a cysteine residue within the enzyme.¹⁷ Kai Johnsson's lab used this technology to target O⁶-benzylguanosine (BG) derivatives containing fluorescent probes to POIs (Figure 2A). This labeling approach has several attractive properties: the size of hAGT is small (207 amino acids); it can be fused to either the N or C termini of POI and retains its function; the ligated dye is covalently linked to the hAGT with a 1:1 stoichiometry; and, the chemistry of BG-modification chemistry has been established very well in the literature. Several studies have successfully shown the applications of this tag *in vitro* and in living cells.¹⁸⁻²¹ However, the inspiration from the DNA damage repair protein also has its disadvantages. Since Alkylguanine-DNA alkyltransferase (AGT) is intrinsically present in cells for DNA repair, special cell lines that are deficient in AGT should be utilized in studies with SNAP-tag. Cell lines that have endogenous AGT show a detectable labeling of AGT in the nucleus. This can be a major limitation for the general application of the SNAP-tag technology, especially when the studies involve targeting proteins in the nucleus, or studying proteins that may translocate to the nucleus. The second disadvantage to this technology comes from the high concentration of the substrate, typically ~10 μ M for labeling cultured cells. Several dyes show non-specific binding as well as dye-dye interactions at such high concentrations and thus may interfere with fluorescence observations. Finally, washing the unreacted BG derivatives may be cumbersome and needs optimization with each cell type and experimental condition.

CLIP-tag: The CLIP-tag is a logical extension of the SNAP-tag technology where the molecular recognition consists of an AGT mutant that reacts specifically with an O²-

benzylcytosine (BC) derivative (Figure 2A).¹⁹ The discovery of the CLIP-tag allowed for simultaneous and specific labeling of two different proteins with spectrally resolvable fluorescent probes. The CLIP-tag can be used in conjunction with the SNAP-tag due to the marked differences between the molecular recognition mechanisms of AGT (SNAP) and its mutant (CLIP). The labeling achieved through the simultaneous use of the two probes can be attributed to the lack of interactions between AGT and BC due to the hydrogen bonding between Tyr114 and the N³ of guanine. Further since cytosine is a less bulky group and has different hydrogen binding interactions, the AGT mutants (CLIP) did not show any cross reactivity towards the BG derivatives. One of the key breakthroughs that the CLIP-tag achieves over the SNAP-tag is in the labeling of cell lines that are not deficient in endogenous AGT. Since the CLIP-tag uses a mutant of AGT, BC derivatives do not react with endogenous AGT in cell lines. The CLIP-tag has been applied to studies involving pulse chase measurements, superresolution microscopy and chromophore assisted light inactivation of proteins.²² Similar to the SNAP-tag the CLIP-tag labeling requires high concentrations of the BC derivatives and extensive wash steps prior to imaging. Both SNAP-tag and CLIP-tag constructs, dyes and targeting moieties (reactive versions of BG and BC) are available commercially from New England Biolabs.

HaloTag: The HaloTag is a commercially available, versatile probe from Promega that utilizes similar principles as the SNAP and CLIP-tags. The tag uses a mutant of Rhodococcus dehalogenase (DhaA.H272F/K175M/C176G/Y273L) that reacts specifically and at a fast rate with haloalkanes.²³ The underlying chemistry involves the nucleophilic displacement of the terminal chloride with Asp¹⁰⁶, forming an alkyl-enzyme intermediate. The H272F mutation ensures that the hydrolysis of this intermediate is not catalyzed and hence trapped as the stable product (Figure 2B). The utility and versatility

of the HaloTag arises primarily from the underlying linker chemistry. Since the ester bond formed with the Asp¹⁰⁶ is seated deeply inside a hydrophobic pocket, it is stable under stringent conditions such as boiling with SDS, or even in the presence of formaldehyde. A direct application of this property is the use of HaloTag in fixed cell assays.²⁴ Secondly, alkyl dehalogenases are absent in *E. coli* and eukaryotic cells making this probe useful in a wide variety of cell types and organisms. Finally, the HaloTag technology has been used in a wide variety of assays owing to the generality of the approach and optimization of the chloroalkane linker that proves to be an excellent handle for performing cellular imaging, protein-protein and protein-DNA interaction studies, SDS-PAGE, western blotting, and a variety of in-vivo and in-vitro assays. For live cell imaging, the probes are incubated at concentrations of 1-5 μ M for 45 mins, and require extensive washing, limiting their applications in the imaging of real time protein interactions during the labeling.

BL-tag: Throughout the course of evolution, cells have developed a wide variety of electrophiles and nucleophiles to carry out chemical reactions required for biosynthesis and metabolism. The β -lactamase enzymes found in *E. coli* are similar to the hAGT proteins in that regard. They cleave β lactam moieties in several compounds very well, and have been used widely as genetic reporters for colorimetric and fluorogenic assays. The Kukuchi lab utilized the underlying chemistry behind the β -lactamase in a mutant of the TEM-1- β -lactamase from *E. coli* to specifically covalently couple to substrates containing β -lactams (Figure 2C).²⁵ The BL-tag is similar to the HaloTag in that it traps the reaction intermediate of the WT enzyme through a site specific mutation. In the WT-TEM-1, Ser70 attacks the β -lactam ring to form an acyl intermediate. This is followed by the nucleophilic attack of Glu166 on the intermediate that releases the substrate and regenerates WT-TEM-1. In the BL-tag, an E166N mutation uses an ineffective

nucleophile (Asn) in the active site instead of Glu, trapping the acyl intermediate, and covalently linking the dye to form a stable product. The TEM-1 mutant is not found endogenously in bacterial or eukaryotic cells, making the method widely applicable in intracellular and cell surface protein imaging.²⁶ However, background β -lactamase catalytic activity in cells may reduce the availability of the tag in the cellular context. The BL-tag is orthogonal to SNAP-tag and thus can be used in combination with it and with similar technologies. A potential disadvantage of the method is the high concentrations of probe that are incubated with the cells (typically 5 μ M) that may lead to non-specific binding based on the cell type and dye used. Hence, optimization of incubation times and concentrations need to be performed when using the BL-tag for cell imaging. Additionally, for both HaloTag and BL-tag, there are limited choices of probes for intracellular imaging.

Covalent A-TMP-tag: The Cornish lab utilized rational design principles to synthesize an acrylamide conjugate of 2,4-diamino-5-(3,4,5-trimethoxybenzyl) pyrimidine (acrylamine Trimethoprim or A-TMP) that could specifically covalently link to a single engineered cysteine in an E. coli derived dihydrofolate reductase mutant (eDHFR:L28C) (Figure 2D).²⁷ This tag could be used in wild type mammalian cell lines with great success as TMP selectively binds to eDHFR ($K_d = 1\text{nM}$) with over three orders of magnitude higher affinity compared to mammalian DHFR ($K_d = 4\mu\text{M}$). Live cell imaging of proteins inside nuclear compartments could be performed using this tag owing to the excellent cell permeability of TMP. Moreover, only 1 μM of fluorescently labeled A-TMP is needed for live cell imaging. It is important to point out here that the reaction forming the eDHFR:A-TMP covalent bond takes $\sim 2\text{h}$ for $> 95\%$ completion. This tag can be used for single molecule imaging owing to the irreversible binding of the fluorophore to the target

protein. This can also be used in conjunction with the non-covalent TMP tag as discussed later.

Non covalent labels

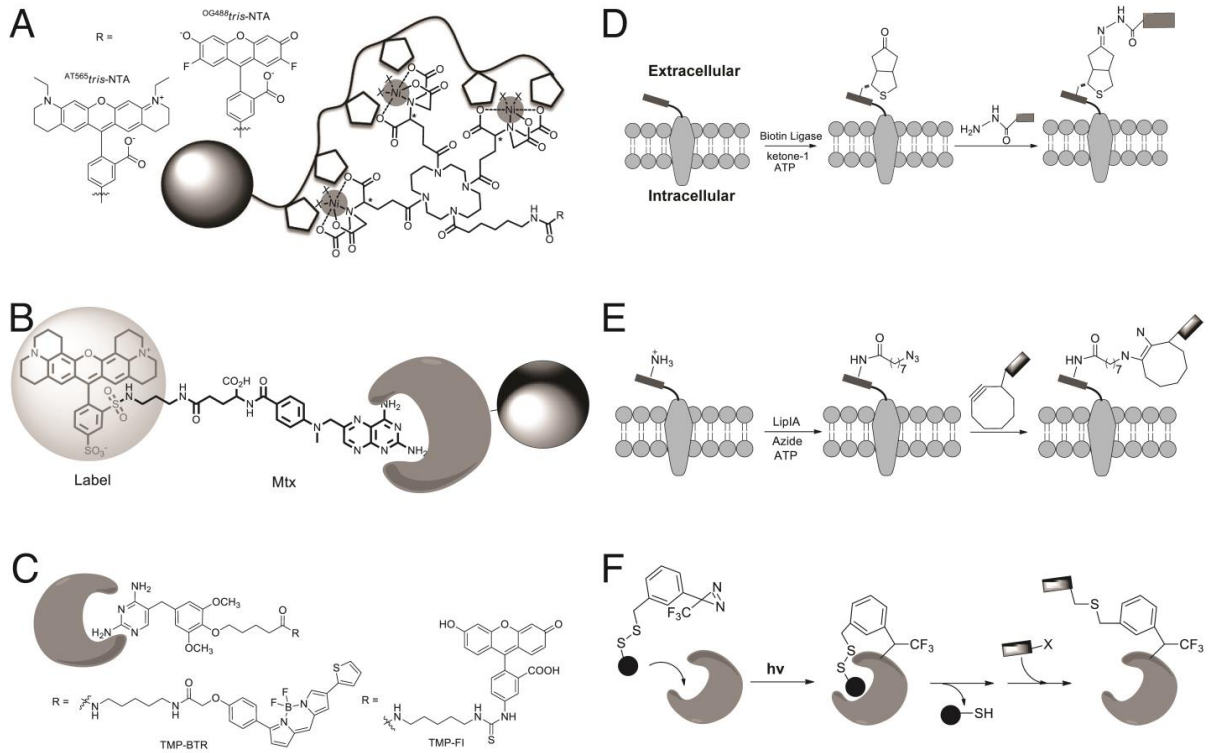


Figure 3. A. Common tris-NTA probes and schematic showing the binding of Ni:NTA to His₆ motif on a POI. B. Mechanism of action of a Mtx tag binding to DHFR. C. Binding mechanism of the non-covalent TMP tag and some of the commonly used fluorophores for this technology. D. Mechanism of action of the BirA-ketone-1 tagging technology. E. Mechanism of action of the LipIa-azide tagging technology. F. Mechanism of labeling using P-PALM probes.

Poly-Histidine tags: Poly-histidine tags have been widely used in affinity purification of proteins utilizing non-covalent binding with Ni²⁺:Nitrilotriacetic acid (Ni:NTA). The Ebright lab first demonstrated the successful targeting of Ni:NTA conjugated cyanine dyes to proteins expressing a hexa-Histidine (His₆) tag.²⁸ They optimized the number of Ni:NTA

per dye molecule such that, while mono Ni:NTA conjugated cyanine dyes showed a K_d in excess of 10 μ M, the Bis-Ni:NTA conjugates of the same dyes exhibited a K_d of 0.4-1 μ M for binding a His₆ tag. The Piehler lab further improved on this technology by synthesizing tris-NTA conjugates of commercially available organic dyes that bound His₆ and His₁₀ residues on POIs with high affinity and fast on rates, ultimately achieving sub-nanomolar affinities with His₁₀ and tris-Ni:NTA chelates (Figure 3A).²⁹ The poly-His:Ni:NTA binding is reversible in the presence of 20-100 mM imidazole; a method used very frequently in affinity purification of proteins, and useful for reversal of labeling under moderate conditions at the cell surface. A critical drawback of poly-His tagging arises from the quenching of the fluorophores upon conjugation with the Ni:NTA owing to the electronic interactions with the empty d-orbitals of Ni²⁺. There is typically further quenching of the fluorophore upon binding with the His-tagged protein. The combined quenching effect can sometimes lead to a loss of up to 80% in QY of the respective fluorophores. The Hamachi lab developed a complementary extension of this technology through the use of oligo-Aspartate sequences, and corresponding multinuclear Zn(II) complexes.³⁰ While moderate binding affinities weaken the signal due to incomplete labeling, there is no quenching of the fluorophore in this tag due to the d10 configuration of Zn(II). One challenge with these metal coordination based tags is that the poly-His and poly-Asp tags consist of clustered charges at the N-terminus or C-terminus of the protein, and may interfere with protein solubility, interactions and functions in cellular environments.

DHFR-Mtx: The Cornish lab utilized the non-covalent interaction between eDHFR and fluorescent conjugates of a small molecule, methotrexate (Mtx) (Figure 3B).³¹ The equilibrium and kinetic properties of DHFR-Mtx complex, further make this approach very attractive. DHFR binds Mtx with sub-nanomolar affinities ($K_d = 25$ pM) with a

sufficiently slow dissociation rate constant (k_{off}) of 10^{-4} s^{-1} in solution. Further, the formation of the DHFR-Mtx complex is thermodynamically favorable and it provides additional stability to DHFR particularly against proteolytic degradation. Finally, the chemical modification of Mtx is performed at the γ -carboxylate position that does not interfere with the receptor-binding moiety. Cell imaging using membrane and nuclear targeting DHFR in DHFR deficient cell lines was performed using a Texas Red conjugate of Mtx (Mtx-TR) at concentration of $2 \mu\text{M}$ (incubation with cells for 20h), which is less than half of that used for the SNAP-tag and Halotag. Key disadvantages of the DHFR-Mtx labeling strategy arise from the fact that the interaction is non-covalent and hence reversible, and the Mtx-TR for example, dissociates from DHFR tagged proteins on the order of 1-2 hours. Further, because methotrexate binds to both human and bacterial DHFR, this approach has to be used in cell lines that are DHFR-deficient to reduce background that arises from the labeling of endogenous DHFR.

DHFR-TMP-tag: The TMP-tag is a rationally designed tag that improves over the DHFR-Mtx tag and exploits the advantages of a non-covalent label. The Cornish lab used it as a binding partner for the E. coli DHFR for imaging in wild type mammalian cell lines, due to the previously described 4000:1 selectivity of TMP for eDHFR compared to hDHFR (Figure 3C).³² The conjugation of TMP to fluorescent dyes is straightforward and does not interfere with the binding to eDHFR. Owing to the high affinity and excellent cell permeability, the dye conjugated TMP tags can be used at low concentrations (10nM) with 5-15 min incubation times. Therefore, TMP tags deliver low background imaging with fast binding kinetics for cell biology studies. Because TMP is recognized by both the mutant eDHFR and wt-eDHFR, these TMP-tagged dyes can be used with the covalent A-TMP-eDHFR tags for pulse chase experiments.

Coiled-coil tag: The Coiled-Coil (CC) tagging approach is unique from the previously discussed approaches in that it uses complementary heptad-repeat peptide coil combinations for labeling cellular proteins.³³ Since it doesn't involve metal ions, a quenching of the probe is not observed. Briefly, the approach uses four peptides K3 (KIAALKE)₃, K4 (KIAALKE)₄, E3 (EIAALEK)₃ and E4 (EIAALEK)₄. The K peptides are positively charged whereas, the E peptides are negatively charged (K#, E#; # indicating the net charge). K3 and E3 probes were expressed on the extracellular N-terminus of membrane proteins in mammalian cells and TMR labeled complementary probes (E3 and K3 respectively) were used for live cell imaging. Although this approach should be very modular, fluorescent labeling could only be achieved with the K probes and E3 peptide expressed on the POI at the cell surface. The labeling concentrations of the probes were low (< 70 nM) and the incubation time was typically ~5 mins. Finally the probes were non-toxic even at concentrations of 10 μM in the media. Because the charged peptides do not cross the plasma membrane, the CC-tag approach is presently limited to labeling membrane proteins.

Indirect labeling

Indirect labeling approaches, for the purposes of discussion in this chapter, are defined as approaches where the formation of a covalent bond between a genetically encoded peptide sequence on the POI and a small molecule is mediated by enzymes or photochemically. Several of these methods are inspired by post-translational modifications on proteins. Specific enzymes catalyze the formation of a covalent bond between many small molecules such as biotin, acetyl coenzyme A and lipoic acid to specific short peptides in native proteins. These reactions can be exploited using the native enzymes or mutant and recombinant enzymes to form linkages between these peptides and dyes or other bio-orthogonal reactive groups.

Enzyme mediated labeling

BirA labeling with biotin: The streptavidin-biotin complex has one of the highest known affinities among non-covalent complexes. The high affinity and the extremely slow off rates make this system very attractive for fluorescent labeling of proteins. Further, the systematic optimization of the bacterial biotin holoenzyme synthetase, BirA has fueled the application of biotinylated proteins in pull-down assays, immunofluorescence and single molecule studies in vitro and in cells.³⁴⁻³⁷ Of particular interest are the studies targeting streptavidin conjugated Alexa Fluor dyes and streptavidin conjugated QDots to enzymatically biotinylated proteins on the cell surface, such as the cystic fibrosis transmembrane conductance receptor, the epidermal growth factor receptor, and α -amino-3-hydroxy-5-methyl-4-isoxazolepropionate receptor.^{35, 36}

BirA labeling with ketone-1: The Ting lab developed a cell surface protein labeling method derived from this approach to ligate an unnatural biotin analog (ketone-1) onto the AP (Figure 3D).³⁷ This required a combination of the unnatural biotin analog and a mutant BirA that could selectively ligate this new analog preferentially to native biotin. Because most biomolecules do not have a ketone group on them, this label can provide a very specific site for covalent labeling of POIs with ketone-1 modified APs using mild hydrazide chemistry. This approach was used to label AP-tagged EGFR and other transmembrane proteins with ketone-1 followed by covalent labeling with hydrazide conjugates of fluorescent dyes. The method is used to label surface proteins and cannot yet be applied inside cells because some intracellular molecules may be reactive towards hydrazides. This approach requires relatively long incubation times of the ketone-1-BirA complex followed by the fluorescent target incubation (20-120 mins). The reaction between ketone-1 and the dye conjugated to a hydrazide is carried out at pH 6.2 (faster hydrazine formation), limiting the application in complex tissues or cells that

may be pH sensitive. This method requires initial washing of the ketone prior to labeling with the dye, as well as washing of the unreacted fluorescent dye label.

Lipoic acid ligase: The reaction between an alkyne and an azide can be used to provide high specificity in cellular environments not only because they are generally not found in cells but also because they are not cytotoxic. The lipoic acid ligase (LipIA) tag exploits this principle and has been shown to label cell surface proteins with fluorescent dyes. The Ting lab discovered that an alkyl azide with a linker can bind selectively to the lysine side chain in the acceptor peptide sequence on the POI (Figure 3E).³⁸ Once this was achieved, a fluorescent probe conjugated with a cyclooctyne group could be covalently linked to the azide through the Staudinger ligation. This probe could be used as a complement to BirA labeling on the cell surface. The labeling protocol and wash steps for this approach are similar to the BirA approach. The labeling time is shorter than the BirA approach, yet still requires more than an hour and the lipoic acid and fluorophore cyclooctyne are added in two different steps. The approach can only be used on the cell membrane and requires washing out of the unreacted azide, LipIA and unreacted fluorophores prior to imaging.

PPTase: Yin and coworkers, discovered an enzymatic labeling method utilizing the phosphopantetheinyl transferase (PPTase) enzyme that could catalyze Coenzyme A (CoA) ligation to the serine residue of an 11 aa AP motif.³⁹ The underlying chemistry involves the transfer of the phosphopantetheinyl group from CoA to a specific serine moiety on a peptidyl carrier protein (PCP). Since the size of the PCP tag is slightly larger (80-100 aa), the Yin lab subsequently selected an 11 aa residue through phage display and peptide synthesis, the ybbR AP. This compact tag can be inserted on the N or the C termini of POIs, as well as on a flexible loop within the POI. Further, there were improvements made through the selection of two other AP tags (12 aa) through a phage

display library selection, named the S6 and the A1 tag that served as substrates of Sfp (catalytic efficiency of 442-fold for A1) and AcpS (catalytic efficiency of 30-fold for S6) respectively.⁴⁰ The methodology provided for two selective labels; one utilizing the Sfp pathway while the other utilizes an AcpS pathway. This methodology was successfully applied to image the epidermal growth factor receptor (S6-EGFR) and the transferrin receptor 1 (A1-TfR1) on HeLa cells, labeled with small molecule fluorophores. Although the cell impermeability aspect of the CoA enzyme conjugates has been touted as an advantage, the inability to label intracellular proteins is a key limitation of this method. Secondly, high labeling concentrations and stringent washing conditions further limit the applications of this method.

Light mediated labeling

P-PALM: The Hamachi lab utilized local photochemical reactions in conjunction with electrophilic-nucleophilic substitution principles to obtain a Post-PhotoAffinity Labeling Modification (P-PALM) method (Figure 3F).⁴¹ They used concanavalin A (ConA), a lectin as the protein tag. The probe combined a high affinity target ligand such as α -D-mannoside and α -D-glucoside; a diazirine group that is photoreactive, and a disulfide cleavage site that can generate a chemoselective nucleophilic thiol group upon reduction. After the saccharide moiety binds ConA, bringing the nucleophilic reduction site in close proximity to the protein binding site, UV-irradiation of the probe resulted in the formation of a covalent bond between the diazirine groups of the probe and the ConA tag at the Tyr100 or Tyr12 residues close to the binding pocket. The Hamachi lab further applied this technique to synthesize in a site selective fashion, ConA with two fluorescent labels (Coumarin and Fluorescein). They showed that the fluorescence from fluorescein, that was closer to the protein-sugar binding pocket was somewhat quenched while that of coumarin was invariant to the changes in the microenvironment.

They used this observation to build a ratiometric sensor for mannose type saccharides on the surface of MCF-7 cells. When dual-labeled ConA was bound to the saccharide, the fluorescence from fluorescein was quenched relative to the free dual-labeled ConA in solution. Washing free ConA sensor away revealed cell surface signal related to mannose levels present. The probe could be chased away very easily by using 100 μM 1,6-mannotriose. Photochemical principles have not been exploited very well in protein labeling and this technology may be a starting point in photo-mediated ligation of small molecules to POIs.

Fluorogenic probes

A key limitation of fluorescently labeled affinity tags is that washing steps are required to remove unbound and nonspecifically bound fluorescent labels. Further, incubation times are generally low only when the fluorescent probe is used at high concentrations, giving rise to non-specific binding with intrinsic cellular proteins. A logical solution to these limitations would be the use of probes that light-up only when bound to the specific target protein. A fluorogen is a small, non-fluorescent molecule that shows a fluorescent enhancement upon binding a partner protein. Fluorogens have been realized using three basic concepts: chemical cleavage produces an aromatic and fluorescent conjugated dye molecule; chemical cleavage removes a fluorescence quenching group or binding results in enhancement of fluorescent properties of molecular rotor-like molecules. While one of the first attempts at protein labeling was fluorogenic (Tetracysteine tags), only a handful of fluorogenic probes have since been discovered. Although the concept of fluorogenic detection is well established and highly effective in DNA detection, many of these molecules are unsuitable for fluorogenic protein labeling due to background from DNA and RNA activation. Fluorogenic labeling is a very attractive approach for both cell surface and intracellular labeling, but is presently limited by a small selection of robust

fluorogenic dyes with high brightness and low nonspecific activation with good cell-penetrating properties.

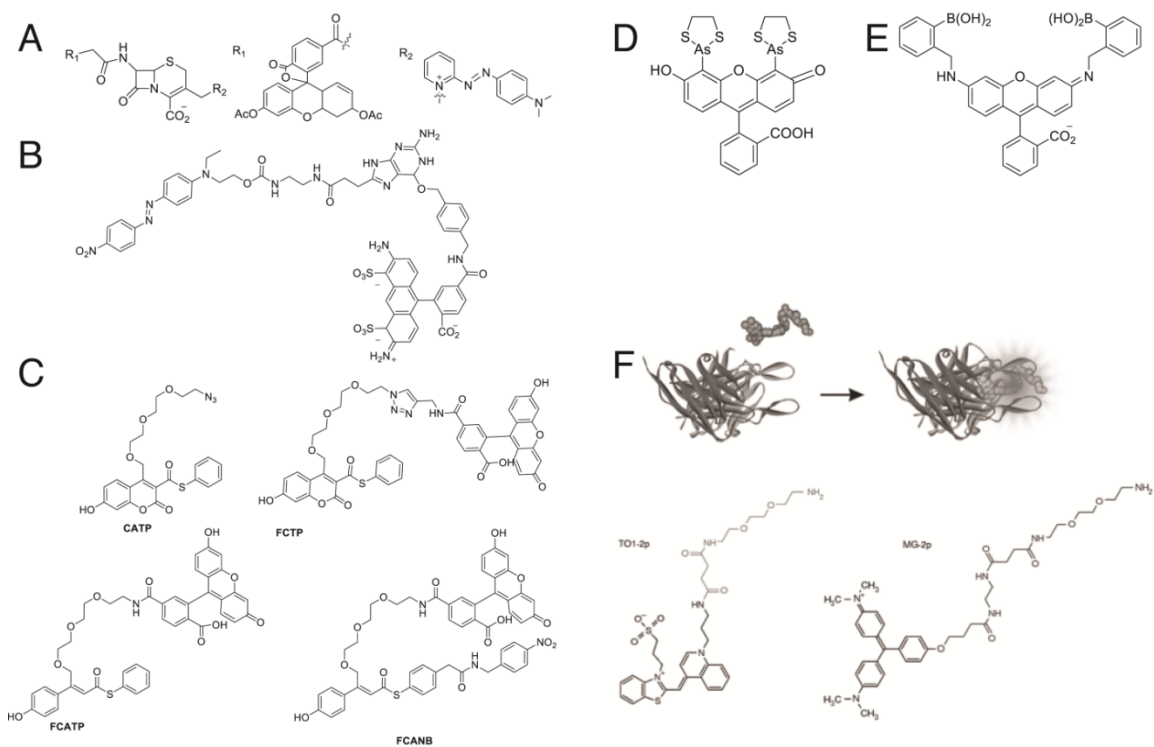


Figure 4. A. Fluorogenic BL-tag probes showing the structures of the fluorophore and the quencher. B. Structure of the fluorogenic SNAP-tag probe. C. Structures of some commonly used PYP-tag probes. D. FIAsh. E. RhoBo fluorogen. F. Fluorogen activating peptide technology and the structure of the commonly used fluorogens.

Covalent fluorogenic probes

BL-tag: The BL-tag, as discussed in the fluorescent dye labeling approach, employs the site specific covalent labeling of small molecule conjugated to β -lactams and the TEM-1- β lactamase. In a related approach, the Kikuchi lab synthesized a three component fluorogenic probe that consisted of a single organic dye (7-hydroxycoumarin, Fluorescein or TAMRA), cephalosporin and a collisional fluorescence quencher, DABCYL or azopyridine (Figure 4A).⁴² The fluorescence of the respective organic dyes

are quenched in the presence of the DABCYL or azopyridine until the cephalosporin β -lactam ring cleaves followed by the elimination of the 3' bonded quencher. The remaining cephalosporin-dye adduct remained bound to the β -lactamase labeled EGFR on HEK-293 cell surface. Although the probe is fluorogenic, high concentration of the fluorogen ($\sim 10 \mu\text{M}$) have to be used with cells for long incubation times (~ 2 hours), achieving a fluorescence activation of 142-fold. Also, the fluorescence signal of the FCD reaches its maximum in over 200 minutes, limiting the application of this probe to experiments where fast labeling is not crucial.

SNAP-tag: While the benzylguanine motif in SNAP tag probes is a fluorescence quencher for certain organic dyes, only a 30-fold fluorescence enhancement was achieved using this approach.⁴³ More recently, the Urano lab developed a SNAP-tag BG probe that has a disperse red-1 quencher at the C8 position of the BG motif.⁴⁴ They synthesized a disperse red-BG-Fluorescein (DRBG-488) (Figure 4B) and a membrane permeant version with a diacetyl protection (DRBFFL-DA) for labeling proteins. The fluorescence activation of these probes upon binding the SNAP-tag was 300 fold and they did not need any washing of the unreacted label owing to their negligible background fluorescence. SNAP-EGFR expressing COS7 cells could be imaged using $2 \mu\text{M}$ of the DRBG-488 probe without washing within 40 mins. These probes were successfully employed to study membrane trafficking in COS7 cells as well as cell migration of MDCK cells. This approach was used to study protein delivery on the HEK-293 cell surface in real time, as opposed to the single time point measurements offered by pulse-chase for probes where rigorous washing is needed.

PYP tag: PYP-tag is based on a 125 kDa photoactive yellow protein found in bacteria. It can covalently bind to a variety of compounds containing a 7-hydroxycoumarin-3-carboxylic acid thioester through transthioesterification with its Cys₆₉ residue.⁴⁵⁻⁴⁷ When

the probe is in solution without the PYP-tag, the fluorescence from fluorescein is quenched due to intramolecular interactions between the coumarin thioester derivative and fluorescein. On covalently binding to the PYP-tag, the location of coumarin in the protein binding pocket disrupts its interaction with fluorescein and fluorescence emission from fluorescein is observed. Common PYP probes are shown in Figure 4C. CATP is a cell permeable dye while the other dyes can be only used on the cell surface. In another probe designated FCANB, nitrobenzene is used as a quencher for fluorescein. All but the environment sensitive probes designated TMBDMA and CMBDMA, need washing after incubation for ~30 mins at several micromolar concentrations. They could be incubated at 1 μ M concentration for 30 mins to label mammalian cells. The key limitation of PYP-tags is the use of fluorescein as the primary fluorophore. This limits the available colors when performing an experiment with PYP-tags.

Non covalent fluorogenic probes

Tetracysteine: The tetracysteine tag is the first example of a hybrid tag and was systematically developed and reported by Roger Tsien's lab in 1998.¹⁶ It utilizes a 6-12 epitope containing the sequence CCXBCC where X and B can be any amino acids except cysteine and mostly Proline and Glycine. The four cysteines bind to biarsenical dyes such as FIAsH (Figure 4D), ReAsH, CrAsH, CHoXAsH and AsCy3.⁴⁸⁻⁵⁰ The tetracysteine motif has sub-picomolar affinity for the FIAsH and ReAsH probes and there is a 1000-fold fluorescence enhancement of the probes upon binding the tetracysteine motif. This combination of tight binding and high fluorogenicity, results in a labeling system that does not require any washing prior to imaging the specifically labeled proteins. The biarsenical dyes are always administered with dithiols to minimize background labeling arising from their affinity for monothiol, and to protect cells from arsenic toxicity. Typical labeling concentrations are 1 μ M and the incubation times are long, often up to 1 hour.

As the first hybrid tags that were developed and implemented in two colors, the biarsenicals have been used in a variety of applications, including affinity purification, pulse chase labeling, chromophore assisted light inactivation, correlative light and electron microscopy, and protein synthesis detection and *in vivo* studies of protein folding to name just a few.⁸

Tetraserine tags: Tetraserine tags, developed by the Schepartz lab, to some extent solve the problems of cytotoxicity and background that are observed with TC tags. A rhodamine derived bis-boronic acid dye (RhoBo) (Figure 4E) can bind specifically with sub-micromolar affinity, to tetraserine motifs (SSPGSS) on POIs. RhoBo has higher QY (0.91) than FIAsH (0.5).⁵¹ RhoBo is a cell permeant dye and has been used at a concentration of 1 μ M with 30 mins of incubation time for the fluorescence imaging of intrinsic proteins inside HeLa cells. The relatively higher K_d (347 nM) and the abundance of proteins containing the SSPGSS motifs (particularly Myosin), in human cell lines pose the main limitations to the use of this probe for live cell imaging.

Fluorogen Activating Peptides: While non-covalent, fluorogenic labeling has several advantages; there is a constant trade-off between the binding affinity, on-rate and brightness. Also, for some applications, having a reversible binding of the fluorescent complex can be very useful. Most importantly, the ability to target the probe to any location, on or inside the cell is still an unmet need due to the limitations on the available tags and probes. Fluorogen activating peptides are excellent hybrid labeling agents that address these limitations. They consist of a genetically encoded protein tag and a small molecule fluorogen. The fluorogen, in solution has rotational freedom around its pi-bond system that disrupts conjugation and fluorescence. However, when it is bound to a protein in a non-covalent fashion, the rotational freedom is restricted and fluorescence results from the formation of a planar, conjugated π -system. Derivatives of Malachite

Green (MG) and Thiazole Orange (TO1) were the first reported fluorogens with this technology (Figure 4F).⁵² The last five years have seen a rapid increase in the number and type of fluorogens for this technology: covering the visible and far red spectrum as well as providing a variety of functionalities, such as resonance energy transfer, leading to signal amplification and pH sensing.⁵³⁻⁵⁷ The fluorogens used with this technology show a fluorescence enhancement of up to 18000-fold, the highest reported enhancement for any protein based fluorogen. This ensures a completely wash free system for cell imaging. Finally, since the interaction between the peptide and the fluorogen is non-covalent, it has been possible to obtain through directed evolution, a vast variety of peptide-fluorogen pairs with varying affinities (6 pM to ~500 nM).⁵⁸ The protein-fluorogen binding is instantaneous, even at a ~100 nM of the fluorogen. Directed evolution also allows for tunability of photochemical properties, and has led to the discovery of fluorogens with enhanced photostability. This technology has been applied for single molecule detection and superresolution microscopy on fixed and live cells.^{52, 59}

Conclusions and future outlook

During the first wave of developing fluorophores, synthetic chemistry enabled us to provide the desired spectroscopic, photochemical and targeting properties to a variety of fluorophores and fluorogens. The development of FP technology further fueled discovery through genetically encoded protein tagging techniques. The last 18 years, in what may be termed as a bio-inspired third wave of protein tagging, have seen some very smart systems that mimic natural enzymes and proteins to label POIs. During this period, most of the efforts have been towards the modification of the protein tag. Fluorogenic probes are catching up with other techniques and a surge in the number and variety of these probes has been observed in the last four years. While these wash free labels will continue to be developed, in the future, we would finally like to have a “tag-less” labeling system. For this to be achieved, the principles of fluorogenicity and bio-inspired specificity have to be utilized in sync. A recent example of that approach was the development of fluorescent saxitoxins by the Moerner lab.⁶⁰ These small molecule probes directly bind to a protein of interest and show a fluorogenic response. While it is hard to fathom that we would be able to find a selective fluorogen for every protein possible, it is definitely a good target for the design of the fourth generation protein labeling approaches. These may enable the direct detection of a specific native protein in the complex cellular environment.

Tables

Table 1: Properties and labeling conditions for fluorescent hybrid tags discussed in this study.

Name (MW/kDa)	Steps	[Probe] (μ M)/Incubation time (min)	Wash	Cell permeability
SNAP [¶] (20)	1	5/ 25	3x	Yes
CLIP (21)	1	5/ 20	3x	Yes
Halo (33)	1	5/ 15	3x	Yes
BL (29)	1	10/ 30-120	1x	Yes
A-TMP (18)	1	1/ 10	2x	Yes
<i>Poly-His (1)</i>	1	0.1/ 5	1x	No
<i>DHFR-Mtx[¶] (18)</i>	1	2/ 20h	2x	Yes
<i>DHFR-TMP (18)</i>	1	0.1-10/ 5-120	3x	Yes
<i>Coiled Coil (6)</i>	1	0.005/ 5	1x	No
<i>BirA-Biotin[*] (2)</i>	1	<1/ instantaneous	1x	No
BirA-Ketone-1 [*] (2)	2	1000/ 60-120	2x	No
LipoicAl [*] (0.2)	2	100-400/ 20	3x	No
PPTase [*] (1)	1	1/ 20	5x	Yes
P-PALM ^{**} (27)	1	0.3-1/ 0-60	1x	Yes

* Enzyme mediated; ** Light mediated, [¶] Deficient cell lines needed; Non-covalent probes are italicized

Table 2: Properties and labeling conditions for fluorogenic hybrid tags discussed in this study

Name (MW/kDa)	Mechanism	$F_{\text{bound}}/F_{\text{free}}$	[Probe] (μM)/ Incubation time (min)	$K_d(\mu\text{M})/$ $k_{\text{off}}(\text{s}^{-1})$	Cell permeability
BL (29)	Chromophore Quenching	142	10/ 30	--	No
SNAP (20)	Chromophore Quenching	300	2/ 10-40	--	No
PYP (14)	Chromophore Quenching	22	1/ 30	--	No
<i>Tetra-Cys</i> (0.6)	<i>Disruption of Conjugation</i>	<i>1000</i>	<i>1/ 60</i>	--	Yes
<i>Tetra-Ser</i> (0.6)	<i>Disruption of Conjugation</i>	<i>3</i>	<i>0.05/ 20</i>	<i>0.3/ --</i>	Yes
<i>FAP</i> (26)	<i>Disruption of Conjugation</i>	<i>18000</i>	<i>0.1/ 5</i>	<i>6E-6/ 1E-5</i>	Yes

Non-covalent probes are italicized

Bibliography

1. Fernández-Suárez, M.; Ting, A. Y., Fluorescent probes for super-resolution imaging in living cells. *Nature Reviews Molecular Cell Biology* **2008**, 9 (12), 929-943.
2. Yildiz, A.; Selvin, P. R., Fluorescence imaging with one nanometer accuracy: application to molecular motors. *Accounts of chemical research* **2005**, 38 (7), 574-582.
3. Xie, X. S.; Trautman, J. K., Optical studies of single molecules at room temperature. *Annual Review of Physical Chemistry* **1998**, 49 (1), 441-480.
4. Eggeling, C.; Widengren, J.; Rigler, R.; Seidel, C. A. M., Photostability of fluorescent dyes for single-molecule spectroscopy: mechanisms and experimental methods for estimating photobleaching in aqueous solution. In *Applied fluorescence in chemistry, biology and medicine*, Springer: 1999; pp 193-240.
5. Depry, C.; Mehta, S.; Zhang, J., Multiplexed visualization of dynamic signaling networks using genetically encoded fluorescent protein-based biosensors. *Pflügers Archiv - European Journal of Physiology* **2013**, 465 (3), 373-381.
6. Wysocki, L. M.; Lavis, L. D., Advances in the chemistry of small molecule fluorescent probes. *Current Opinion in Chemical Biology* **2011**, 15 (6), 752-759.
7. Remington, S. J., Green fluorescent protein: A perspective. *Protein Science* **2011**, 20 (9), 1509-1519.
8. Giepmans, B. N. G.; Adams, S. R.; Ellisman, M. H.; Tsien, R. Y., The fluorescent toolbox for assessing protein location and function. *Science Signaling* **2006**, 312 (5771), 217.

9. Coons, A. H.; Kaplan, M. H., Localization of antigen in tissue cells II. Improvements in a method for the detection of antigen by means of fluorescent antibody. *The Journal of experimental medicine* **1950**, *91* (1), 1-13.
10. Tsien, R. Y., THE GREEN FLUORESCENT PROTEIN. *Annual Review of Biochemistry* **1998**, *67* (1), 509-544.
11. Day, R. N.; Davidson, M. W., The fluorescent protein palette: tools for cellular imaging. *Chemical Society Reviews* **2009**, *38* (10), 2887-2921.
12. Shcherbo, D.; Murphy, C.; Ermakova, G.; Solovieva, E.; Chepurnykh, T.; Shcheglov, A.; Verkhusha, V.; Pletnev, V.; Hazelwood, K.; Roche, P., Far-red fluorescent tags for protein imaging in living tissues. *Biochem. J* **2009**, *418*, 567-574.
13. Kremers, G.; Hazelwood, K. L.; Murphy, C. S.; Davidson, M. W.; Piston, D. W., Photoconversion in orange and red fluorescent proteins. *Nature methods* **2009**, *6* (5), 355-358.
14. Farinas, J.; Verkman, A. S., Receptor-mediated targeting of fluorescent probes in living cells. *Journal of Biological Chemistry* **1999**, *274* (12), 7603-7606.
15. Schlessinger, J.; Shechter, Y.; Willingham, M. C.; Pastan, I., Direct visualization of binding, aggregation, and internalization of insulin and epidermal growth factor on living fibroblastic cells. *Proceedings of the National Academy of Sciences* **1978**, *75* (6), 2659-2663.
16. Griffin, B. A.; Adams, S. R.; Tsien, R. Y., Specific covalent labeling of recombinant protein molecules inside live cells. *Science* **1998**, *281* (5374), 269-272.
17. Keppler, A.; Gendreizig, S.; Gronemeyer, T.; Pick, H.; Vogel, H.; Johnsson, K., A general method for the covalent labeling of fusion proteins with small molecules in vivo. *Nature biotechnology* **2002**, *21* (1), 86-89.

18. Regoes, A.; Hehl, A. B., SNAP-tag-mediated live cell labeling as an alternative to GFP in anaerobic organisms. *Biotechniques* **2005**, 39 (6), 809.
19. Gautier, A.; Juillerat, A.; Heinis, C.; Corrêa Jr, I. R.; Kindermann, M.; Beaufils, F.; Johnsson, K., An Engineered Protein Tag for Multiprotein Labeling in Living Cells. *Chemistry & Biology* **2008**, 15 (2), 128-136.
20. Srikun, D.; Albers, A. E.; Nam, C. I.; Iavarone, A. T.; Chang, C. J., Organelle-targetable fluorescent probes for imaging hydrogen peroxide in living cells via SNAP-Tag protein labeling. *Journal of the American Chemical Society* **2010**, 132 (12), 4455-4465.
21. Maurel, D.; Comps-Agrar, L.; Brock, C.; Rives, M.-L.; Bourrier, E.; Ayoub, M. A.; Bazin, H.; Tinel, N.; Durroux, T.; Prézeau, L., Cell-surface protein-protein interaction analysis with time-resolved FRET and snap-tag technologies: application to GPCR oligomerization. *Nature methods* **2008**, 5 (6), 561-567.
22. Hinner, M. J.; Johnsson, K., How to obtain labeled proteins and what to do with them. *Current Opinion in Biotechnology* **2010**, 21 (6), 766-776.
23. Los, G.; Darzins, A.; Karassina, N.; Zimprich, C.; Learish, R.; McDougall, M.; Encell, L.; Friedman-Ohana, R.; Wood, M.; Vidugiris, G., HaloTag™ Interchangeable labeling technology for cell imaging and protein capture. *Cell Notes* **2005**, 11, 2-6.
24. Schröder, J.; Benink, H.; Dyba, M.; Los, G. V., In vivo labeling method using a genetic construct for nanoscale resolution microscopy. *Biophysical journal* **2009**, 96 (1), L1-L3.
25. Watanabe, S.; Mizukami, S.; Hori, Y.; Kikuchi, K., Multicolor Protein Labeling in Living Cells Using Mutant β -Lactamase-Tag Technology. *Bioconjugate chemistry* **2010**, 21 (12), 2320-2326.

26. Watanabe, S.; Mizukami, S.; Akimoto, Y.; Hori, Y.; Kikuchi, K., Intracellular Protein Labeling with Prodrug-Like Probes Using a Mutant β -Lactamase Tag. *Chemistry-A European Journal* **2011**, *17* (30), 8342-8349.
27. Gallagher, S. S.; Sable, J. E.; Sheetz, M. P.; Cornish, V. W., An in vivo covalent TMP-tag based on proximity-induced reactivity. *ACS chemical biology* **2009**, *4* (7), 547-556.
28. Kapanidis, A. N.; Ebright, Y. W.; Ebright, R. H., Site-specific incorporation of fluorescent probes into protein: hexahistidine-tag-mediated fluorescent labeling with (Ni²⁺: nitrilotriacetic acid) n-fluorochrome conjugates. *Journal of the American Chemical Society* **2001**, *123* (48), 12123-12125.
29. Lata, S.; Gavutis, M.; Tampe, R.; Piehler, J., Specific and stable fluorescence labeling of histidine-tagged proteins for dissecting multi-protein complex formation. *Journal of the American Chemical Society* **2006**, *128* (7), 2365-2372.
30. Ojida, A.; Honda, K.; Shinmi, D.; Kiyonaka, S.; Mori, Y.; Hamachi, I., Oligo-Asp tag/Zn (II) complex probe as a new pair for labeling and fluorescence imaging of proteins. *Journal of the American Chemical Society* **2006**, *128* (32), 10452-10459.
31. Miller, L. W.; Sable, J.; Goelet, P.; Sheetz, M. P.; Cornish, V. W., Methotrexate conjugates: a molecular in vivo protein tag. *Angewandte Chemie* **2004**, *116* (13), 1704-1707.
32. Miller, L. W.; Cai, Y.; Sheetz, M. P.; Cornish, V. W., In vivo protein labeling with trimethoprim conjugates: a flexible chemical tag. *Nature methods* **2005**, *2* (4), 255-257.
33. Yano, Y.; Yano, A.; Oishi, S.; Sugimoto, Y.; Tsujimoto, G.; Fujii, N.; Matsuzaki, K., Coiled-Coil Tag-Probe System for Quick Labeling of Membrane Receptors in Living Cells. *ACS chemical biology* **2008**, *3* (6), 341-345.

34. Beckett, D.; Kovaleva, E.; Schatz, P. J., A minimal peptide substrate in biotin holoenzyme synthetase-catalyzed biotinylation. *Protein Science* **1999**, *8* (04), 921-929.
35. Bates, I. R.; Hébert, B.; Luo, Y.; Liao, J.; Bachir, A. I.; Kolin, D. L.; Wiseman, P. W.; Hanrahan, J. W., Membrane lateral diffusion and capture of CFTR within transient confinement zones. *Biophysical journal* **2006**, *91* (3), 1046-1058.
36. Howarth, M.; Takao, K.; Hayashi, Y.; Ting, A. Y., Targeting quantum dots to surface proteins in living cells with biotin ligase. *Proceedings of the National Academy of Sciences of the United States of America* **2005**, *102* (21), 7583-7588.
37. Chen, I.; Howarth, M.; Lin, W.; Ting, A. Y., Site-specific labeling of cell surface proteins with biophysical probes using biotin ligase. *Nature methods* **2005**, *2* (2), 99-104.
38. Fernández-Suárez, M.; Baruah, H.; Martínez-Hernández, L.; Xie, K. T.; Baskin, J. M.; Bertozzi, C. R.; Ting, A. Y., Redirecting lipoic acid ligase for cell surface protein labeling with small-molecule probes. *Nature biotechnology* **2007**, *25* (12), 1483-1487.
39. Yin, J.; Straight, P. D.; McLoughlin, S. M.; Zhou, Z.; Lin, A. J.; Golan, D. E.; Kelleher, N. L.; Kolter, R.; Walsh, C. T., Genetically encoded short peptide tag for versatile protein labeling by Sfp phosphopantetheinyl transferase. *Proceedings of the National Academy of Sciences of the United States of America* **2005**, *102* (44), 15815-15820.
40. Zhou, Z.; Cironi, P.; Lin, A. J.; Xu, Y.; Hrvatin, S. a.; Golan, D. E.; Silver, P. A.; Walsh, C. T.; Yin, J., Genetically encoded short peptide tags for orthogonal protein labeling by Sfp and AcpS phosphopantetheinyl transferases. *ACS chemical biology* **2007**, *2* (5), 337-346.

41. Hayashi, T.; Hamachi, I., Traceless affinity labeling of endogenous proteins for functional analysis in living cells. *Accounts of chemical research* **2012**, *45* (9), 1460-1469.
42. Mizukami, S.; Watanabe, S.; Akimoto, Y.; Kikuchi, K., No-wash protein labeling with designed fluorogenic probes and application to real-time pulse-chase analysis. *Journal of the American Chemical Society* **2012**, *134* (3), 1623-1629.
43. Stöhr, K.; Siegberg, D.; Ehrhard, T.; Lymperopoulos, K.; Oñz, S.; Schulmeister, S.; Pfeifer, A. C.; Bachmann, J.; Klingmüller, U.; Sourjik, V., Quenched substrates for live-cell labeling of SNAP-tagged fusion proteins with improved fluorescent background. *Analytical chemistry* **2010**, *82* (19), 8186-8193.
44. Komatsu, T.; Johnsson, K.; Okuno, H.; Bito, H.; Inoue, T.; Nagano, T.; Urano, Y., Real-time measurements of protein dynamics using fluorescence activation-coupled protein labeling method. *Journal of the American Chemical Society* **2011**, *133* (17), 6745-6751.
45. Hori, Y.; Nakaki, K.; Sato, M.; Mizukami, S.; Kikuchi, K., Development of Protein-Labeling Probes with a Redesigned Fluorogenic Switch Based on Intramolecular Association for No-Wash-Live-Cell Imaging. *Angewandte Chemie International Edition* **2012**, *51* (23), 5611-5614.
46. Hori, Y.; Ueno, H.; Mizukami, S.; Kikuchi, K., Photoactive yellow protein-based protein labeling system with turn-on fluorescence intensity. *Journal of the American Chemical Society* **2009**, *131* (46), 16610-16611.
47. Sadhu, K. K.; Mizukami, S.; Hori, Y.; Kikuchi, K., Switching modulation for protein labeling with activatable fluorescent probes. *ChemBioChem* **2011**, *12* (9), 1299-1308.
48. Uljana Mayer, M., CrAsH: a biarsenical multi-use affinity probe with low non-specific fluorescence. *Chemical communications* **2006**, (24), 2601-2603.

49. Adams, S. R.; Campbell, R. E.; Gross, L. A.; Martin, B. R.; Walkup, G. K.; Yao, Y.; Llopis, J.; Tsien, R. Y., New biarsenical ligands and tetracysteine motifs for protein labeling in vitro and in vivo: synthesis and biological applications. *Journal of the American Chemical Society* **2002**, *124* (21), 6063-6076.
50. Cao, H.; Xiong, Y.; Wang, T.; Chen, B.; Squier, T. C.; Mayer, M. U., A red cy3-based biarsenical fluorescent probe targeted to a complementary binding peptide. *Journal of the American Chemical Society* **2007**, *129* (28), 8672-8673.
51. Halo, T. L.; Appelbaum, J.; Hobert, E. M.; Balkin, D. M.; Schepartz, A., Selective recognition of protein tetraserine motifs with a cell-permeable, pro-fluorescent bis-boronic acid. *Journal of the American Chemical Society* **2008**, *131* (2), 438-439.
52. Szent-Gyorgyi, C.; Schmidt, B. F.; Creeger, Y.; Fisher, G. W.; Zakel, K. L.; Adler, S.; Fitzpatrick, J. A.; Woolford, C. A.; Yan, Q.; Vasilev, K. V., Fluorogen-activating single-chain antibodies for imaging cell surface proteins. *Nature biotechnology* **2007**, *26* (2), 235-240.
53. Pow, C. L.; Marks, S. A.; Jesper, L. D.; Silva, G. L.; Shank, N. I.; Jones, E. W.; Burnette III, J. M.; Berget, P. B.; Armitage, B. A., A rainbow of fluoromodules: A promiscuous scFv protein binds to and activates a diverse set of fluorogenic cyanine dyes. *Journal of the American Chemical Society* **2008**, *130* (38), 12620-12621.
54. Shank, N. I.; Zanotti, K. J.; Lanni, F.; Berget, P. B.; Armitage, B. A., Enhanced photostability of genetically encodable fluoromodules based on fluorogenic cyanine dyes and a promiscuous protein partner. *Journal of the American Chemical Society* **2009**, *131* (36), 12960-12969.
55. Shank, N. I.; Pham, H. H.; Waggoner, A. S.; Armitage, B. A., Twisted Cyanines: A Non-Planar Fluorogenic Dye with Superior Photostability and its Use in a

- Protein-Based Fluoromodule. *Journal of the American Chemical Society* **2012**, *135* (1), 242-251.
56. Grover, A.; Schmidt, B. F.; Salter, R. D.; Watkins, S. C.; Waggoner, A. S.; Bruchez, M. P., Genetically encoded pH sensor for tracking surface proteins through endocytosis. *Angewandte Chemie International Edition* **2012**, *51* (20), 4838-4842.
57. Szent-Gyorgyi, C.; Schmidt, B. F.; Fitzpatrick, J. A. J.; Bruchez, M. P., Fluorogenic dendrons with multiple donor chromophores as bright genetically targeted and activated probes. *Journal of the American Chemical Society* **2010**, *132* (32), 11103-11109.
58. Szent-Gyorgyi, C.; Stanfield, R. L.; Andreko, S.; Dempsey, A.; Ahmed, M.; Capek, S.; Waggoner, A. S.; Wilson, I. A.; Bruchez, M. P., Malachite Green Mediates Homodimerization of Antibody V_L Domains to Form a Fluorescent Ternary Complex with Singular Symmetric Interfaces. *Journal of molecular biology* **2013**, *425* (22), 4595-4613.
59. Fitzpatrick, J. A.; Yan, Q.; Sieber, J. J.; Dyba, M.; Schwarz, U.; Szent-Gyorgyi, C.; Woolford, C. A.; Berget, P. B.; Waggoner, A. S.; Bruchez, M. P., STED nanoscopy in living cells using fluorogen activating proteins. *Bioconjugate chemistry* **2009**, *20* (10), 1843-1847.
60. Ondrus, A. E.; Lee, H.-I. D.; Iwanaga, S.; Parsons, W. H.; Andresen, B. M.; Moerner, W.; Du Bois, J., Fluorescent saxitoxins for live cell imaging of single voltage-gated sodium ion channels beyond the optical diffraction limit. *Chemistry & Biology* **2012**, *19* (7), 902-912.

Chapter II: Fluorogen encapsulation and exchange for photostable imaging

Introduction

The phenomenon of fluorescence has been the tool of choice for scientists and engineers engaged in a wide variety of fields in the last 30 years. Sir John Herschel was the first to report fluorescence from quinine sulfate.¹ A century and a half later, we have come a great distance to the discovery of new fluorescent compounds and their applications to cell biology.² While the phenomenon observed by Herschel was not well understood back then, we now have a complete understanding of the molecular basis of fluorescence and the category of compounds that exhibit the phenomenon. Fluorescence is typically exhibited by aromatic molecules with conjugated pi bonds such as coumarins, xanthenes, aromatic cyanines, naphthalenes, oxazines and rhodamines.³ It is these conjugated π bonds that upon excitation by light of suitable wavelength, excite to different electronic states and in some cases, exhibit fluorescence upon de-excitation.⁴ While this may sound simple, there are several possibilities that may arise between the absorption and the emission of light. The Jablonski diagram is the spectroscopist's tool to describe and understand fluorescence from any system as shown in Figure 1.⁵ In a simplified case of light absorption by a fluorophore in the absence of photobleaching, the fluorophores populate the excited singlet state (S_1) upon absorption, a process that lasts *ca.* 10^{-15} s and populates the S_1 state. The S_1 state starts depopulating through fluorescence emission, radiationless internal conversion and intersystem crossing to the triplet state (T_1).⁶ When the pathway is fluorescence, some of the energy is lost due to vibrational relaxation in S_1 on the order of 10^{-12} s. This makes the energy of the emitted photon lower than the energy of the absorbed photon and

gives rise to the separation between the excitation and emission spectra known as Stokes shift.⁷

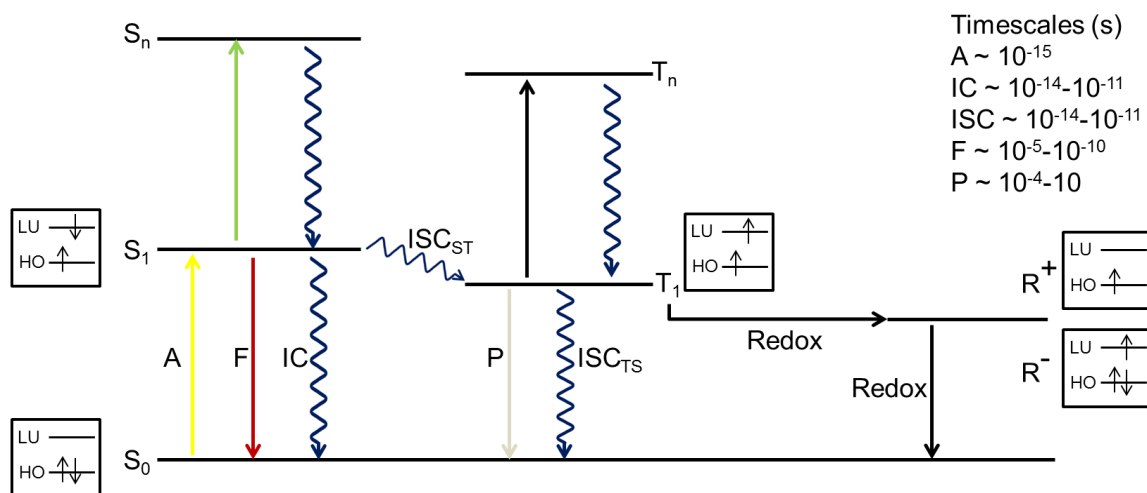
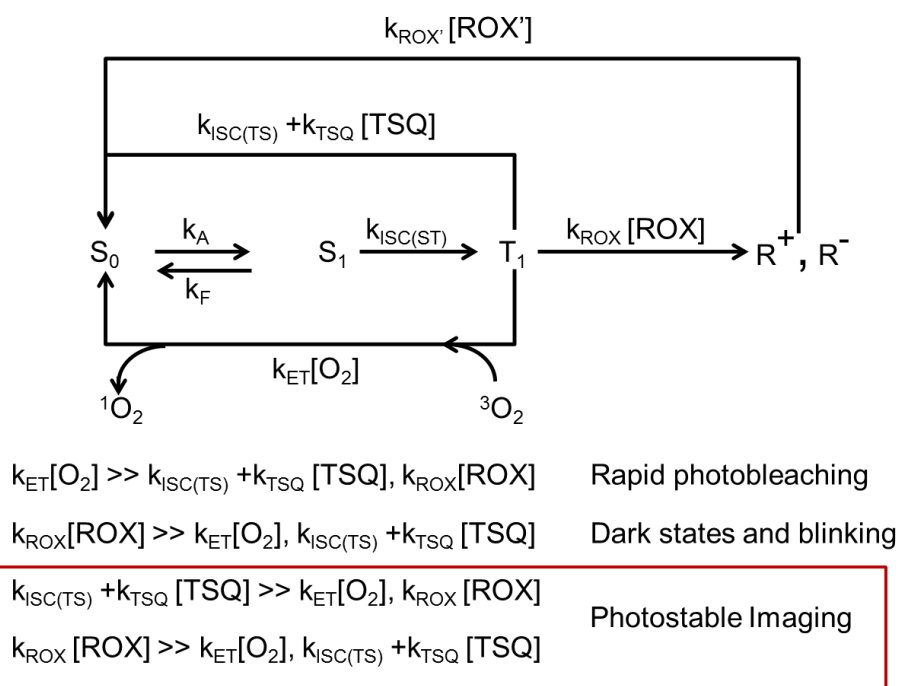


Figure 1. Jablonski diagram for electron absorption and deactivation pathways and the lifetimes of different processes. S_0 : The ground state of the fluorophore, S_1 : first singlet excited state, T_1 : First triplet excited state, R^+ and R^- : Cationic and anionic radical states respectively, S_n and T_n : Higher energy singlet and triplet excited states respectively, A: Photon absorption, F: Fluorescence, IC: Internal conversion, P: Phosphorescence, ISC: Intersystem crossing from S_1 to T_1 (ST) and T_1 to S_0 (TS) respectively, Redox: reduction or oxidation, LU: Lowest unoccupied molecular orbital, HO: Highest occupied molecular orbital. Arrows in the boxes represent electronic spins.

In an ideal system, only two states S_0 and S_1 contribute to fluorescence or internal conversion. In a real system however, the fluorophore can go from S_1 to T_1 through an intersystem crossing. This event has a very low quantum yield for typical organic fluorophores (<0.01).⁸⁻¹⁰ However, the triplet state has a high energy and a long lifetime of the order of 10^{-6} to 10^{-4} s.¹⁰⁻¹² This makes the T_1 state reactive and a determinant of the fate of the fluorophore. T_1 has been implicated in blinking as well as redox reactions with molecular oxygen, impurities in the system and biomolecules in the vicinity.¹³ The role of molecular oxygen, and its ground triplet state, which is present at a concentration

of 300 μM in aqueous solutions at ambient pressure, becomes very important from the point of view of the reactive triplet state of the dye.¹⁴ The T_1 state can form a non-fluorescent cationic state by reacting with molecular oxygen, also producing a superoxide radical anion ($\text{O}_2^{\cdot-}$) in the process. The other pathway that leads to photobleaching is the triplet-annihilation mediated formation of singlet oxygen ($^1\text{O}_2$) that is a stronger oxidizing agent than ground state molecular oxygen. The various reactive oxygen species (ROS) that can be produced downstream of these processes may include $\text{HO}\cdot$, $\text{HO}_2\cdot$ and H_2O_2 and these may also react with a ground state molecule and oxidize it.^{15, 16} Additionally, in a biological system, these ROS can also react with biomolecules and cause photo-toxicity.^{17, 18} Scheme 1 describes the various pathways that can lead to fluorophore instability under excitation as well as kinetic considerations for these pathways.



Scheme 1. A kinetic platform for understanding fluorophore behavior. TSQ: Triplet state Quencher, ROX: Reducing agent, ROX': Oxidizing agent. The diagram was developed using the mechanistic discussion outlined in references 12, 24 and 48.

While oxygen has a critical role in the bleaching of organic dyes, the photobleaching of genetically encoded fluorescent proteins (FP) is generally independent of the oxygen concentrations. FPs have the chromophore embedded inside their β -barrel.¹⁹ This gives rise to a plethora of interesting properties such as a solvation mediated dynamic stokes shift, a quadratic stark effect and a chromophore involving an excited state proton transfer.²⁰⁻²² It is the photon budget (photons emitted before photobleaching) where FPs remain up to a 100 fold shy compared to organic dye molecules.^{23, 24} FPs undergo dark state conversion through two different mechanisms.²⁵⁻²⁷ The protonation of the p-hydroxybenzylidene is a pH dependent pathway that gives rise to dark states.^{28, 29} In another pH independent pathway an environmental change or conformational change of the chromophore drives the FP to a dark state.^{26, 30, 31} Unlike organic fluorophores, FPs are unaffected by oxygen in their bleaching rates. This is attributed to the protection of the chromophore by the β -barrel.³² As we will discuss later, the same protection against oxygen is observed in fluorogen activating peptides where the chromophore is embedded inside the protein binding pocket.³³

Our understanding of photobleaching mechanisms has led to the development of methods to prevent photobleaching during fluorescence microscopy. For organic fluorophores, oxygen and the fluorophore triplet state have been primarily implicated in photobleaching. While molecular oxygen is primarily responsible for photo-oxidation and photobleaching, it is also responsible for triplet state quenching.³⁴ Therefore, an obvious preventive measure against photobleaching was the addition of oxygen scavengers supplemented with alternative triplet state quenchers (TSQ) to the imaging buffer. Enzymatic oxygen scavenging system (OSS), glucose oxidase and catalase converts glucose and O₂ to gluconic acid and water in a two-step reaction that results in a net loss of 1 equivalent of O₂ from the system.³⁵⁻³⁷ Another popular OSS is the protocatechuic

acid and protocatechuate-3,4-dioxygenase.³⁸ These systems have been used in combination with TSQs such as Trolox, β -mercaptoethanol (BME), 1,3,5,7-cyclooctatetraene (COT) and 4-nitrobenzylalcohol (NBA), whose structures are shown in Figure 2.^{11, 39-41} Most of these TSQs were believed to act through a collisional mechanism and there have not been detailed studies on their precise mechanism. However, the mechanism of action of Trolox has been investigated in detail and it has been concluded that Trolox quenches the triplet state through electron transfer and leads to anti-blinking through a redox mechanism that involves its quinoid derivative.⁴² Despite the lack of mechanistic knowledge on some of the TSQs, they have been immensely useful and have been employed in a majority of single molecule measurements in the last decade.^{43, 44}

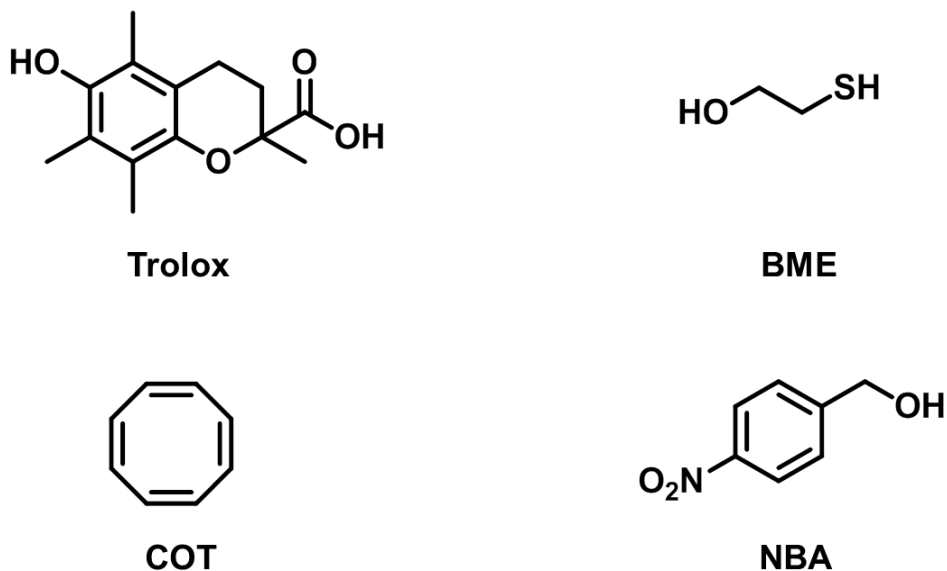


Figure 2. Chemical structures of common triplet state quenchers used in single molecule imaging as well as in self-healing fluorophores.

While several efforts have been made in engineering dye molecules to improve their optical properties, aqueous solubility and biosensing abilities, not much work had been done until a couple of years ago to extend dye engineering for improved photostability. Working forward from solution based demonstrations of the effect of TSQs on organic dye photostability, the Blanchard lab developed cyanine dyes conjugated with TSQs such as NBA, Trolox and COT.^{12, 45, 46} This approach showed remarkable enhancements in photostability, even compared to a solution based approach with TSQs present at near saturating concentrations of 1mM. The approach was extended to all available cyanine fluorophores and the photostabilizing effect was consistent throughout the series. It was also observed that COT conjugated fluorophores showed the highest increase in performance from a photon output perspective. This enhancement was a function of the distance between COT and the fluorophore and established a collision dependent mechanism for COT, resulting in up to a 68 fold decrease in the triplet state lifetimes for the optimum linker.¹² Additionally, it was confirmed that NBA and Trolox operated through a charge transfer mechanism to enhance photostability. This self-healing fluorophore theory is still very recent and has been criticized to some extent by Tinnefeld and Cordes for the lack of generality as well as the speculation that the mechanism should work on all dye classes.⁴⁷ Despite the criticism, the approach lays a solid foundation for chemical engineering of dyes for enhanced photostability and its potential in improving other dye families such as rhodamines remains to be seen.

Molecular encapsulation is another approach that has been shown to render encapsulated dye molecules more photostable. Since the first reported encapsulation of azo dyes in cyclodextrins in 1967, several other compounds such as rotaxanes, polymeric dendrimers and inorganic matrices have been used for molecular encapsulation.^{48, 49} These approaches are not very popular with dyes used for biological

imaging mostly due to solubility issues. However, the discovery of the green fluorescent protein and its crystal structure showed that nature had utilized molecular encapsulation for millennia. The chromophore in fluorescent proteins is covalently attached to the β -barrel and is embedded inside it. While this encapsulation imparts significant protection to these chromophores, they do undergo bleaching. Due to the covalent bonding, these chromophores cannot be replaced by un-bleached chromophores in biological systems. To this end, having a non-covalent interaction may be very useful from a photochemical standpoint. As pointed out in the previous chapter, fluorogen activating peptides bind the fluorogen in a non-covalent fashion. Therefore, while encapsulation of the fluorogen can impart photostability, an exchange mechanism cannot be ruled out. This chapter discusses the mechanisms behind the photostability of some of these peptides. It also outlines some of the methods targeted towards the discovery of scFvs with varying kinetic and equilibrium properties through flow cytometry, with the aim of obtaining scFvs with a higher photon output. Additionally, the role of molecular oxygen as well as the triplet states will be examined for fluorogen activating peptides with slow off rates.

Results

Proposed Mechanism for the kinetic dependence of photostability

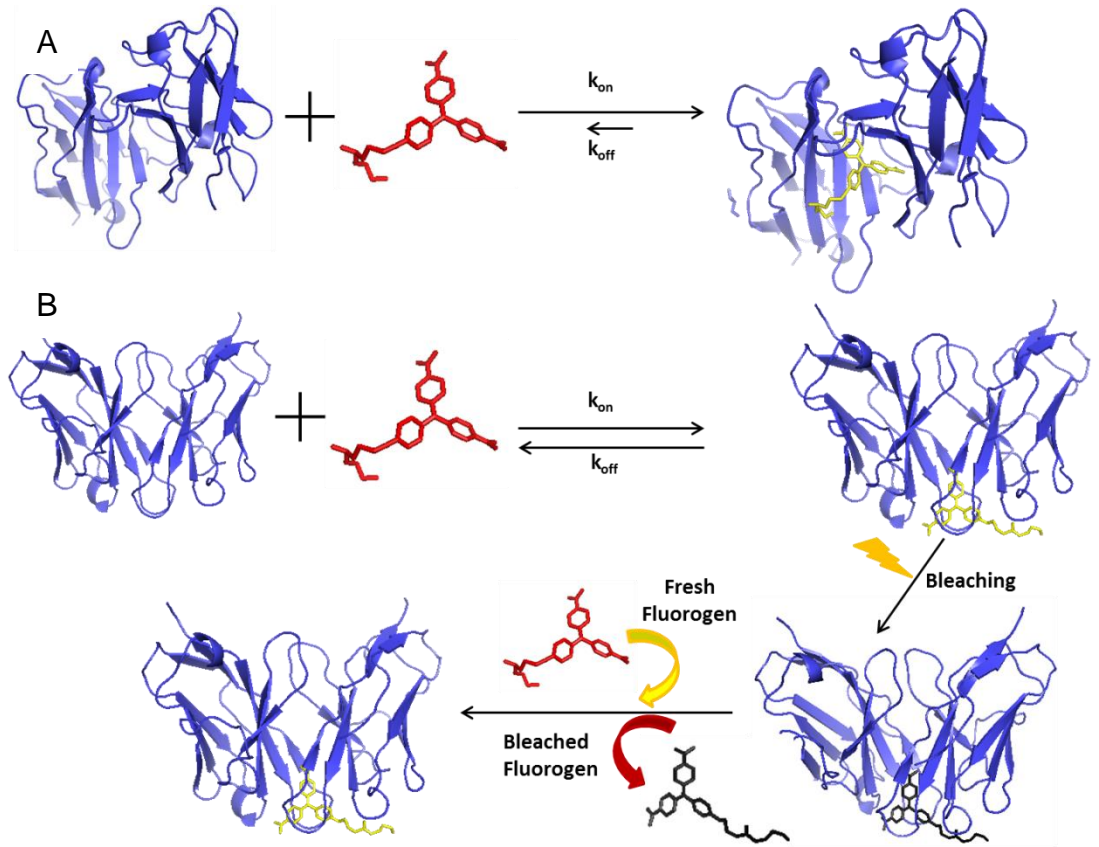


Figure 3. Mechanistic platform to understand the enhanced photostability of fluorogen activating peptides. A. For complexes exhibiting slow off rates, the fluorogen is encapsulated by the protein and is thus protected from ROS that gives rise to photostability enhancement. B. Complexes that exhibit fast off rates can exchange the fluorogen rapidly before or after bleaching and can display enhanced photostability in the presence of excess fluorogen.

As pointed out earlier, fluorogen activating peptides (FAP) bind non-covalently to the fluorogen. This gives rise to an interesting hypothesis that outlines two possible pathways behind enhanced photostability. The first mechanism is molecular encapsulation, whereby a complex that has a very slow off-rate, once formed

photobleaches before dissociation. Classic examples of this mechanism are the FAPs, dL5 and HL4-NP149 (Table 1). These complexes dissociate on the order of hours whereas their photobleaching occurs on the order of tens of seconds under typical single molecule excitation conditions. These slow off-rate FAPs are similar to fluorescent proteins in that once bleached, they are rendered useless. Another mechanism that can be responsible for imparting high photostability to these complexes is fluorogen exchange. FAP-fluorogen complexes that dissociate on the order of photobleaching timescales can be very powerful tools in live cell imaging. This is primarily because the unbound fluorogen is practically dark and on binding shows a fluorescence enhancement of four orders of magnitude. This implies that in the presence of excess fluorogen, for FAPs that exchange, we can achieve high photostability with minimal background. In the remaining part of this chapter we will discuss experimental results that shed some light on these two mechanisms behind enhanced photostability.

FAP	Fluorogen	MW (kDa)	$\lambda_{Ex}:\lambda_{Em}$ (nm)	ϕ_F	K_d (nM)	k_{off} (s^{-1})
dL5	MG	28	640:667	0.20	0.018	>6E-5
HL4NP149	MG	26	629:649	0.16	500	2E-4
ScFv1	TO1	26	510:527	0.47	300	1E-1
dL9.3x	MG	25	630:667	0.04	70	1E-2

Table 1. Physical, spectroscopic, kinetic and equilibrium properties of Fluorogen activating peptides discussed in this chapter.

Photostability enhancement through encapsulation

Before testing the encapsulation or exchange hypothesis with dL5-MG complex, we assessed the enhancement in stability that the fluorogen achieved upon binding dL5. For this, we performed a chemical bleaching experiment where 500nM MG-2PEG (MG-2p) was exposed to 0.1 M H_2O_2 and absorbance was monitored over time. An absorbance measurement was needed in this case (instead of fluorescence) since MG-2p does not exhibit fluorescence in the absence of dL5. Figure 4 shows a rapid bleaching of MG-2p in the presence of 0.1 M H_2O_2 , but we saw negligible (<2%) bleaching with a pre-complexed solution of dL5-MG-2p (2 μ M : 500 nM). To ensure that this protection is complex-specific, we compared the protection of another scFv, AM2-2 that does not bind MG-2p, confirming that chemical bleaching is not prevented by free protein.

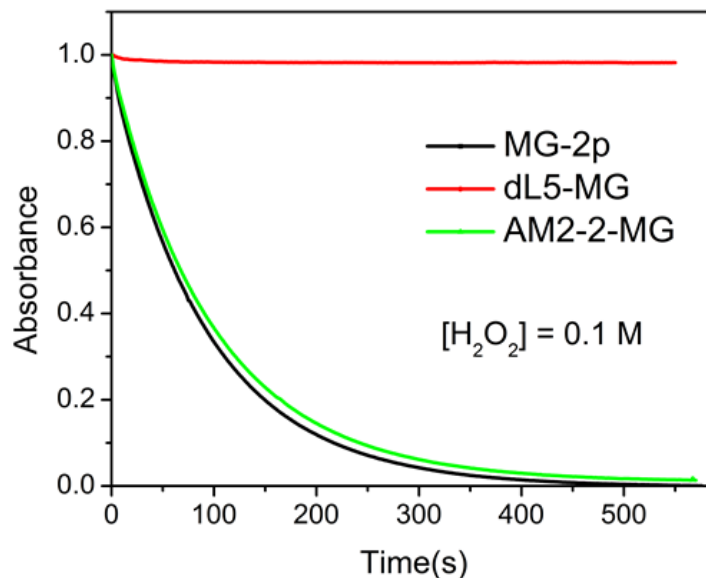


Figure 4. Bleaching experiments performed by measuring absorbance in the presence of 0.1 M H_2O_2 . We observe that dL5 protects the fluorogen from H_2O_2 through molecular encapsulation, whereas the fluorogen bleaches rapidly in the same environment when it is present without dL5 or with a non-cognate scFv such as AM2-2.

This experiment proves that dL5 has a protective effect on MG-2p through encapsulation. Additionally, the protective effect imparts the complex excellent stability against oxidation in extremely harsh oxidative environments even up to 0.1 M H₂O₂. The concentration of H₂O₂ in the human body is on the order of tens of micromolar. Therefore, the dL5-MG complex can provide for highly photostable imaging *in vivo*.

Once molecular encapsulation was established for the dL5-MG complex, we measured the photostability of the complex against a known standard that was spectrally similar to the complex. The cyanine dye, Cy5, has an excitation maximum at 650 nm and it emits at 670 nm. These spectral features made possible the photobleaching comparison of dL5-MG with Cy5. The dL5-MG complex was bleached under a 639 nm laser excitation in limiting concentrations of MG. We found that Cy5 photobleaches completely in 60 minutes under the excitation, while the dL5-MG complex only bleaches by 10% in the same time. Further, to investigate if this photostability was a result of exchange of the fluorogen, the photobleaching experiment was performed such that there was excess MG in the system. Even in this case, we obtained the same bleaching curve as we did in the presence of limiting MG concentration. These results are shown in Figure 5. This proves that the complex does not exchange the fluorogen significantly with the time scales used for photobleaching. This is indeed true as seen from the off-rate measurements performed using the dL5-MG complex. The off-rate for the complex is $6 \times 10^{-5} \text{ s}^{-1}$ which is much longer than photobleaching time scales. A common misconception of non-covalent complexes is that lower affinities give rise to faster off rates. We found that this is not always the case. For this, we used another FAP, HL4-NP149 that has a K_d of $\sim 500 \text{ nM}$. While this complex showed enhanced photostability as well, the off rate for the complex is of the order of $2 \times 10^{-4} \text{ s}^{-1}$. Therefore, we established

through this series of experiments that it is the kinetics and not the equilibrium, which decides the photon budget for these FAPs.

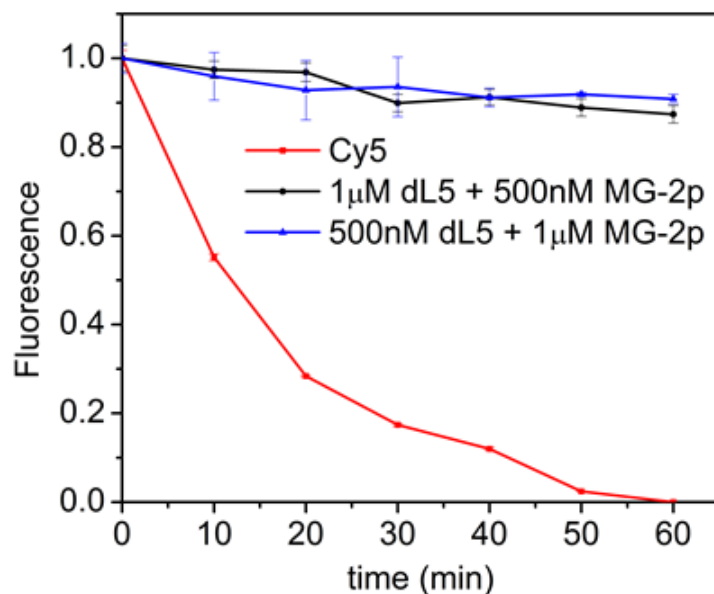


Figure 5. Ensemble photobleaching of purified dL5-MG complex and a comparison with Cy5. The dL5-MG complex only bleaches by 10% in the same time that Cy5 bleaches completely under the excitation conditions used in the experiment. Additionally, excess fluorogen does not have any impact on the photostability of the complex. This proves that the complex is unable to exchange the fluorogen in solution on the time scales of photobleaching in this experiment.

We also performed single molecule experiments to compare the photostability of the dL5-MG complex against Cy5. For this, a biotinylated version of dL5 was used and the complex was captured on a streptavidin surface. Total internal reflection fluorescence microscopy was performed on these samples to measure the photoelectrons detected before photobleaching from the complex. The histograms generated from the experiment are shown in Figure 6A. From these measurements we can say that the dL5-MG complex emits ~2.5 times more photons before photobleaching. This is in agreement with the ensemble data as well as the molecular

brightness of Cy5 and dL5-MG complex. Additionally, from the time traces of the dL5-MG complex we could see that the complex showed single step bleaching even in the presence of excess fluorogen as shown in Figure 6B.

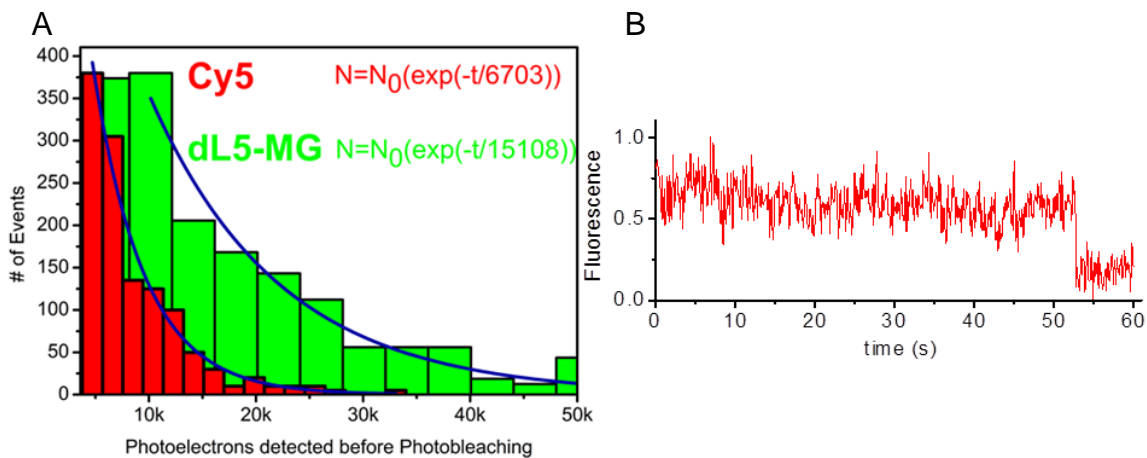


Figure 6. A. Comparison of dL5-MG complex with Cy5 at a single molecule level. The dL5-MG complex emits about twice as many photons compared to Cy5 at a single molecule level. B. Even in the presence of excess MG-2p, we find a single step photobleaching behavior as shown by a typical single molecule time trace for dL5-MG on the right.

Finally, we tested if the *in vitro* results were consistent with results on the cell surface. For this, we performed bleaching experiments under an epi-fluorescence microscopy setup on JAR200 cells expressing dL5 on the cell surface. We found negligible bleaching of the complex under the excitation conditions used, which are typical for epi-fluorescence microscopy. Further, the bleaching behavior of the complex was insensitive to the concentrations of MG in the imaging media as shown in Figures 7A and B. This proves that the complex is photostable through encapsulation and not exchange, even on the cell surface.

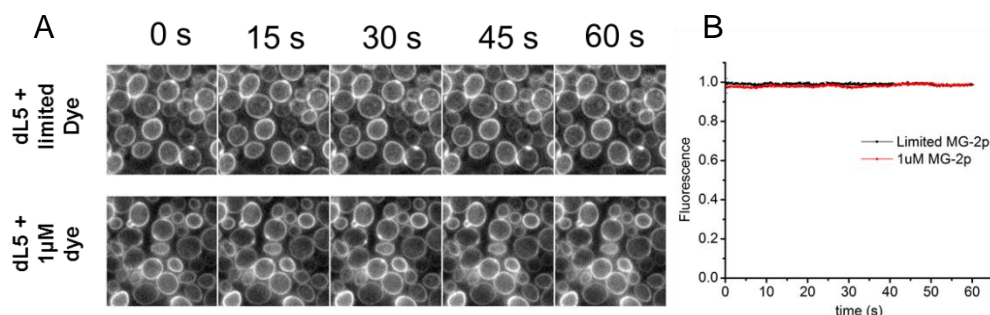


Fig 7. A. Photobleaching measurements performed with the dL5-MG complex on the surface of JAR200 cells expressing the FAP and, B. corresponding bleaching curves. We see that the complex shows negligible bleaching under standard epi-fluorescence microscopy excitation flux. Additionally, there is no difference in the bleaching behavior in the presence of excess fluorogen. This proves that dL5 enhances the photostability of MG through encapsulation and not exchange.

The role of molecular oxygen and the triplet state

As outlined in the introduction to this chapter, molecular oxygen and triplet states of fluorophores are two important factors that contribute to photobleaching. In order to understand the role of these two species we performed photobleaching experiments in the presence of oxygen scavengers and triplet quenchers at a single molecule level with dL5-MG and HL4-NP149-MG complexes. We used the well characterized dye Cy5 for a direct comparison with the FAP-MG complexes. The use of glucose oxidase-catalase (GOD-CAT) system enhances the photostability of the FAP-MG system to the highest extent (Figure 8). While Trolox also enhances the photostability of the complexes compared to the system without any additives, the enhancement is not as high as in the case of GOD-CAT system. An interesting observation was that the photostability of these complexes as well as that of Cy5 go down if a combination of Trolox and GOD-CAT is used, relative to GOD-CAT alone. This suggests that at the concentrations of GOD-CAT and Trolox that we used (see methods), $^1\text{O}_2$ plays a major role in the

photobleaching of the fluorophores. When we use an oxygen scavenger, we eliminate the T_1 to S_0 process that generates 1O_2 , thereby preventing photobleaching. At the same time, oxidation products that may be formed by reaction with oxidizing species can go back to state S_0 from R^+ to give fluorescent molecules back in the ground state. Trolox quenches the triplet state through collisions, and since the MG is protected in the FAP binding pocket, its effect is not as pronounced as GOD-CAT.

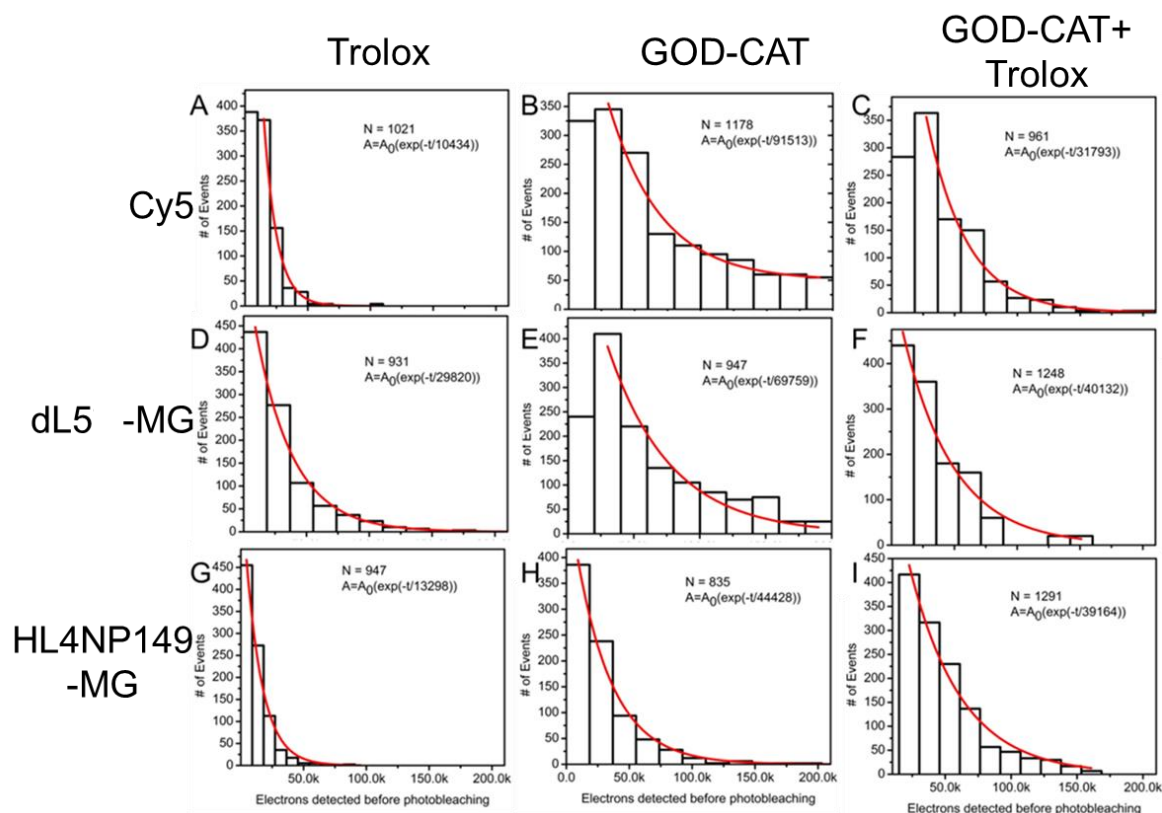


Figure 8. Histograms of photoelectrons detected before photobleaching for single Cy5 and FAP-MG molecules imaged using a TIRF setup in the presence of stabilizing additives such as Trolox and GOD-CAT system. At the concentrations of Trolox and GOD-CAT used and the excitation flux that we have, oxygen scavengers enhance the photostability of the fluorophores more than triplet state quenchers.

Additionally, for each case we see a higher photostability enhancement for the FAP-MG complex with a higher binding affinity. This possibly indicates that the tighter the fluorogen is bound to the FAP, the more is the protection through molecular encapsulation.

Photostability enhancement through exchange

From the first screen to isolate FAPs that bind to TO1 a clone scFv1 was discovered that showed some signs of exchange of the fluorogen. Therefore, this was the first scFv that we considered for testing the mechanisms of exchange. Additionally, a FAP K7 was reported to be photostable by the exchange of the fluorogen Dimethylindole red (DIR) and the mechanisms for the complex stability were carried out carefully and reported.⁵⁰ We used a 488 nm laser line to irradiate purified scFv1 complexed with TO1-2p (1:1 complex). Within 20 mins of irradiation, the complex lost about 90% of fluorescence. On the addition of 0.86 equivalents of TO1-2p to the cuvette, the fluorescence signal came back to 85% showing that the FAP was able to bind the fresh fluorogen that was provided. The signal never went to the initial level even on adding more fluorogen indicating that there was some irreversible damage to the protein. The emission spectra from this experiment are shown in Figure 9.

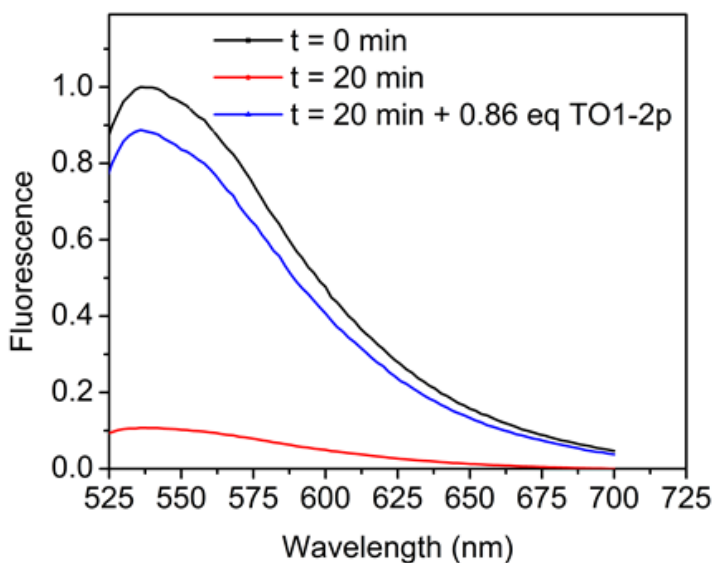


Figure 9. Emission spectrum of scFv1-TO1 complex during ensemble photobleaching using a 488 nm laser source for excitation. The sample bleaches by 90% in 20 mins. On addition of 0.86eq of TO1-2p the signal is regained that proves exchange by the FAP.

Additionally, we performed photobleaching of the complex in two cases, one where the protein was in excess and the other where the fluorogen was in excess. While the sample with limiting fluorogen bleaches completely in about 20 mins of irradiation, the sample with excess fluorogen only lost 30% of its initial fluorescence signal as seen in Figure 10. These results further tie up the hypothesis that scFv1 maintains its photostability through exchange. This is also useful because scFv1-TO1-2p- is a very photo-unstable fluoromodule and having a way to perform long time scale measurements at 488 nm excitation is very useful.

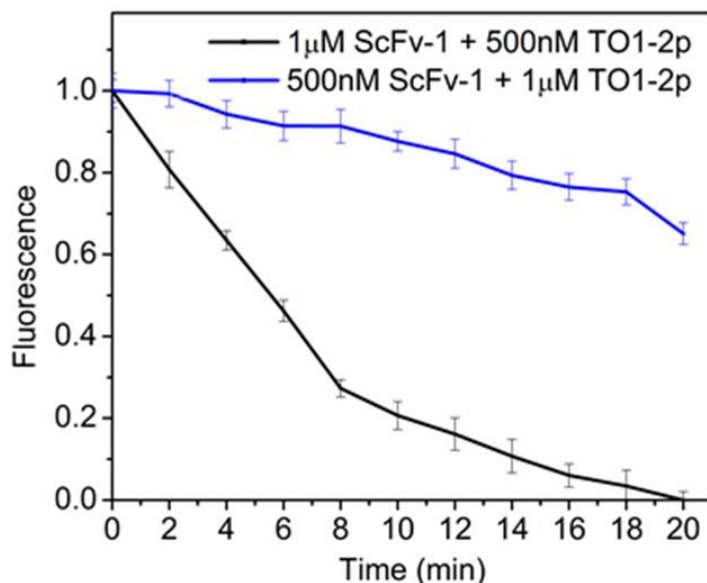


Figure 10. Photobleaching curves for scFv1-TO1-2p complexes in the presence of limiting and excess amounts of the fluorogen. We can see that the complex only bleaches to 70% in the presence of 1 μM fluorogen whereas there is complete bleaching when there is limiting amount of the fluorogen, thus establishing exchange by the FAP.

We purified a biotinylated scFv1 protein and performed single molecule measurements with it in the presence of limiting and excess amounts of TO1-2p. The histograms in Figure 11A indicate that there is a three-fold enhancement in the

photoelectrons detected before photobleaching in the presence of excess fluorogen. Further time traces of a single scFV-1-TO1-2p complex showed multiple on-off cycles in the presence of excess fluorogen, as seen in Figure 11B. With this established, we have mechanistically proven FAPs that exchange and thus show enhanced photostability. Combined with the K7-DIR complex, this gives us two colors to perform highly photostable imaging where the signal can be regenerated just by the addition of fresh fluorogen in the system.

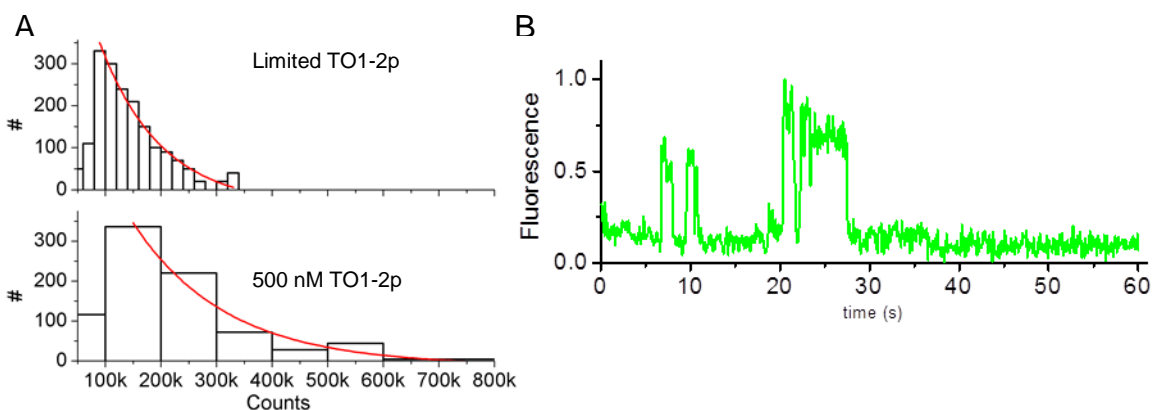


Figure 11. A. Histograms showing the number of photoelectrons detected after photobleaching for scFv1-TO1-2p complex under single molecule imaging. In the presence of excess fluorogen the complex is about twice as photostable compared to the limiting fluorogen case. B. Additionally, in the presence of excess fluorogen, we see a time trace consisting of several on and off cycles before photobleaching.

Finally, in order to establish that exchange properties were not affected on the cell surface, we performed photobleaching experiments in the presence and absence of excess TO1-2p. We can see from Figures 12A and B that there is a concentration dependent photostability enhancement of the complex on the yeast cell surface. Also noticeable is the negligible background that we get in the presence of even 5 μ M TO1-2p. These results, combined with the in vitro results prove that the scFv-1 FAP

exchanges TO1-2p rapidly and can be used for long time scale imaging experiments in the presence of excess fluorogen.

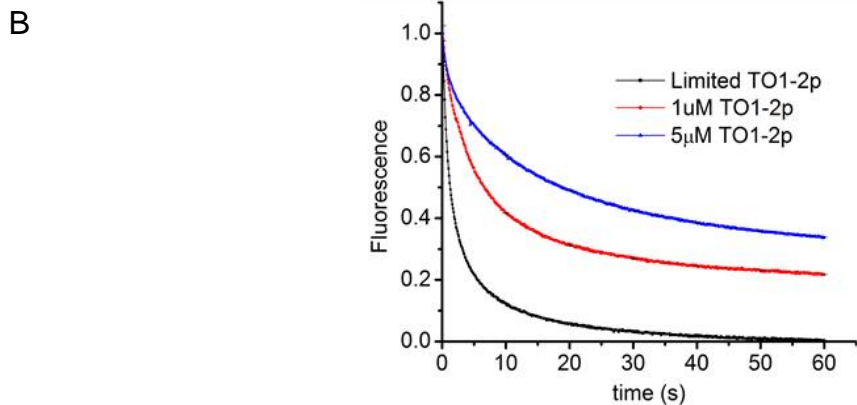
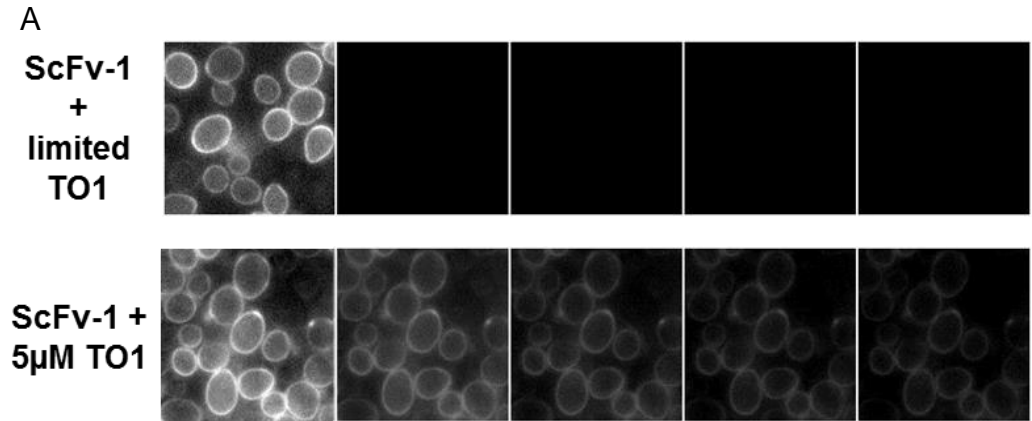


Figure 12.A. Photobleaching experiments on JAR200 cell surface expressing scFv1. We see that in the presence of excess fluorogen, there is enhanced photostability exhibited by the complex. B. Also shown are the photobleaching curves at different concentrations of the fluorogen on the yeast cell surface.

Exchangers by rational design and screening

While the two reported FAPs that exhibit exchange were isolated purely by serendipity, we continued to ask if it was possible to rationally design a FAP that could exchange. From known structures of dL5 FAP, we could tell that a deeply buried

fluorogen in the protein binding pocket is expected to have a slow dissociation rate. Therefore, it is likely that a complex where the fluorogen is bound more superficially can dissociate faster. This was the rationale behind selecting an L9 based library for screening for exchangers. A preliminary (unpublished: Stanfield and Wilson) x-ray crystal structure indicates that the complex of L9 with cognate fluorogen (MG) is relatively exposed near the surface of the protein, and thus offers a reasonable candidate for mutagenesis and screening efforts to isolate exchanging FAP/fluorogen pairs. A library of approximately 10^7 colony forming units was constructed from dL9.5 (now Mars1Cy) via random mutagenesis as described by Chao and colleagues.⁵¹ Screening was performed by flow cytometry with selection for exchange of MG for MG-Cy7 (as monitored by far-red and NIR emission filters). Briefly, FAP-expressing cells were labeled by excess MG-2p, rapidly washed (wash time of 120 seconds), and re-labeled by MG-Cy7. Cells that exhibited high Cy7 emission were collected. Mutations from the most promising clones were grafted into dL9.5 to create dL9.5X, a symmetric light chain dimer that hosts the sum of mutations from three clones (T17A, K49E, V97G; identical mutations in the second monomer). Off-rate measurements of dL9.5X revealed that fluorogen could be exchanged on the order of minutes. However, the brightness of the fluoromodule was significantly lower than the parent dL9.5 complex (See materials and methods).

Previous work had isolated a clone designated dL9.3 (H96Y, relative to dL9.5). Since this amino acid variation occurs adjacent to the V97G mutation isolated from exchanger screens, those mutations (T17A, K49E, V97G) were propagated into dL9.3 in order to explore whether a tyrosine at position 96 on each monomer could improve the brightness of the resulting clone (dL9.3X) while retaining the ability to exchange fluorogen (See materials and methods). This indeed turned out to be the case and

dL9.3X was able to exchange MG-2p on the order of 90 seconds in ensemble measurements.

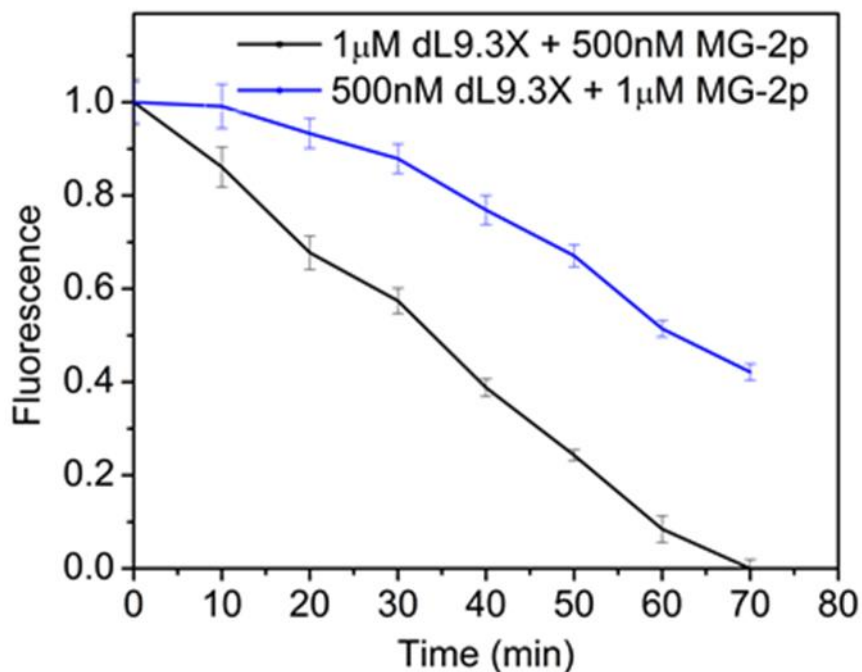


Figure 13. Photobleaching curves for dL9.3X-MG-2p complexes in the presence of limiting and excess amounts of the fluorogen. We can see that the complex only bleaches to 40% in the presence of 1uM fluorogen whereas there is complete bleaching when there is limiting amount of the fluorogen, thus establishing exchange by the FAP.

Ensemble experiments could be performed with this FAP and we could show exchange through the same experiments that were used for scFv-1, as shown in Figure 13. However, single molecule experiments posed a challenge for this clone. The brightness of the clone was still poor (20% of that of dL5-MG). We were able to perform single molecule measurements with this complex by condensing the laser excitation to a central spot on the image plane by using a 0.5x de-magnifying lens. The photoelectrons detected before photobleaching show a 2.3 fold enhancement in the presence of excess MG-2p as shown in Figure 14A. Also, single molecule traces of the complex in the

presence of excess MG-2p show multiple on and off cycles that point towards exchange as shown in Figure 14B. With the addition of dL9.3X to our K7 and scFv-1 exchanging FAPs, we have the potential to perform three-color imaging using fluorogen exchange as a means to enhance photostability and enable long time scale imaging.

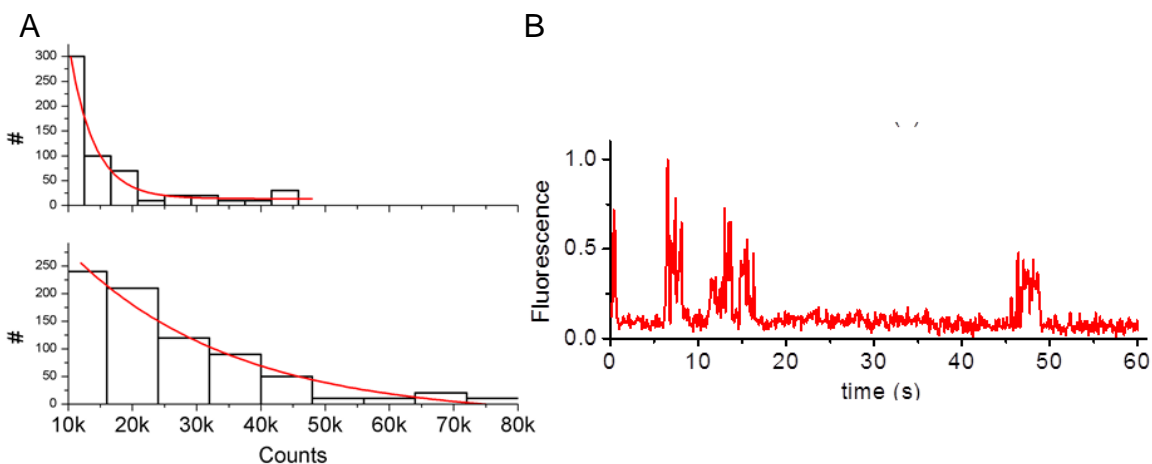


Figure 14. A. Histograms showing the number of photoelectrons detected after photobleaching for dL9.3X-MG-2p complex under single molecule imaging. In the presence of excess fluorogen the complex is about twice as photostable compared to the limiting fluorogen case. B. Additionally, in the presence of excess fluorogen, we see a time trace consisting of several on and off cycles before photobleaching.

Finally, we performed imaging of dL9.3X on the surface of JAR200 yeast cells. Again we can see the challenge in imaging dL9.3X due to its low quantum yield as shown in Figure 15A. As soon as we wash MG-2p from the cells, we can barely see the signal from the FAP. However, in the presence of 1 μ M MG-2p and greater, we see a remarkable photostability over the time scale of imaging. This FAP, in fact turns out to be a better FAP than the naturally selected FAP scFV-1 in that lower concentrations of MG-

2p are needed to impart exceptional photostability as can be seen from the bleaching curves in Figure 15B.

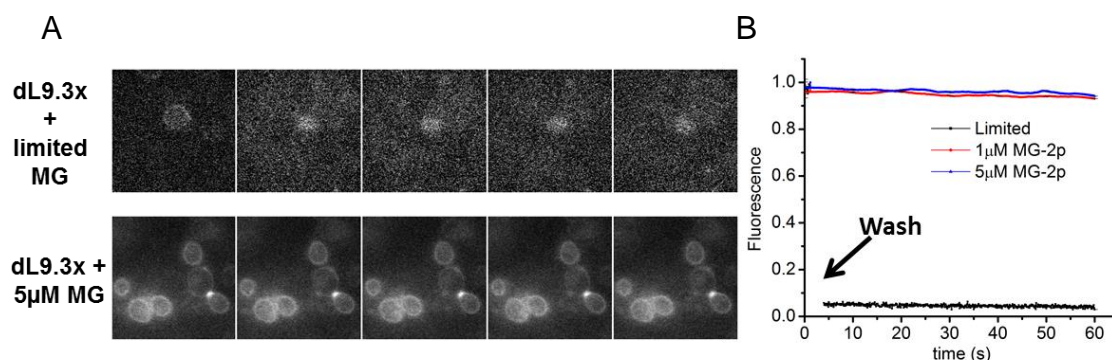


Figure 15. A. Photobleaching experiments on JAR200 cell surface expressing dL9.3X. We see that in the presence of excess fluorogen, there is enhanced photostability exhibited by the complex. B. Also shown are the photobleaching curves at different concentrations of the fluorogen on the yeast cell surface. Note that on the cell surface we do not see much signal after the dye is washed due to the low quantum yield of the complex.

New directions to screen for exchangers using flow cytometry

The isolation of dL9.5X using MG-Cy7 as a chasing reagent gave us the idea of a systematic method for isolating FAPs with fast off rates. Through rigorous trials, we were able to optimize two different methods to screen for fast exchangers, namely BleachSort and ChaseSort as shown in Figure 16.

In the Bleachsort method, we designed a home-built LED based illumination system that could bleach Cy5 on the yeast cell surface in less than 30 seconds. We took a library of JAR200 cells that was known to bind to MG-2p and after incubating the cells with the fluorogen and washing it off, we exposed the library (in solution tubes) to the LED illumination for 5-10 mins. These cells were analyzed through FACS and gave us the control scatter plot for the sample. 1 µM MG-2p was added to a second tube that was bleached using the same protocol and cells were sorted based on the gates that

were drawn for the control cells. Cells showing higher signal than the control population were collected from this sort.

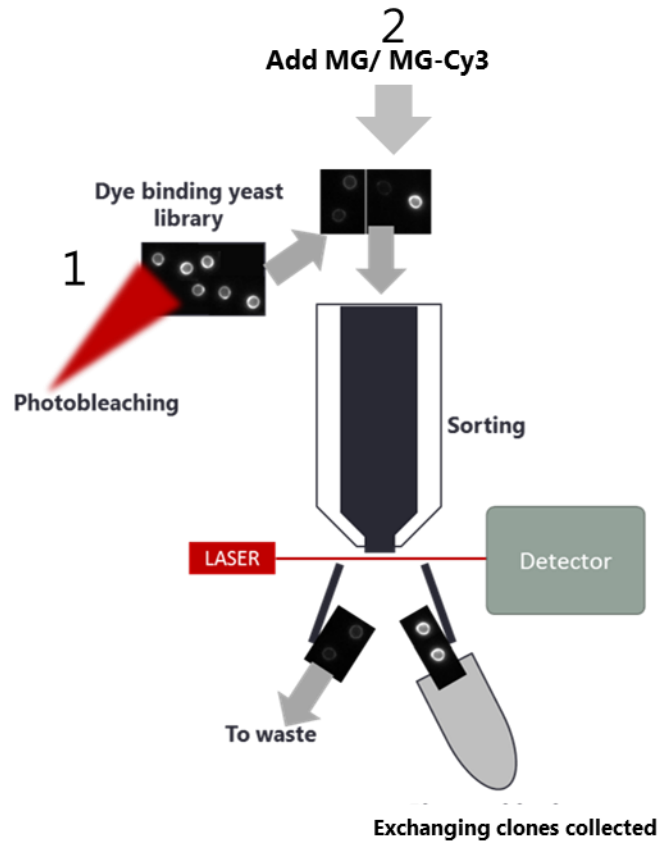


Figure 16. Schematic illustrating the BleachSort and the ChaseSort methods for screening for exchangers. In the BleachSort technique (1), the dye binding library is photobleached and quickly incubated with MG and sorted. For the ChaseSort method, no bleaching is performed and MG-Cy3 is added in excess amounts to the library and FRET signal is monitored.

The ChaseSort system built upon the initial screening of dL9.5X using MG-Cy7. In this case, we used another tandem dye, MG-Cy3. Once bound to a FAP, the donor fluorescence is quenched and energy is transferred from the donor to the acceptor. Therefore, in this experiment we incubated the cells with MG-2p followed by the addition of 2 μ M of MG-Cy3 just before sorting. The excitation was at 532 nm (Cy3 excitation)

whereas we looked for emission in the 685/70 channel for MG. Using a combination of these techniques, we were able to isolate over a hundred clones. Off rate measurements were performed on these clones expressed on a yeast cell surface in a 96 well format. The 20 best clones are shown in Figure 17.

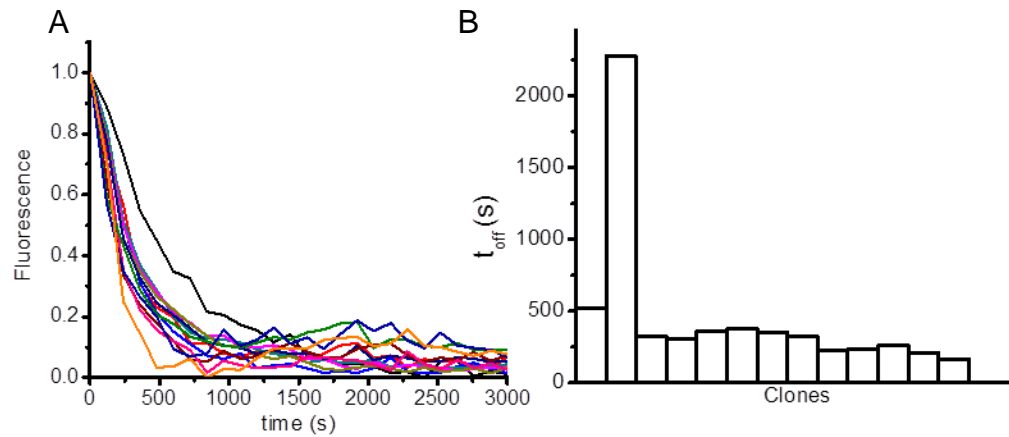


Fig 17. A. Off rate curves on the yeast cell surface for the clones that were isolated using BleachSort and ChaseSort methods. B. Also shown is a distribution of dissociation times ($t_{1/2}$ of dissociation) for the selected clones. We can see that using both the methods, we were able to obtain clones that exhibit an off time of the order of 100s.

Discussion

An overarching desire to improve the photon budget of genetically encoded fluorescent labels has fueled the discovery of highly photostable probes through chemical modifications. We have furthered this quest through the use of biochemical and flow cytometry tools to obtain fluorogen activating peptides with enhanced photostability. We have exploited the non-covalent binding between the protein and the fluorogen to isolate complexes that undergo exchange of the fluorogen. This makes the technology platform a very powerful one, since the fluorogen is dark when it is not bound to the peptide. We are now at a point where we have well characterized, highly photostable FAPs that work on the exchange mechanism and are available in multiple colors to enable simultaneous labeling of up to three targets on the cell surface and possibly in the cytoplasm.

Future directions for working with these FAPs involve superresolution microscopy techniques that utilize the stochastic blinking of probes to achieve nanometer resolution. Additionally, an elegant experiment in this direction could be the simultaneous detection of two or more proteins, such as actin and myosin beyond the diffraction limit. These exchanging FAPs can be exploited for chase measurements *in vivo* and *in vitro*, using a tandem dye pair containing one of the exchangeable fluorogens. This also extends the useable palette of colors at our disposal. One area of improvement for the MG exchanging FAP, the amino acids of the dL9.3x can be further mutagenized in the protein binding pocket to improve the quantum yield. This problem can also be attacked from a synthetic chemistry point of view where the addition of electron withdrawing groups to the chromophore can give rise to a shift in the emission spectrum and/ or enhanced molecular brightness. Finally, there is room for improvement towards the automation of the BleachSort and ChaseSort methods to enable faster dye addition followed by detection to obtain even faster exchange kinetics.

Materials and methods

Protein purification

Expression of recombinant proteins was carried out in the *E.coli* strain Rosetta-gami 2 (DE3) (Novagen). The plasmids were transformed into competent cells and fresh colonies were grown in 5ml overnights with 12.5 µg/mL tetracycline, 34 µg/mL chloramphenicol, and 50 µg /mL ampicillin. The 5mL cultures were then added to 500mls LB+GB (10g/L tryptone, 5g/L yeast extract, 4g/L NaCl with 100mM phosphate pH 7.2 and supplemented with 20mM succinic acid, 0.4% glycerol) to an OD of 0.8 at 37°C, the temperature was dropped to 22°C for 1 hour and then cultures were induced with 500µM IPTG and supplemented with 0.4% glucose for 18h growth at 22°C. Cells were pelleted and washed once with cold PBS before freezing at -20°C. The pellets were resuspended in 3mL of wash buffer A (50mM Tris-Cl pH 7.5, 750mM NaCl, 0.1% Triton X-100, 0.02% Tween-20, 50 mM imidazole) and sonicated with 10x15sec pulses prior to dilution with 15mL of wash buffer A. This lysate was centrifuged 30 min at 20,000g and the supernatant was incubated with Ni-NTA agarose beads (Thermo Fisher) for 2 hours at 4°C with agitation. After binding, beads were washed with 10mL of wash buffer A and then put on column and washed with wash buffer G (same as wash buffer A but with 150mM NaCl). His tagged HRV 3C protease was used to cleave the FAP away from His-GST at 4°C overnight and any unbound protease was removed by incubating with additional Ni-NTA beads at 4°C for 2 hours. Protein released by the proteolysis digestion was collected as flow through and was then purified on Superdex 75 Gel Filtration Column (GE Healthcare) by fast protein liquid chromatography (BioLogic DuoFlow, Biorad). Purity was evaluated using SDS-PAGE and protein was quantified using a DU730 UV/Vis spectrophotometer based on the absorbance at 280nm (Beckman

Coulter Inc.). Further purity and the amount of functional protein was confirmed using a fluorogen binding assay.

Off rate measurements:

Off-rate measurements were performed using purified proteins for all FAPs using a QuantaMaster fluorimeter (PTI, Edison, NJ). Briefly, a solution of the FAP and fluorogen was prepared in PBSp buffer (PBS+0.01% pF127 at pH7.4) at a concentration such that the [Fluorogen] = $100 \times K_d$ and the [FAP] = $500 \times K_d$ of the complex. 200 μ L of this solution was added to 1.9mL buffer in a quartz cuvette with a magnetic stir bar in it to enable fast mixing. Fluorescence was measured as a function of time by exciting the complex at its excitation maximum and recording emission at the emission maximum. The excitation slits were set such that there was no photobleaching of the complex. This was ensured by performing a bleaching experiment on the complex for time scales longer than the observation time scale for the off rates. The dissociation curves were modeled using a 1:1 complex stoichiometry and fit to a single exponential decay curve. The half-lives of dissociation were used to calculate the off rates that are reported in table 1.

Ensemble bleaching experiments

Ensemble bleaching experiments were performed using the purified protein-fluorogen complex such that the protein was at a tenfold excess concentration compared to the fluorogen. The fluorogen concentration was tenfold higher than the K_d of the complex. The complex was incubated overnight at 4°C to ensure complete binding before performing any photobleaching experiments. Excitation and emission spectra of the complex were measured before photobleaching. Photobleaching was performed in a cuvette with a magnetic stir bar for mixing. The illumination source was a 250mW solid state laser (639nm). The beam from the laser was defocused enough so as to make a circular spot on the cuvette but not outside it. Excitation and emission spectra were

recorded in the QuantaMaster fluorimeter as above, every 10 mins for the MG binding FAPs, dL5 and dL9.3X and every 2 mins for the TO1 binding FAP scFv1.

Yeast cell surface bleaching experiments

Photobleaching measurements were performed on the surface of JAR200 yeast cells expressing the FAPs from a pPNL6 surface display plasmid. All strains (JAR200) were grown in 3 mL growth media (20g Dextrose, 5g Casamino acids, 1.7g Yeast nitrogen base, 5.3g Ammonium sulfate, 7.4g Sodium citrate, 2.2g Citric acid per liter at pH 4) at 30° C for 24 hours. For induction, 0.7 mL of yeast cells from the 24 hour culture were added to 35 mL of SG/R-CAA induction media (1g Dextrose, 20g Raffinose, 20g Galactose, 5g Casamino acids, 1.7g Yeast nitrogen base, 5.3g Ammonium sulfate, 60mg Uracil per liter at pH 7.4) at 20° C for 72 hours. 1 mL of this culture was spun down and media was removed. Cells were then washed 3x with 1 mL PBS and incubated at 4° C for 2 hours in 100 μ L of PBS with 1 μ M fluorogen. Unbound fluorogen was then removed and cells were washed 2x with 1 mL PBS. These cells were plated on concanavalin A coated glass bottom dishes. For experiments where excess fluorogen was required, we mixed the fluorogen at the desired concentrations in the imaging buffer (PBS). Imaging was performed on a Nikon Ti Eclipse inverted epi-fluorescence microscope using solid state laser illumination at 488nm (scFv1) and 639nm (dL5-MG, dL9.3X, HL4NP149) and appropriate emission filter sets. Time lapse images were acquired at 100ms exposure for a total duration of 1 minute (600 frames). To generate photobleaching curves from these images, a HiLo filter was used in ImageJ software package to remove regions that were saturated with signal in the first frame. For non-saturated regions, up to ten different 4X4 pixel regions of interest (ROI) were selected on different cells and the mean intensity over those pixels was measured over time. These bleaching curves were averaged and normalized to the signal in the first frame.

Surface preparation for single molecule experiments

Single molecule experiments were performed on glass coverslips that were derivatized to have biotin on them at low density in an otherwise PEG conjugated glass surface to minimize nonspecific binding of the protein. Briefly, coverslips were rinsed with acetone in 250 mL beaker. They were transferred to a new beaker and 100 mL of 50% MeOH in ultrapure water was added to the beaker followed by sonication for 20 mins. The coverslips were dried after this at room temperature. They were transferred to a flat bottom flask. H_2O_2 was added followed by very slow addition of H_2SO_4 such that the volume ratio of H_2O_2 : H_2SO_4 is 3:7. The coverslips are treated in this Piranha solution for 30 mins followed by a wash in ultrapure water and sonication in HPLC grade methanol for 20 min. Coverslips were placed in a staining rack that was placed in a beaker. 400 mL MeOH+20mL Acetic acid + 4 mL (3-aminopropyl)-trimethoxysilane were mixed together and added to the beaker so that the coverslips were immersed in the solution for 30 mins. They were rinsed with ultrapure water and a 100 μL solution containing 0.4 mg Biotin PEG-succinimidyl carboxymethyl ester [MW=3400], 5mg m-PEG-succinimidyl carboxymethyl ester [MW=5000] (Laysan Bio inc.) and 100 μL NaHCO_3 solution was added to each coverslip and they were kept in a closed humidified chamber overnight.

Single molecule photobleaching experiments

Single molecule photobleaching experiments were performed on the glass coverslips that were functionalized with PEG-Biotin. 100 μL of 0.2mg/mL streptavidin was added to these coverslips for 10 mins followed by rinsing with PBSp buffer (pH7.4). A solution containing 100nM Biotin-FAP and 250nM Biotin was then added to the imaging chamber and washed after 20 mins of incubation. This was followed by the addition of 10pM – 1nM fluorogen (K_d dependent) to the chamber. Single molecule imaging was performed Imaging was performed on the same system as above, utilizing 488nm or 639nm

excitation in the total internal reflection (TIR) mode. The microscope was equipped with a TIRF objective (100x, 1.49NA, Nikon) and appropriate TIRF filter cubes and emission filters corresponding to each fluoromodule. Images were acquired using the EMCCD camera as above at an exposure time of 100ms. Image acquisition was performed using Micromananger software package. Single particle tracking and time trace analyses were performed using particle tracking code written in Matlab.

BleachSort

BleachSort is the screening method where sorting was performed followed by bleaching the cells that expressed FAPs that bind MG-2p. A home built LED based bleaching device was made that could produce a power density of 100 W/cm^2 at the center of the LED beam at a distance of 10cm from the LED. We used a 300lm LED source with peak emission wavelength at 635nm for bleaching. MG binders were isolated through the first two rounds of sorting and the cells were subjected to bleaching before sorting in the third round and after. Cells were bleached for 10 mins and the fluorescence was recorded and compared against cells that were not subjected to any bleaching. $1\text{E-}6\text{M}$ MG-2p was added to the bleached cells and fluorescence was observed. Cells that showed binding of fresh dye and hence an increase in signal that was above the cells that were in the bleached gate; were collected. This process was repeated for 3 rounds to enrich for exchanging FAPs.

ChaseSort

In the ChaseSort technique, we chased MG bound to FAPs off with MG-TM-Cy3 and MG-tTEG-Cy3. In this approach, the scFv library was incubated with saturating concentrations of MG (up to $2\text{E-}6\text{M}$) and the fluorescence signal from the cells was monitored in the FRET and the direct excitation channels. The FRET channel being 532nm excitation and 680 emission. The direct excitation channel had the same

emission settings but the excitation was performed at 639nm. Once these cells were observed and the gates were drawn to mark the population, MG-Cy3 dye was added rapidly to the sorting tube and fluorescence was monitored in the FRET and direct excitation channels. Clones that were positive in the FRET channel only were selected and grown on SD-CAA induction plates.

Peptide sequences of L9 mutants and dL9.3x (I would align these and show where the mutations are.)

dL9.1

SYELTQPPSVSVSPGQTARITCSGDALPKQYTYWYQQKAGQAPVLVIYKDTERPSGIPE
RFSGTSSGTTATLTISGVQAEDEADYYCQSADSSGSYVFFGGGTKVTVLS

SYELAQSPSVSVSPGQTARITCSGDALPKQYTYWYQQKAGQAPVLVIYKDTERPSGIP
ERFSGTSPGTTVTLTISGVQAEDEADYYCQSADSSGSYVFFGGGTKVTVLS

dL9.2

SYELTQPPSVSVSPGQTARITCSGDALPKQYTYWYQQKAGQAPVLVIYKDTERPSGIPE
RFSGTSSGTTATLTISGVQAEDEADYYCQSADSSGSYVFFGGGTKVTVLS

SYELTQPPSVSVSPGQTARITCSGDALPKQYTYWYQQKAGQAPVLVIYKDTERPSGIPE
RFSGTSSGTTVTLTISGVQAEDEADYYCQSADSSGSYVFFGGGTKVTVLS

dL9.3

SYELTQPPSVSVSPGQTARITCSGDALPKQYTYWYQQKAGQAPVLVIYKDTERPSGIPE
RFSGTSSGTTATLTISGVQAEDEADYYCQSADSSGSYVFFGGGTKVTVLS

SYELTQPPSVSVSPGQTARITCSGDALPKQYTYWYQQKAGQAPVLVIYKDTERPSGIPE
RFSGTSSGTTATLTISGVQAEDEADYYCQSADSSGSYVFFGGGTKVTVLS

dL9.5

SYELTQPPSVSVSPGQTARITCSGDALPKQYTYWYQQKAGQAPVLVIYKDTERPSGIPE
RFSGTSSGTTATLTISGVQAEDEADYYCQSADSSGSHVFFGGGKVTVLS

SYELTQPPSVSVSPGQTARITCSGDALPKQYTYWYQQKAGQAPVLVIYKDTERPSGIPE
RFSGTSSGTTATLTISGVQAEDEADYYCQSADSSGSHVFFGGGKVTVLS

dL93x01

SYELTQPPSVSVSPGQTARITCSGDALPKQYTYWYQQKAGQAPVLVIYEDTERPSGIPE
RFSGTSSGTTATLTISGVQAEDEADYYCQSADSSGSYVFFGGGKVTVLSGGGGP
GSGGGSGGGSGGG

SYELTQPPSVSVSPGQTARITCSGDALPKQYTYWYQQKAGQAPVLVIYKDTERPSGIPE
RFSGTSSGTTATLTISGVQAEDEADYYCQSADSSGSYGFFGGGKVTVLS

dL93x03

SYELTQPPSVSVSPGQTARITCSGDALPKQYTYWYQQKAGQAPVLVIYEDTERPSGIPE
RFSGTSSGTTATLTISGVQAEDEADYYCQSADSSGSYVFFGGGKVTVLSGGGGP
GSGGGSGGGSGGG

SYELTQPPSVSVSPGQTARITCSGDALPKQYTYWYQQKAGQAPVLVIYKDTERPSGVP
ERFSGTSSGTTATLTISGVQAEDEADYYCQSADSSGSYGFFGGGKVTVLS

dL9.3X

SYELTQPPSVSVSPGQAARITCSGDALPKQYTYWYQQKAGQAPVLVIYEDTERPSGIP
ERFSGTSSGTTATLTISGVQAEDEADYYCQSADSSGSYGFFGGGKVTVLS

SYELTQPPSVSVSPGQAARITCSGDALPKQYTYWYQQKAGQAPVLVIYEDTERPSGIP
ERFSGTSSGTTATLTISGVQAEDEADYQCQSADSSGSYGFFGGGKVTVLS

Bibliography

1. Herschel, J. F. W., On a Case of Superficial Colour Presented by a Homogeneous Liquid Internally Colourless. *Philosophical Transactions of the Royal Society of London* **1845**, 135, 143-145.
2. Giepmans, B. N. G.; Adams, S. R.; Ellisman, M. H.; Tsien, R. Y., The Fluorescent Toolbox for Assessing Protein Location and Function. *Science* **2006**, 312 (5771), 217-224.
3. Liu, J.; Liu, C.; He, W., Fluorophores and Their Applications as Molecular Probes in Living Cells. *Current Organic Chemistry* **2013**, 17 (6), 564-579.
4. Harris, D. C.; Bertolucci, M. D., *Symmetry and spectroscopy: an introduction to vibrational and electronic spectroscopy*. Courier Dover Publications: 1978.
5. Jaboski, A., Efficiency of anti-Stokes fluorescence in dyes. *Nature* **1933**, 131, 839-840.
6. Valeur, B.; Berberan-Santos, M. N., *Molecular fluorescence: principles and applications*. John Wiley & Sons: 2013.
7. Stokes, G. G., On the change of refrangibility of light. *Philosophical Transactions of the Royal Society of London* **1852**, 463-562.
8. Webb, J. P.; McColgin, W. C.; Peterson, O. G.; Stockman, D. L.; Eberly, J. H., Intersystem Crossing Rate and Triplet State Lifetime for a Lasing Dye. *The Journal of Chemical Physics* **1970**, 53 (11), 4227-4229.
9. Menzel, R.; Thiel, E., Intersystem crossing rate constants of rhodamine dyes: influence of the amino-group substitution. *Chemical physics letters* **1998**, 291 (1), 237-243.

10. Chibisov, A. K.; Zakharova, G. V.; Gorner, H., Effects of substituents in the polymethine chain on the photoprocesses in indodicarbocyanine dyes. *Journal of the Chemical Society, Faraday Transactions* **1996**, *92* (24), 4917-4925.
11. Widengren, J.; Chmyrov, A.; Eggeling, C.; Loefeldahl, P. A. K.; Seidel, C. A. M., Strategies to Improve Photostabilities in Ultrasensitive Fluorescence Spectroscopy. *The Journal of Physical Chemistry A* **2006**, *111* (3), 429-440.
12. Zheng, Q.; Jockusch, S.; Zhou, Z.; Altman, R. B.; Warren, J. D.; Turro, N. J.; Blanchard, S. C., On the mechanisms of cyanine fluorophore photostabilization. *The journal of physical chemistry letters* **2012**, *3* (16), 2200-2203.
13. Turro, N. J.; Ramamurthy, V.; Scaiano, J. C., *Principles of molecular photochemistry: an introduction*. University science books: 2009.
14. Montalti, M.; Credi, A.; Prodi, L.; Gandolfi, M. T., *Handbook of photochemistry*. CRC press: 2006.
15. Kuramoto, N.; Kitao, T., The contribution of singlet oxygen to the photofading of triphenylmethane and related dyes. *Dyes and Pigments* **1982**, *3* (1), 49-58.
16. Byers, G.; Gross, S.; Henrichs, P., Direct and sensitized photooxidation of cyanine dyes. *Photochemistry and photobiology* **1976**, *23* (1), 37-43.
17. Sies, H.; Menck, C. F., Singlet oxygen induced DNA damage. *Mutation Research/DNAging* **1992**, *275* (3), 367-375.
18. Davies, M. J., Reactive species formed on proteins exposed to singlet oxygen. *Photochemical & Photobiological Sciences* **2004**, *3* (1), 17-25.
19. Tsien, R. Y., The green fluorescent protein. *Annual review of biochemistry* **1998**, *67* (1), 509-544.
20. Drobizhev, M.; Tillo, S.; Makarov, N. S.; Hughes, T. E.; Rebane, A., Color hues in red fluorescent proteins are due to internal quadratic Stark effect. *The Journal of Physical Chemistry B* **2009**, *113* (39), 12860-12864.

21. Abbyad, P.; Childs, W.; Shi, X.; Boxer, S. G., Dynamic Stokes shift in green fluorescent protein variants. *Proceedings of the National Academy of Sciences* **2007**, *104* (51), 20189-20194.
22. Chatteraj, M.; King, B. A.; Bublitz, G. U.; Boxer, S. G., Ultra-fast excited state dynamics in green fluorescent protein: multiple states and proton transfer. *Proceedings of the National Academy of Sciences* **1996**, *93* (16), 8362-8367.
23. Shaner, N. C.; Lin, M. Z.; McKeown, M. R.; Steinbach, P. A.; Hazelwood, K. L.; Davidson, M. W.; Tsien, R. Y., Improving the photostability of bright monomeric orange and red fluorescent proteins. *Nature methods* **2008**, *5* (6), 545-551.
24. Harms, G. S.; Cognet, L.; Lommerse, P. H.; Blab, G. A.; Schmidt, T., Autofluorescent proteins in single-molecule research: applications to live cell imaging microscopy. *Biophysical journal* **2001**, *80* (5), 2396-2408.
25. Haupts, U.; Maiti, S.; Schwille, P.; Webb, W. W., Dynamics of fluorescence fluctuations in green fluorescent protein observed by fluorescence correlation spectroscopy. *Proceedings of the National Academy of Sciences* **1998**, *95* (23), 13573-13578.
26. Heikal, A. A.; Hess, S. T.; Baird, G. S.; Tsien, R. Y.; Webb, W. W., Molecular spectroscopy and dynamics of intrinsically fluorescent proteins: coral red (dsRed) and yellow (Citrine). *Proceedings of the National Academy of Sciences* **2000**, *97* (22), 11996-12001.
27. Schwille, P.; Kummer, S.; Heikal, A. A.; Moerner, W.; Webb, W. W., Fluorescence correlation spectroscopy reveals fast optical excitation-driven intramolecular dynamics of yellow fluorescent proteins. *Proceedings of the National Academy of Sciences* **2000**, *97* (1), 151-156.

28. Hendrix, J.; Flors, C.; Dedecker, P.; Hofkens, J.; Engelborghs, Y., Dark states in monomeric red fluorescent proteins studied by fluorescence correlation and single molecule spectroscopy. *Biophysical journal* **2008**, *94* (10), 4103-4113.
29. Mudalige, K.; Habuchi, S.; Goodwin, P. M.; Pai, R. K.; De Schryver, F.; Cotlet, M., Photophysics of the Red Chromophore of HcRed: Evidence for Cis \rightarrow Trans Isomerization and Protonation-State Changes. *The Journal of Physical Chemistry B* **2010**, *114* (13), 4678-4685.
30. Malvezzi-Campeggi, F.; Jahnz, M.; Heinze, K. G.; Dittrich, P.; Schwille, P., Light-induced flickering of DsRed provides evidence for distinct and interconvertible fluorescent states. *Biophysical journal* **2001**, *81* (3), 1776-1785.
31. Schenk, A.; Ivanchenko, S.; RÄ¶tjcker, C.; Wiedenmann, J. r.; Nienhaus, G. U., Photodynamics of red fluorescent proteins studied by fluorescence correlation spectroscopy. *Biophysical journal* **2004**, *86* (1), 384-394.
32. Chalfie, M.; Kain, S. R., *Methods of Biochemical Analysis, Green Fluorescent Protein: Properties, Applications and Protocols*. John Wiley & Sons: 2005; Vol. 47.
33. Szent-Gyorgyi, C.; Schmidt, B. F.; Creeger, Y.; Fisher, G. W.; Zakel, K. L.; Adler, S.; Fitzpatrick, J. A.; Woolford, C. A.; Yan, Q.; Vasilev, K. V., Fluorogen-activating single-chain antibodies for imaging cell surface proteins. *Nature biotechnology* **2008**, *26* (2), 235-240.
34. Song, L.; Hennink, E. J.; Young, I. T.; Tanke, H. J., Photobleaching kinetics of fluorescein in quantitative fluorescence microscopy. *Biophysical journal* **1995**, *68* (6), 2588-2600.
35. Gordon, M. P.; Ha, T.; Selvin, P. R., Single-molecule high-resolution imaging with photobleaching. *Proceedings of the National Academy of Sciences of the United States of America* **2004**, *101* (17), 6462-6465.

36. Taguchi, H.; Ueno, T.; Tadakuma, H.; Yoshida, M.; Funatsu, T., Single-molecule observation of protein-protein interactions in the chaperonin system. *Nature biotechnology* **2001**, *19* (9), 861-865.
37. Rasnik, I.; McKinney, S. A.; Ha, T., Nonblinking and long-lasting single-molecule fluorescence imaging. *Nature methods* **2006**, *3* (11).
38. Aitken, C. E. a.; Marshall, R. A.; Puglisi, J. D., An Oxygen Scavenging System for Improvement of Dye Stability in Single-Molecule Fluorescence Experiments. *Biophysical journal* **2008**, *94* (5), 1826-1835.
39. Dave, R.; Terry, D. S.; Munro, J. B.; Blanchard, S. C., Mitigating unwanted photophysical processes for improved single-molecule fluorescence imaging. *Biophysical journal* **2009**, *96* (6), 2371-2381.
40. Grunwell, J. R.; Glass, J. L.; Lacoste, T. D.; Deniz, A. A.; Chemla, D. S.; Schultz, P. G., Monitoring the conformational fluctuations of DNA hairpins using single-pair fluorescence resonance energy transfer. *Journal of the American Chemical Society* **2001**, *123* (18), 4295-4303.
41. Glazer, A. N., Fluorescence-based assay for reactive oxygen species: a protective role for creatinine. *The FASEB Journal* **1988**, *2* (9), 2487-2491.
42. Cordes, T.; Vogelsang, J.; Tinnefeld, P., On the Mechanism of Trolox as Antiblinking and Antibleaching Reagent. *Journal of the American Chemical Society* **2009**, *131* (14), 5018-5019.
43. Joo, C.; Balci, H.; Ishitsuka, Y.; Buranachai, C.; Ha, T., Advances in Single-Molecule Fluorescence Methods for Molecular Biology. *Annual review of biochemistry* **2008**, *77* (1), 51-76.
44. Klein, T.; Proppert, S.; Sauer, M., Eight years of single-molecule localization microscopy. *Histochemistry and cell biology* **2014**, 1-15.

45. Altman, R. B.; Terry, D. S.; Zhou, Z.; Zheng, Q.; Geggier, P.; Kolster, R. A.; Zhao, Y.; Javitch, J. A.; Warren, J. D.; Blanchard, S. C., Cyanine fluorophore derivatives with enhanced photostability. *Nature methods* **2012**, *9* (1), 68-71.
46. Altman, R. B.; Zheng, Q.; Zhou, Z.; Terry, D. S.; Warren, J. D.; Blanchard, S. C., Enhanced photostability of cyanine fluorophores across the visible spectrum. *Nature methods* **2012**, *9* (5), 428-429.
47. Tinnefeld, P.; Cordes, T., 'Self-healing'dyes: intramolecular stabilization of organic fluorophores. *Nature methods* **2012**, *9* (5), 426-427.
48. Cramer, F.; Saenger, W.; Spatz, H.-C., Inclusion compounds. XIX. 1a The formation of inclusion compounds of $\hat{\alpha}$ -cyclodextrin in aqueous solutions. Thermodynamics and kinetics. *Journal of the American Chemical Society* **1967**, *89* (1), 14-20.
49. Arunkumar, E.; Forbes, C. C.; Smith, B. D., Improving the properties of organic dyes by molecular encapsulation. *European journal of organic chemistry* **2005**, *2005* (19), 4051-4059.
50. Shank, N. I.; Zanotti, K. J.; Lanni, F.; Berget, P. B.; Armitage, B. A., Enhanced Photostability of Genetically Encodable Fluoromolecules Based on Fluorogenic Cyanine Dyes and a Promiscuous Protein Partner. *Journal of the American Chemical Society* **2009**, *131* (36), 12960-12969.
51. Chao, G.; Lau, W. L.; Hackel, B. J.; Sazinsky, S. L.; Lippow, S. M.; Wittrup, K. D., Isolating and engineering human antibodies using yeast surface display. *Nature protocols* **2006**, *1* (2), 755-768.

Chapter III: Targeting Quantum dots using fluorogenic haptens

Introduction

Biological systems are chaotic, in the sense that there is a vast diversity in the number and type of biomolecules, both reactive and inert in any biological micro-environment. Biochemistry is a very powerful tool that enables studying these complex systems in isolation and thus provides for simplistic models of bio-molecular function. However, the amount of information that can be obtained from systems that are studied in isolation of their micro-environments is very limited and often not an exact picture of a real system. For instance, a binding between DNA and an RNA polymerase molecule in the presence of the transcription machinery may be totally different in the presence of molecular crowding agents, which is a natural state of all living cells.¹ The study of cellular systems is therefore needed to gain a better understanding of biological processes. Imaging biomolecules in a cell poses several challenges such as delivery of the probe in a site specific manner, selective labeling and high sensitivity. The sensitivity aspect is of critical importance when the biomolecules under observation are few in number. The immune system is a classic example of the problem at hand. Less than ten peptide-major histocompatibility complex (pMHC) glycoproteins are needed to bind the T cell receptor and initiate an immune response.^{2, 3} More importantly, these signaling responses occur on the order of tens of seconds.⁴ Therefore, the number of photons emitted per second by the fluorophore is the most critical parameter for obtaining better limit of detection and temporal resolution. Typical fluorophores such as organic dyes and fluorescent proteins are limited in the photon budget to about tens of thousands of photons.⁵ A rapid development in the field of nanotechnology has provided us with nanoparticles that have superior optical properties for sensitive detection.

The use of nanotechnology tools for detecting or manipulating biological systems requires robust approaches to direct nanomaterials to biological targets. Developments in nanotechnology have led to nanoparticles of engineered size and shape in a variety of materials, including noble metals, insulators, semiconductors, magnetic materials and composite structures available with a range of surface modifications and physical properties.⁶⁻¹⁰ While gold and silicon nanoparticles have been primarily used for surface enhanced Raman spectroscopy, electron microscopy and magnetic resonance imaging, Quantum Dots (QDs) have been the nanoparticles of choice for fluorescence imaging¹¹,¹² due to their excellent quantum yields, long-term photostability and advantageous spectroscopic properties. For these properties to be exploited for biological objectives, the nanoparticles should be precisely located at sites of biological interest on or inside live and fixed cells. The conventional labeling approach has delivered a variety of nanoparticles to live cells using antibody, peptide, DNA and aptamer conjugates, but requires robust affinity molecules for a specific target.¹³⁻¹⁵ In contrast, genetically encoded epitope tags¹⁶ and fluorescent proteins¹⁷ have been fused to nearly every eukaryotic protein, allowing detection of each target in a cellular context. The power of genetic targeting arises from the resulting protein-level fusion, carrying the tag where the target is directed by the cell. The development of orthogonal and modular genetic targeting approaches is required to effectively exploit the properties of nanomaterials in biological systems.

Since the first demonstrations of bioconjugated Quantum Dots (QDs), several approaches at the interface of nanotechnology and biology have led to an increase in the use of QDs for live cell imaging.^{18, 19} QDs have been used extensively for labeling and imaging cellular proteins particularly at the single molecule level.^{20, 21} Their brightness, photostability and multicolor properties make single molecule imaging

possible at very high speeds and low exposures, thus improving temporal resolution.²² Traditionally, QDs have been targeted to proteins of interest as antibody or biomolecule conjugates, resulting in a large, typically multivalent probe that may interfere with protein function.²³⁻²⁵ Recently, there have been several efforts to target QDs using smaller affinity tags. QDs functionalized with fluorescein were used to target a mouse prion protein fused to an anti-fluorescein scFv.^{26, 27} Another approach showed the tracking of single poly-Histidine tagged proteins using QDs functionalized with Ni²⁺ tris-nitrilotriacetic acid.^{28, 29} More recently, QDs functionalized with haloTag protein were used to target single LDL receptor proteins on the cell surface that had been previously tagged using a lipoic acid ligase directed-10-bromodecanoate substrate.^{30, 31} Similar methods have been used in conjunction with biotin tags to target streptavidin (sav) functionalized QDs after biotin modification of the proteins. While these approaches enabled targeting of QDs to cell surface proteins, their general application is limited by the synthetic steps required to prepare the functionalized QDs. In addition, the post-labeling approach is not easy to implement for multiplexing. The shared excitation and narrow emission spectra of QDs can be exploited for simultaneous multiplexing, but lacking robust orthogonal targeting approaches, multiplex labeling has been limited to complex pre-labeling procedures (i.e. biotin ligase and lipoic acid ligase treatment), multicolor labeling of a single target or antibody pre-complexation.^{32, 33} In this chapter, we report a modular approach to target commercially available sav-QDs using biotinylated hapten molecules that specifically bind to small genetically encoded proteins with high affinities. The schematic for the targeting method is shown in Figure 1. Due to the high affinity and fast on rate of the hapten-protein complex formation, the labeling is instantaneous and requires only one washing step before imaging. The large number of available haptens with specific cognate proteins provides a highly modular labeling scheme, potentially limited only by the number of resolvable detection channels. We show that this method can achieve

orthogonal labeling for at least three targets on the surface of cells, functions to label multiple cell surface proteins for simultaneous single molecule tracking at high speeds and over long timescales and can be applied to target sav-QDs to intracellular proteins. The QDs, due to the ease of multiplexed detection, serve as a robust targeting model for various nanoparticles, demonstrating that this approach can specifically target 3 or more different nanoparticles to genetically specified locations, as long as those nanoparticles are available as biotin-binding conjugates.

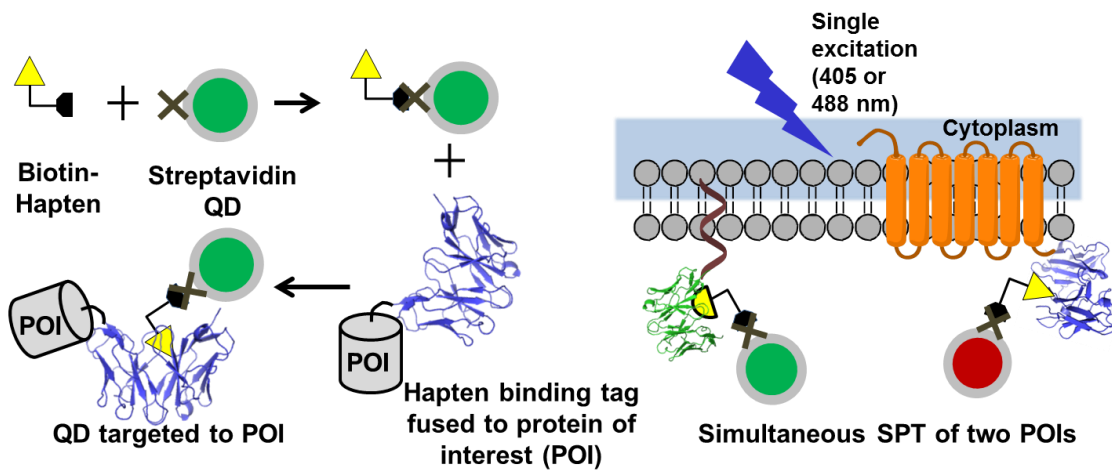


Figure 1. A scheme for genetically targeting streptavidin QDs to proteins using biotinylated haptens. The QD-hapten complex can be assembled and then targeted to the cognate protein for the hapten that in turn may be fused to any protein of interest. These proteins of interest may be on the cell surface and this methodology can enable the simultaneous tracking of two or more proteins on the cell surface using different QDs but the same excitation wavelength owing to the broad excitation spectrum of the QDs.

Results

Streptavidin QDs can be targeted to proteins through biotinylated haptens

A robust genetically encoded targeting approach must be both specific and selective for the expressed protein tag. Single chain variable fragment (scFv) antibodies with molecular recognition properties for fluorescent and fluorogenic dye haptens have been established with dissociation constants (K_d) ranging from low nanomolar to picomolar ranges.^{34, 35} We demonstrate that biotinylated analogues of these dye-based haptens can target commercially available QD streptavidin conjugates to the cognate genetically encoded binding protein. The chemical structures of the dye based haptens are shown in Figure 2.

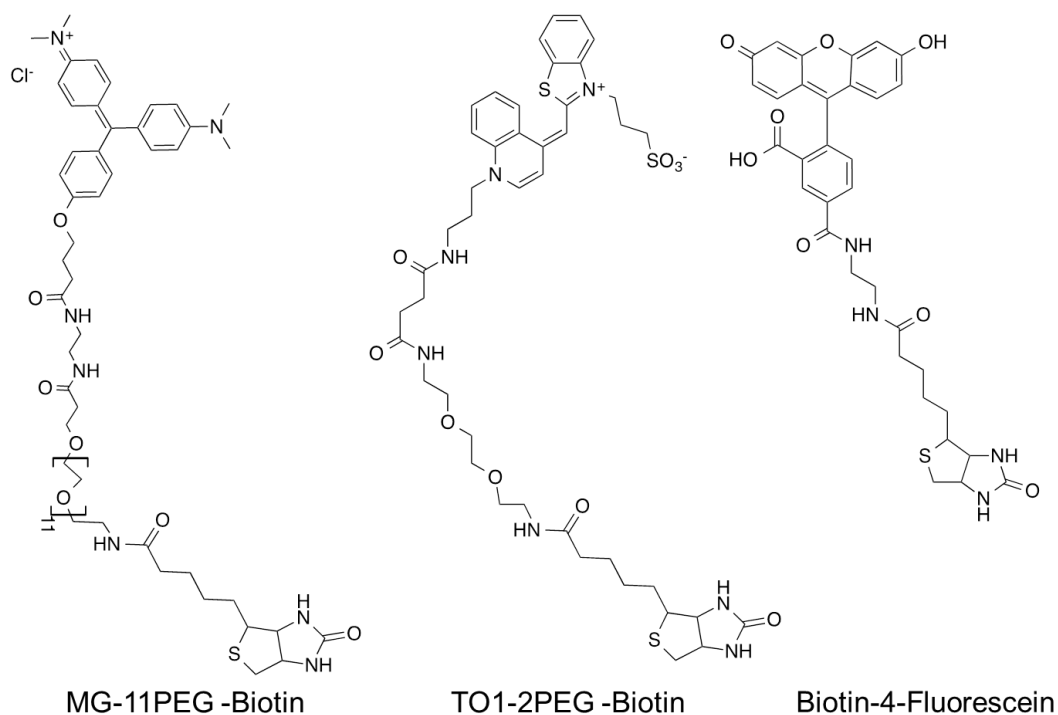


Figure 2. Chemical structures of the biotin conjugated haptens used for targeting streptavidin QDs. While MG and TO1 are fluorogenic, Fluorescein is intrinsically fluorescent. This approach can be applied to any haptens as long as a cognate protein for it is available.

Selectivity of targeting ensured through haptens targeted to cognate proteins

Pre-binding of biotinylated hapten to QD streptavidin conjugates can also selectively label cognate protein tags on cells. scFvs that bind to MG (dL5**), a sulfonated thiazole orange (TO1) analog (HL1.0.1) and fluorescein (E2) were expressed on the yeast cell wall as above.^{34, 35, 37} QD655-sav was pre-incubated with saturating amounts of the respective biotinylated hapten, separated from excess hapten and then incubated with JAR200 cells expressing each protein. Imaging of the cells revealed that the QD-hapten complex labels only the cognate protein for the bound hapten, demonstrating the modularity and orthogonality of the labeling strategy with three distinct hapten-scFv pairs, MG-dL5**, TO1-HL1.0.1 and FI-E2.

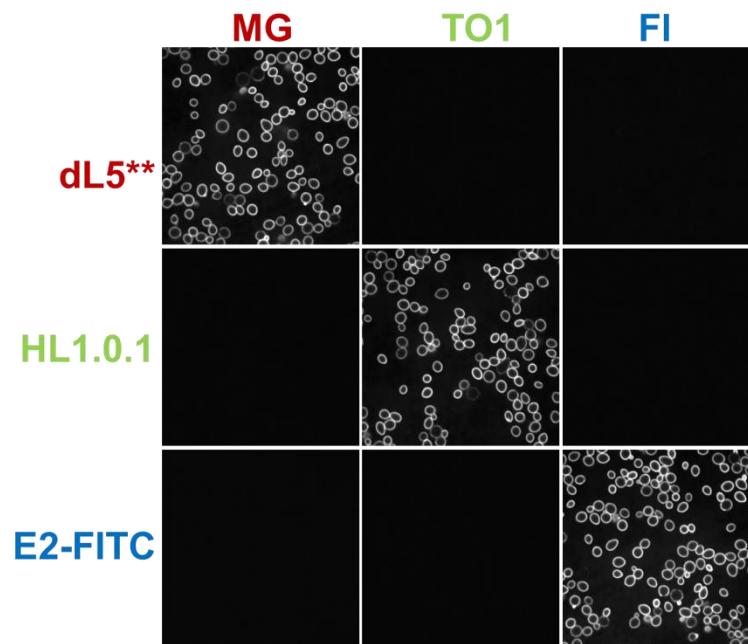


Figure 4. Pre-complexation of the QDs and haptens allows selective targeting of QDs to cognate expressed scFvs. The targeting is specific and QD signal is only observed when the QDs are bound to the correct hapten for the cognate protein. Here, dL5** binds MG, HL1.0.1 binds TO1 and E2-FITC binds Fluorescein (FI). No labeling is seen with any non-cognate pairs.

Thus, these protein-hapten pairs are suitable for simultaneous multicolor use since the expressed protein tags recognize only one dye. JAR200 yeast cells labeled with sav-QDs using this strategy were imaged with an epi-fluorescence microscope using 405nm excitation laser as shown in Figure 4.

Simultaneous multiplexed single particle tracking using QDs

Targeted QDs are retained by the high-affinity hapten-scFv interaction sufficiently for simultaneous multiplexed imaging and single particle tracking, without affecting the protein diffusion behavior. A HEK293 cell line that expressed dL5**- β -2-adrenergic receptor (B2AR) fusion stably (see methods) was transfected to express HL1.0.1 on the cell surface anchored by a single platelet-derived growth factor receptor transmembrane domain (PDGFR-TM) from the pDisplay vector.³⁸ The schematic for the cell surface post-transfection is shown in Figure 5. MG-Bt and TO1-Bt were incubated with sav-QD655 and sav-QD605 respectively to form MG-QD655 and TO1-QD605 complexes.³⁴ These QD-hapten complexes were then added to a glass bottom imaging dish containing the HEK293 cells. Microscopy was performed at the basal surface of the cells at 37° C, using Total Internal Reflection Fluorescence (TIRF) illumination with a dual-view image splitter to simultaneously image QD605 and QD655 under a 405 nm or a 488nm excitation at 40 Hz and 25 millisecond (ms) exposure. The protein labeling schematic is shown in Figure 5A. The images from this experiment are shown in Figure 5B and supplementary movie 3S1. After labeling a sparse subset of receptors with MG-QD605 complex, addition of the MG fluorogen to the media labeled the remaining scFv sites, showing spectrally resolvable ensemble and single molecule imaging.³⁴ Using the 639 nm laser, we could selectively excite the dL5**-MG complex while the 405 nm laser excited bound QD605 as shown in Figure 5B (inset). This combination of ensemble and

single molecule imaging is made possible due to the fluorogenic nature of the haptens used in this study.³⁴

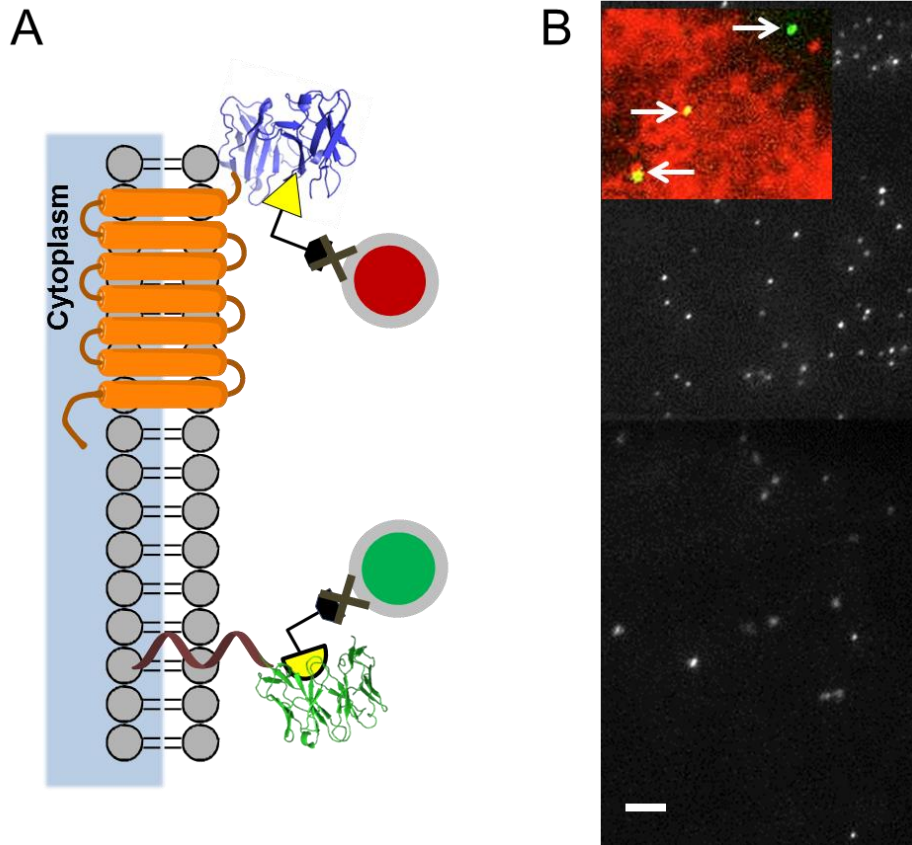


Figure 5. A. Schematic showing dL5⁺-B2AR fusion on the cell membrane bound to MG-QD655 and a transmembrane HL1.0.1 bound to TO1-QD605. B. Single molecule images acquired using a dual-view splitter showing the B2AR molecules labeled with QD655 (top) and the HL1.0.1-TM molecules labeled with QD605. Once the QDs are bound, the remaining receptors can be saturated with the fluorogenic hapten (MG) to perform ensemble imaging using the fluorescence from dL5**⁺-MG (ex 640 nm, em 685/70 nm) and single molecule imaging using QD605 (ex 405 nm, em 605/20 nm) simultaneously (5B, inset); scale bar 1 μ m.**

We performed single particle tracking to determine diffusion coefficients of these proteins on the cell surface using mean squared displacement analysis for each particle trajectory.^{39, 40} Mean trajectory lengths for B2AR and PDGFR-TM were 19 and 13 frames respectively (N>600 tracks, see methods) when no attempts were made to link trajectories due to blinking or diffusion out of the image plane. These trajectories are suitable for mean squared displacement (MSD) analyses using standard methods.⁴¹ While the B2AR shows slow diffusion over short ranges as shown in Figures 6A and B, the trans-membrane protein diffuses rapidly over long ranges as shown in Figures 6C and D. We found the median diffusion coefficient (D) of the HL1.0.1-TM protein to be 4.2 $\mu\text{m}^2/\text{s}$, while the B2AR protein measured on the same cells, under the same conditions, diffuse with a D of 0.1 $\mu\text{m}^2/\text{s}$ as shown in Figures 6B and D. These results are consistent with previous reported diffusion coefficients of B2AR and TM constructs in HEK293 cells.⁴²

Median D values of 4.5 $\mu\text{m}^2/\text{s}$ and 0.1 $\mu\text{m}^2/\text{s}$ were obtained for HL1.0.1-TM and B2AR proteins respectively, when the labeling colors were transposed (MG-QD605:B2AR/TO1-QD655:PDGFR-TM), indicating that the protein, not the quantum dot, is responsible for the observed differences in diffusion. Further, the endocytic sorting of the B2AR is controlled by its interaction with a kinase-regulated PDZ domain.⁴³ An Alanine (Ala) mutation at the carboxy-terminus of the B2AR suppresses its interactions with the PDZ domain. HEK293 cells were transfected with a dL5**⁻B2AR-Ala plasmid. The dL5** protein was labeled using MG-QD655 and single molecule imaging was performed as above. These B2AR-Ala mutant proteins diffused rapidly at a rate of 1.4 $\mu\text{m}^2/\text{s}$ as shown in Figures 6E, F and supplementary movie 3S2. These results are also consistent with previous studies.⁴⁴

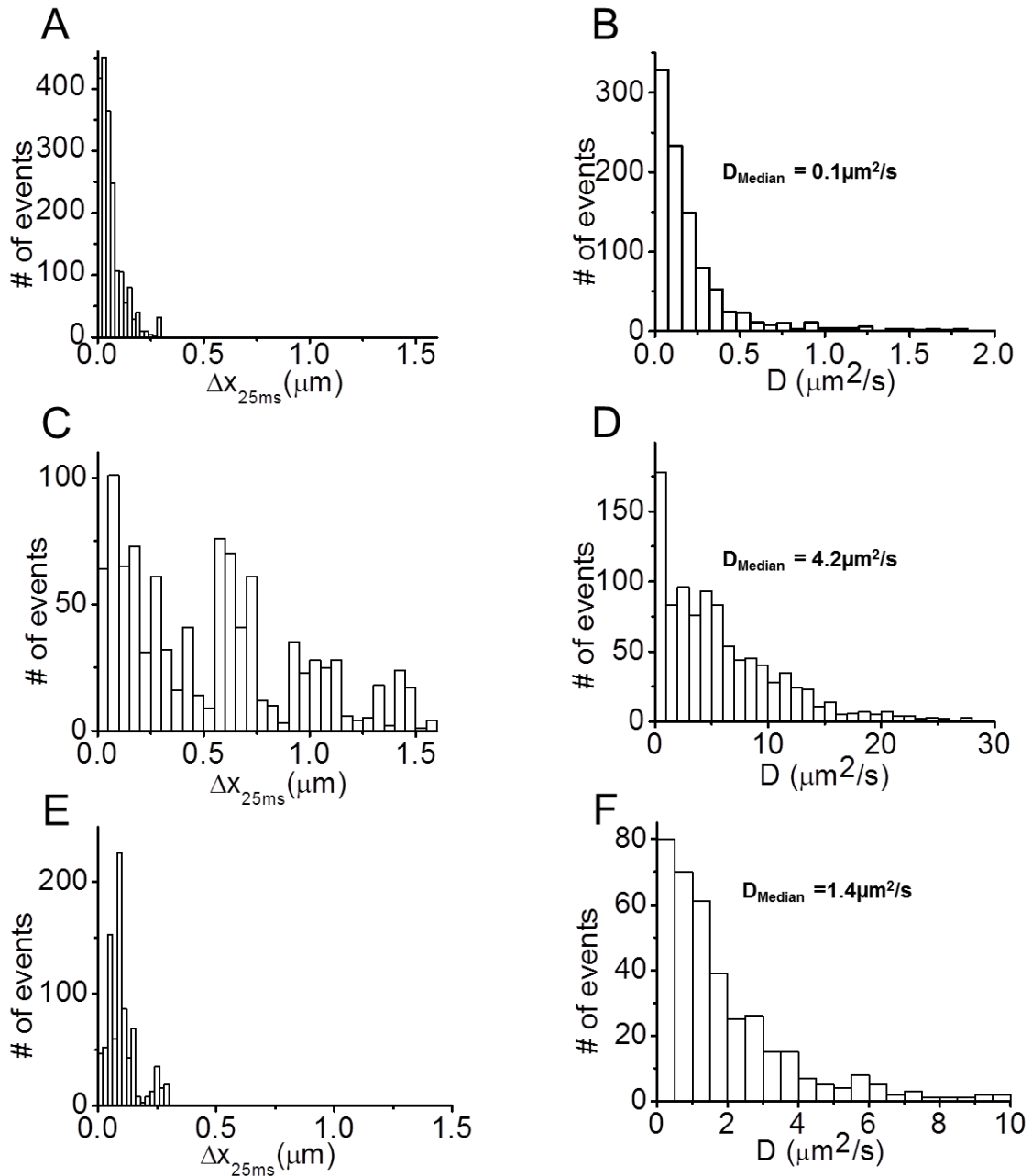


Figure 6. Distribution of jumps and diffusion coefficients of the (A, B) dL5 B2AR; and (C, D) of HL1.0.1-TM on the surface of HEK293 cells, respectively. The TM protein jumps more distance in a 25ms duration and displays ~40x larger diffusion coefficient than the B2AR measured simultaneously on the same cells. (E, F) The B2AR-Ala molecules have jumps and diffusion coefficients significantly larger than WT B2AR molecules owing to the lack of interactions with the PDZ domain.**

Intracellular targeting of QD-haptens

The delivery of a small number of QDs inside the cells is very advantageous since it can enable single molecule studies of QD conjugates using a conventional epi-fluorescence setup. Even at an ensemble level, labeling intracellular targets with QDs is very useful and several methods have been employed to deliver QDs inside the cells. These methods can be broadly classified as passive delivery, facilitated delivery or active delivery.⁴⁵ Passive delivery utilizes the surface functionalization and charge properties of the QD to mediate internalization.^{46, 47} Active delivery relies on the manipulation of the cell through micro-injection, electroporation or scrape loading; techniques that transiently compromise the membrane integrity and thus cause QD uptake.⁴⁸⁻⁵⁰ Finally, facilitated delivery relies on the decoration of the QD surface with specific groups such as peptides, antigens or polymers and allows for intracellular uptake through endocytosis.⁵¹ While passive delivery is really simple and enables the delivery of QDs in high concentrations to the cell, it is often non-specific and the QDs end up in endosomal pathways depending on the cell type and the composition of the QDs. Microinjection or electroporation can enable the delivery of QDs seamlessly into cells but one of the main problems with these methods is the throughput. Each cell has to be injected with the QDs and it becomes a problem in imaging especially when higher magnification is utilized for imaging. Facilitated delivery using peptides in particular has been very useful for QD delivery. NLS, TAT, MTS and RGD peptides have been very popular for delivering QDs to cells.⁵²⁻⁵⁴ The peptide delivery method has an edge over the other methods as the synthesis of QDs with small peptides is straightforward and the peptides are efficient in delivering the QDs to the required targets. Therefore the obvious choice for us to deliver QDs in the cell was using RGD peptides.

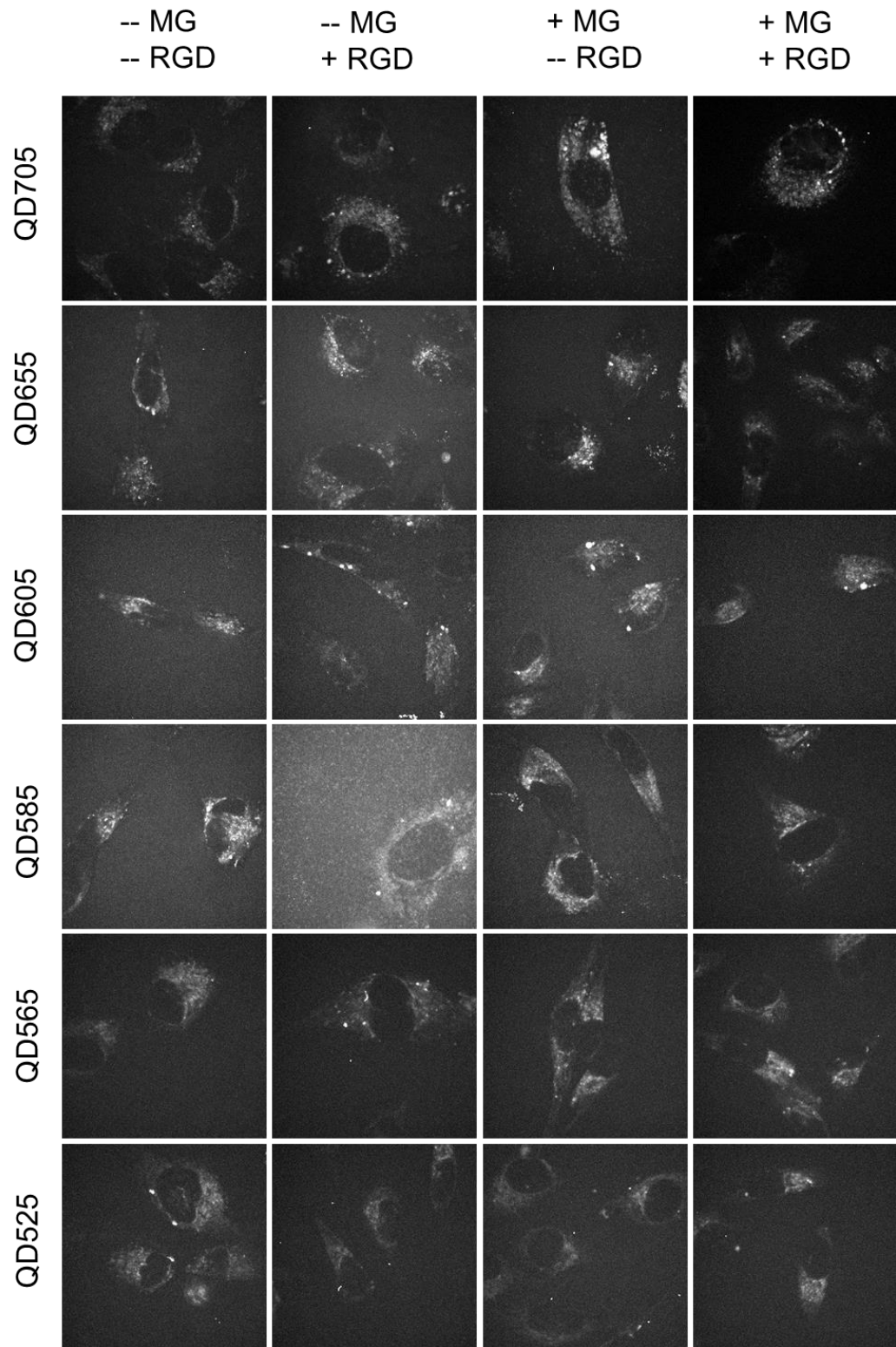


Figure 7. Targeting QDs to dL5-actin in HeLa cells using RGD peptide. While it is clear that more QDs make it inside the cells in the presence of RGD peptide, they are possibly trapped in endosomes or other cellular compartments shown by the lack of specific actin labeling using this approach.**

For this, we utilized two aspects of the streptavidin QDs. First, the tetravalency of streptavidin enabled targeting another biotinylated hapten to the QDs in addition to the fluorogen hapten. Second, the fact that each QD on an average has 2.3 streptavidin molecules conjugated to it, further made it possible to target Biotin-RGD to QDs. Biotin-RGD and Biotin-MG were incubated with streptavidin-QDs in a 2:2:1 ratio for 30 mins followed by the addition of the complex to cell growth media. HeLa cells expressing dL5-Actin were incubated in this media for 6 hours. The media was replaced with fresh media and the cells were imaged using a fluorescence microscope with an excitation wavelength of 405 nm and emission at 655 nm (20 nm bandpass). As a control, cells were incubated with QDs without RGD and without MG. As shown in Figure 7, we could not discern any significant differences between the controls and the case when the QDs were incubated with the cells. While there was a definite increase in the signal in the samples that contained RGD, which is obvious from the high signal to noise ratio in the RGD positive samples, we did not see any localization of these probes to actin cytoskeleton. Even at higher ratios of RGD we did not see a significant localization of the QDs in actin. We believe that, while the RGD facilitates the entry of the QDs past the cell membrane, it does not prevent the QDs from getting trapped in the endosomal pathway. Further work needs to be done in this regard with different peptides to see if the QDs can be targeted site-specifically to intracellular proteins. Next we thought of active targeting methods such as microinjection and scrape loading for the delivery of QDs to intracellular compartments.

The injection of well dispersed, single MG-QD655 using a modified microinjection protocol in wild type HeLa cells showed single particles with significant diffusion (Figure 8A and 8B), while injection into HeLa cells stably expressing dL5**-actin (Figure 8A and 8C) showed rapid immobilization of injected QDs. These results are also shown in supplementary movie 3S3. Diffusion coefficients for MG-QDs bound to dL5**-actin were essentially negligible ($D = 0.002 \mu\text{m}^2/\text{s}$) whereas free MG-QDs in WT cells showed significant diffusion at a rate of $0.10 \mu\text{m}^2/\text{s}$, which is in agreement with the reported diffusion properties of other free QDs in the cytoplasm.⁵⁵

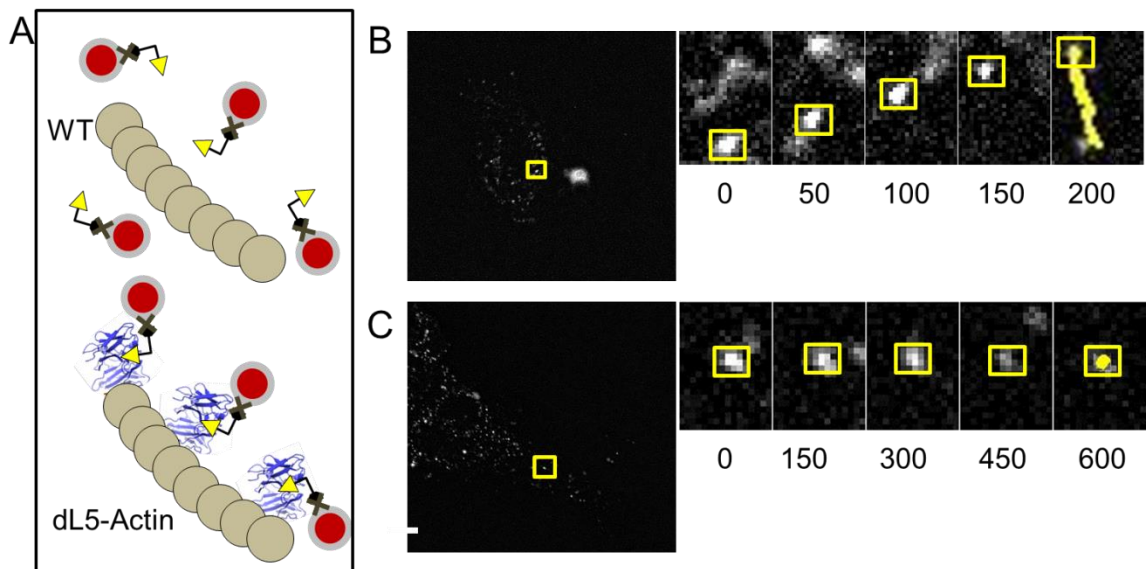


Figure 8. A. Schematic of MG-QD in the cytoskeleton showing that the QDs are targeted to the protein of interest (actin) only when the cognate protein for the hapten (dL5) is present, and otherwise show free diffusion in the cytosol. B. MG-QD655 injected in HeLa cells show rapid diffusion with large jumps, C. as opposed to rapid immobilization when injected in HeLa cells expressing actin-dL5**;** scale bar 4 μm .

The distribution of jumps and diffusion coefficients for dL5**-actin labeled with MG-QD655 and MG-QD655 in cytoplasm are shown in Figure 9. The marked difference between MG-QD complex diffusion in WT and dL5**-actin expressing cells indicates that

the MG-QDs can be targeted to dL5**-actin, and potentially other targets, inside HeLa cells when delivered into the cell through microinjection.

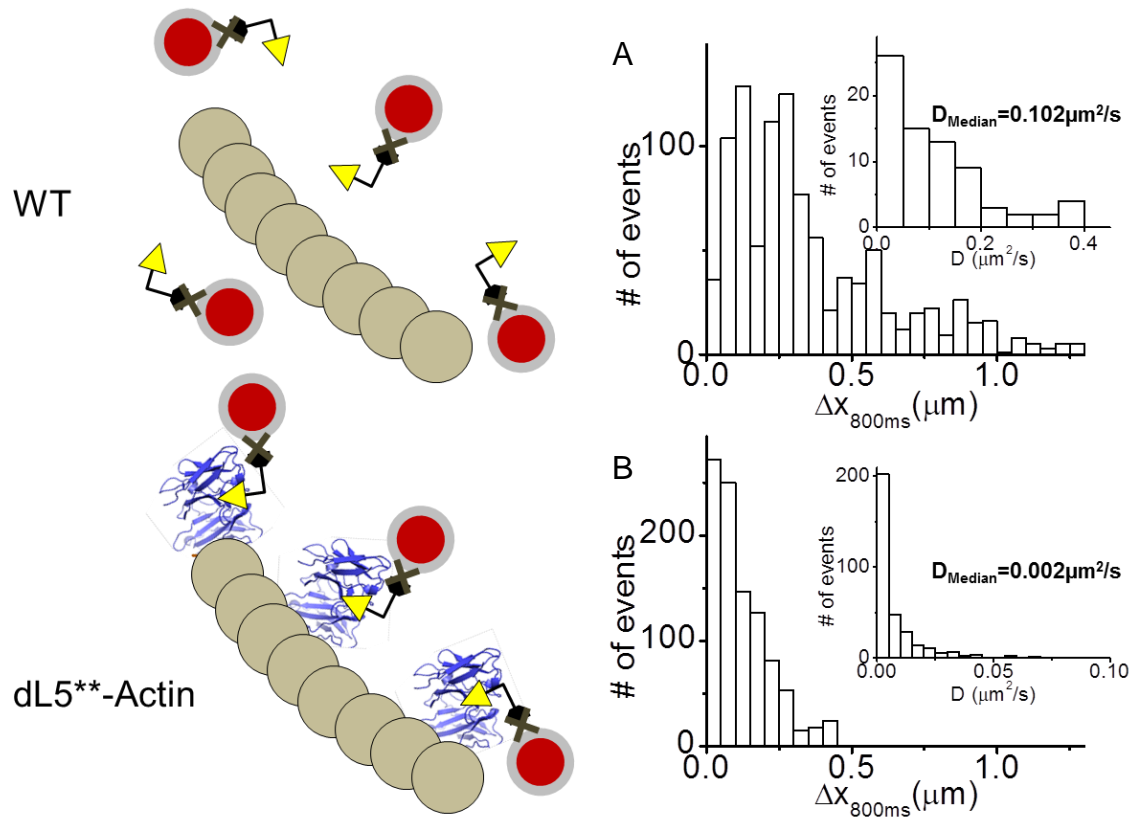


Figure 9. Distribution of the jumps in 800ms as well as diffusion coefficients for the MG-QD655 in WT HeLa cells (A) and HeLa cells expressing actin-dL5 labeled with MG-QD655 (B).**

Discussion

Here we have demonstrated a general genetic targeting and multiplexing approach using commercially available sav-QDs that is useful for specific and multiplexed labeling of genetically encoded tags. We have shown that the targeting using scFv-hapten complexes is specific and depends only on the scFv-hapten pair used. We have established a method for studying two different proteins on the cell surface simultaneously at high speeds (40FPS) and low exposure times (25ms), that can be further improved by using faster cameras and methods to spectrally separate fluorescence into more channels. In addition, we have delivered the MG-QD complexes into live cells for detection of single actin proteins in the cytoskeleton.

The immense selectivity of antibodies and a large structural diversity of haptens suggest that this method may be substantially extended beyond the three orthogonal targets demonstrated here. scFv proteins that recognize various dye molecules, peptides and drug-based haptens have been demonstrated with subnanomolar affinities.^{34, 35} Preparation of biotinylated analogs of these haptens is often required during the selection process, or readily achievable with simple chemical modification; and streptavidin conjugates of various nanoparticles are typically among the first bioconjugates prepared.⁵⁶ Together, these facts suggest that this approach could be rapidly expanded to new protein-hapten pairs and new particle chemistries for multiplexed imaging in biophysics and cell biology. High affinity intracellular protein-ligand complexes (e.g. the trimethoprim-eDHFR complex TMP-tag) may improve the approach for intracellular detection when combined with methods or chemistries that improve delivery of QDs into cells.^{45, 55, 57, 58}

Materials and methods

Yeast cell labeling using QD-Haptens

For yeast cell imaging, all strains (JAR200) were grown in 3 mL growth media (20g Dextrose, 5g Casamino acids, 1.7g Yeast nitrogen base, 5.3g Ammonium sulfate, 7.4g Sodium citrate, 2.2g Citric acid per liter at pH 4) at 30° C for 24 hours. 0.7 mL of yeast cells from the culture were induced in 35 mL of SG/R-CAA (1g Dextrose, 20g Raffinose, 20g Galactose, 5g Casamino acids, 1.7g Yeast nitrogen base, 5.3g Ammonium sulfate, 60mg Uracil per liter at pH 7.4) at 20° C for 72 hours. 1 mL of this culture was spun down and media was removed. Cells were then washed 3x with 1 mL PBS and incubated at 4° C for 2 hours in 100 μ L of PBS with 1 μ M biotin-hapten. Unbound hapten was then removed and cells were washed 2x with 1 mL PBS. Cells were then incubated at 4° C for 30 minutes in 20 μ L PBS with 50 nM QD-sav (Life Technologies, Inc). Unbound QD was then removed and cells were washed 1x with 1 mL PBS. Cells were then re-suspended in 100 μ L of PBS.

Pre-complexation approach using QD-Haptens

5nM QD-sav and 40 nM biotin-hapten were incubated at 4° C in 1 mL PBS for 30 minutes. The complex was then centrifuged in a 10000 MWCO spin filter (Microcon YM10) to remove unbound fluorogen. The retained complex was then added to cells and incubated as above. 20 μ L of the resuspended cells were then imaged in 2 mL PBS on glass bottom dishes (MatTek Corp) coated with concanavalin A.

Yeast cell imaging

Imaging was performed on an epi-fluorescence microscope (Nikon Ti Eclipse inverted microscope), using a planApo-chromat objective (60x, 1.45 N. A., Nikon). The samples were excited using DPSS lasers at 405nm and 488nm through a filter cube consisting of

a quad band excitation filter (405, 488, 561 and 639nm), a quad band dichroic and a 505 longpass emission filter (all from Chroma Technology). We used an additional emission filters for each QD such that the filter was a 20nm bandpass centered at the nominal QD emission peak, except for the 705 QDs that used a 680 nm longpass filter. Images were acquired using an EMCCD camera (iXon DV897, Andor technologies) with an EM gain of 250 and an exposure time of 50ms.

Plasmid and mammalian cell line preparation

pBabe-dL5^{**}-B2AR was generated by inserting the dL5 sequence to pBabeSacADRB2Lac2 using SfiI cutting sites. Stable HEK293 cells were generated by transfecting HEK293 cells with pBabe-dL5^{**}-β2-AR followed by drug selection (1 mg/ml puromycin, Invitrogen) and FACS enrichment (Becton Dickinson FACS Vantage flow cytometer. Excitation: 633 nm; Emission: 685/35 nm).

Mammalian Cell surface protein imaging

For mammalian cell imaging, a stable HEK293 cell population expressing B2AR-dL5^{**} chimera was transfected with HL1.0.1-PDGFR-TM plasmid DNA [3] using Lipofectamine 2000 transfection reagent (Life Technologies) as per the manufacturer's guidelines. Imaging was performed on the same system as above, utilizing 488nm excitation in the total internal reflection (TIR) mode. The microscope was equipped with a TIRF objective (100x, 1.49NA, Nikon) dual view DV2 splitter (Photometrics) consisting of a 625nm dichroic and two band pass filters (605/20 and 655/20, Chroma Technology). TO1-QD605 and MG-QD655 were used to label HL1.0.1-TM and dL5^{**} respectively. Images were acquired using the same EMCCD camera as above at an exposure time of 25ms. Single particle tracking and mean squared displacement analyses were performed using particle tracking code written in Matlab. For MSD analyses, no attempts were made to reconnect broken trajectories. As a result, for dense datasets such as 3S1, the mean

trajectory length was 18 frames compared to sparse datasets such as 3S2 where the mean was 443 frames.

Mammalian cell intracellular imaging

For imaging QDs inside the cells, micro-injection was performed in a HeLa cell line that expressed dL5** on actin. As a control, a HeLa cell line without the dL5** was used. Live cell imaging was done in a system with a motorized stage, on a Nikon Ti Eclipse inverted fluorescent microscope equipped with a 60X plan apo lens (Nikon Inc), fluorescent illuminator (89 North, Burlington, VT), CoolSNAP HQ2 camera (Photometrics) and NIS Elements 4.2. QD imaging was done using an EGFP long pass filter cube (Chroma, C49012) with emission optimized for QDs (either 685/70 or 585/20). Confocal sweptfield imaging was done using the same microscope platform and Andor DU-897 camera. Microinjection used Femtojet, Inject Man Ni 2, and Femtotips II (all by Eppendorf) . We successfully minimized issues of needle clogging by manual needle tip enlargement with brief contact with a cotton ball as suggested in Sutter Pipette Cookbook (Sutter Instrument Co, Novato, CA). Tracking and MSD analyses were done as described above.

Supplementary movies and Matlab codes for particle tracking can be found at <https://www.dropbox.com/sh/12t08ejbcmko4nc/rSuWrijP40h>

Bibliography

1. Tan, C.; Saurabh, S.; Bruchez, M. P.; Schwartz, R.; LeDuc, P., Molecular crowding shapes gene expression in synthetic cellular nanosystems. *Nature nanotechnology* **2013**, *8* (8), 602-608.
2. Irvine, D. J.; Purbhoo, M. A.; Krogsaard, M.; Davis, M. M., Direct observation of ligand recognition by T cells. *Nature* **2002**, *419* (6909), 845-849.
3. Manz, B. N.; Jackson, B. L.; Petit, R. S.; Dustin, M. L.; Groves, J., T-cell triggering thresholds are modulated by the number of antigen within individual T-cell receptor clusters. *Proceedings of the National Academy of Sciences* **2011**, *108* (22), 9089-9094.
4. Huse, M.; Klein, L. O.; Girvin, A. T.; Faraj, J. M.; Li, Q.-J.; Kuhns, M. S.; Davis, M. M., Spatial and temporal dynamics of T cell receptor signaling with a photoactivatable agonist. *Immunity* **2007**, *27* (1), 76-88.
5. Lakowicz, J. R., *Principles of fluorescence spectroscopy*. Springer: 2007.
6. Daniel, M.-C.; Astruc, D., Gold nanoparticles: assembly, supramolecular chemistry, quantum-size-related properties, and applications toward biology, catalysis, and nanotechnology. *Chem. Rev.* **2004**, *104* (1), 293-346.
7. Li, Z.; Barnes, J. C.; Bosoy, A.; Stoddart, J. F.; Zink, J. I., Mesoporous silica nanoparticles in biomedical applications. *Chem. Soc. Rev.* **2012**, *41* (7), 2590-2605.
8. Wu, X.; Wu, M.; Zhao, J. X., Recent development of silica nanoparticles as delivery vectors for cancer imaging and therapy. *Nanomed. Nanotechnol. Biol. Med.* **2014**, *10* (2), 297-312.
9. Laurent, S.; Forge, D.; Port, M.; Roch, A.; Robic, C.; Vander Elst, L.; Muller, R. N., Magnetic iron oxide nanoparticles: synthesis, stabilization, vectorization,

- physicochemical characterizations, and biological applications. *Chem. Rev.* **2008**, *108* (6), 2064-2110.
10. Akerman, M. E.; Chan, W. C. W.; Laakkonen, P.; Bhatia, S. N.; Ruoslahti, E., Nanocrystal targeting in vivo. *Proc. Natl. Acad. Sci. U.S.A.* **2002**, *99* (20), 12617-12621.
 11. Yigit, M. V.; Medarova, Z., In vivo and ex vivo applications of gold nanoparticles for biomedical SERS imaging. *Am. J. Nucl. Med. Mol. Imaging* **2012**, *2* (2), 232.
 12. Margus, H.; Padari, K. r.; Pooga, M., Insights into cell entry and intracellular trafficking of peptide and protein drugs provided by electron microscopy. *Adv. Drug Deliv. Rev.* **2013**, *65* (8), 1031-1038.
 13. Chen, F.; Gerion, D., Fluorescent CdSe/ZnS Nanocrystal-Peptide Conjugates for Long-term, Nontoxic Imaging and Nuclear Targeting in Living Cells. *Nano Lett.* **2004**, *4* (10), 1827-1832.
 14. Tan, W.; Donovan, M. J.; Jiang, J., Aptamers from Cell-Based Selection for Bioanalytical Applications. *Chem. Rev.* **2013**, *113* (4), 2842-2862.
 15. Penn, S. G.; He, L.; Natan, M. J., Nanoparticles for bioanalysis. *Curr. Opin. Chem. Biol.* **2003**, *7* (5), 609-615.
 16. Yang, X.; Boehm, J. S.; Yang, X.; Salehi-Ashtiani, K.; Hao, T.; Shen, Y.; Lubonja, R.; Thomas, S. R.; Alkan, O.; Bhimdi, T.; Green, T. M.; Johannessen, C. M.; Silver, S. J.; Nguyen, C.; Murray, R. R.; Hieronymus, H.; Balcha, D.; Fan, C.; Lin, C.; Ghamsari, L.; Vidal, M.; Hahn, W. C.; Hill, D. E.; Root, D. E., A public genome-scale lentiviral expression library of human ORFs. *Nat. Methods* **2011**, *8* (8), 659-61.
 17. Howson, R.; Huh, W. K.; Ghaemmaghami, S.; Falvo, J. V.; Bower, K.; Belle, A.; Dephoure, N.; Wykoff, D. D.; Weissman, J. S.; O'Shea, E. K., Construction,

- verification and experimental use of two epitope-tagged collections of budding yeast strains. *Comp. Funct. Genomics* **2005**, 6 (1-2), 2-16.
18. Bruchez, M.; Moronne, M.; Gin, P.; Weiss, S.; Alivisatos, A. P., Semiconductor Nanocrystals as Fluorescent Biological Labels. *Science* **1998**, 281 (5385), 2013-2016.
 19. Chan, W. C. W.; Nie, S., Quantum Dot Bioconjugates for Ultrasensitive Nonisotopic Detection. *Science* **1998**, 281 (5385), 2016-2018.
 20. Bruchez, M. P., Quantum dots find their stride in single molecule tracking. *Curr. Opin. Chem. Biol.* **2011**, 15 (6), 775-780.
 21. Pinaud, F.; Clarke, S.; Sittner, A.; Dahan, M., Probing cellular events, one quantum dot at a time. *Nat. Methods* **2010**, 7 (4), 275-285.
 22. Michalet, X.; Pinaud, F. F.; Bentolila, L. A.; Tsay, J. M.; Doose, S.; Li, J. J.; Sundaresan, G.; Wu, A. M.; Gambhir, S. S.; Weiss, S., Quantum Dots for Live Cells, in Vivo Imaging, and Diagnostics. *Science* **2005**, 307 (5709), 538-544.
 23. Dahan, M.; Levi, S.; Luccardini, C.; Rostaing, P.; Riveau, B.; Triller, A., Diffusion Dynamics of Glycine Receptors Revealed by Single-Quantum Dot Tracking. *Science* **2003**, 302 (5644), 442-445.
 24. Bhattacharyya, S.; Bhattacharya, R.; Curley, S.; McNiven, M. A.; Mukherjee, P., Nanoconjugation modulates the trafficking and mechanism of antibody induced receptor endocytosis. *Proc. Natl. Acad. Sci. U.S.A.* **2010**, 107 (33), 14541-14546.
 25. Tekle, C.; Deurs, B. v.; Sandvig, K.; Iversen, T.-G., Cellular trafficking of quantum dot-ligand bioconjugates and their induction of changes in normal routing of unconjugated ligands. *Nano Lett.* **2008**, 8 (7), 1858-1865.
 26. Biju, V.; Itoh, T.; Ishikawa, M., Delivering quantum dots to cells: bioconjugated quantum dots for targeted and nonspecific extracellular and intracellular imaging. *Chem. Soc. Rev.* **2010**, 39 (8), 3031-3056.

27. Iyer, G.; Michalet, X.; Chang, Y.-P.; Pinaud, F. F.; Matyas, S. E.; Payne, G.; Weiss, S., High Affinity scFv-Hapten Pair as a Tool for Quantum Dot Labeling and Tracking of Single Proteins in Live Cells. *Nano Lett.* **2008**, *8* (12), 4618-4623.
28. Roullier, V.; Clarke, S.; You, C.; Pinaud, F.; Gouzer, G. r.; Schaible, D.; Marchi- Artzner, V. r.; Piehler, J.; Dahan, M., High-affinity labeling and tracking of individual histidine-tagged proteins in live cells using Ni²⁺ tris-nitrilotriacetic acid quantum dot conjugates. *Nano Lett.* **2009**, *9* (3), 1228-1234.
29. Los, G. V.; Encell, L. P.; McDougall, M. G.; Hartzell, D. D.; Karassina, N.; Zimprich, C.; Wood, M. G.; Learish, R.; Ohana, R. F.; Urh, M.; Simpson, D.; Mendez, J.; Zimmerman, K.; Otto, P.; Vidugiris, G.; Zhu, J.; Darzins, A.; Klaubert, D. H.; Bulleit, R. F.; Wood, K. V., HaloTag: A Novel Protein Labeling Technology for Cell Imaging and Protein Analysis. *ACS Chem. Biol.* **2008**, *3* (6), 373-382.
30. Liu, D. S.; Phipps, W. S.; Loh, K. H.; Howarth, M.; Ting, A. Y., Quantum Dot Targeting with Lipoic Acid Ligase and HaloTag for Single-Molecule Imaging on Living Cells. *ACS Nano* **2012**, *6* (12), 11080-11087.
31. Howarth, M.; Takao, K.; Hayashi, Y.; Ting, A. Y., Targeting quantum dots to surface proteins in living cells with biotin ligase. *Proc. Natl. Acad. Sci. U.S.A.* **2005**, *102* (21), 7583-7588.
32. Cutler, P. J.; Malik, M. D.; Liu, S.; Byars, J. M.; Lidke, D. S.; Lidke, K. A., Multi-Color Quantum Dot Tracking Using a High-Speed Hyperspectral Line-Scanning Microscope. *PLoS One* **2013**, *8* (5), e64320.
33. Gao, X.; Yang, L.; Petros, J. A.; Marshall, F. F.; Simons, J. W.; Nie, S., In vivo molecular and cellular imaging with quantum dots. *Curr. Opin. Biotechnol.* **2005**, *16* (1), 63-72.

34. Szent-Gyorgyi, C.; Schmidt, B. F.; Creeger, Y.; Fisher, G. W.; Zakel, K. L.; Adler, S.; Fitzpatrick, J. A.; Woolford, C. A.; Yan, Q.; Vasilev, K. V., Fluorogen-activating single-chain antibodies for imaging cell surface proteins. *Nat. Biotechnol.* **2007**, *26* (2), 235-240.
35. Vaughan, T. J.; Williams, A. J.; Pritchard, K.; Osbourn, J. K.; Pope, A. R.; Earnshaw, J. C.; McCafferty, J.; Hodits, R. A.; Wilton, J.; Johnson, K. S., Human antibodies with sub-nanomolar affinities isolated from a large non-immunized phage display library. *Nat. Biotechnol.* **1996**, *14* (3), 309-14.
36. Szent-Gyorgyi, C.; Stanfield, R. L.; Andreko, S.; Dempsey, A.; Ahmed, M.; Capek, S.; Waggoner, A. S.; Wilson, I. A.; Bruchez, M. P., Malachite Green Mediates Homodimerization of Antibody VL Domains to Form a Fluorescent Ternary Complex with Singular Symmetric Interfaces. *J. Mol. Biol.* **2013**, *425* (22), 4595-4613.
37. Holleran, J.; Brown, D.; Fuhrman, M. H.; Adler, S. A.; Fisher, G. W.; Jarvik, J. W., Fluorogen-activating proteins as biosensors of cell-surface proteins in living cells. *Cytometry Part A* **2010**, *77A* (8), 776-782.
38. Grover, A.; Schmidt, B. F.; Salter, R. D.; Watkins, S. C.; Waggoner, A. S.; Bruchez, M. P., Genetically Encoded pH Sensor for Tracking Surface Proteins through Endocytosis. *Angew. Chem. Int. Ed.* **2012**, *51* (20), 4838-4842.
39. Parthasarathy, R., Rapid, accurate particle tracking by calculation of radial symmetry centers. *Nat. Methods* **2012**, *9* (7), 724-6.
40. Saxton, M. J., Single-particle tracking: the distribution of diffusion coefficients. *Biophys. J.* **1997**, *72* (4), 1744-53.
41. Michalet, X., Mean square displacement analysis of single-particle trajectories with localization error: Brownian motion in an isotropic medium. *Phys. Rev. E* **2010**, *82* (4), 041914.

42. Herrick-Davis, K.; Grinde, E.; Cowan, A.; Mazurkiewicz, J. E., Fluorescence Correlation Spectroscopy Analysis of Serotonin, Adrenergic, Muscarinic, and Dopamine Receptor Dimerization: The Oligomer Number Puzzle. *Mol. Pharmacol.* **2013**, *84* (4), 630-642.
43. Cao, T. T.; Deacon, H. W.; Reczek, D.; Bretscher, A.; von Zastrow, M., A kinase-regulated PDZ-domain interaction controls endocytic sorting of the β_2 -adrenergic receptor. *Nature* **1999**, *401* (6750), 286-290.
44. Valentine, C. D.; Haggie, P. M., Confinement of beta(1)- and beta(2)-adrenergic receptors in the plasma membrane of cardiomyocyte-like H9c2 cells is mediated by selective interactions with PDZ domain and A-kinase anchoring proteins but not caveolae. *Mol. Biol. Cell* **2011**, *22* (16), 2970-82.
45. Delehanty, J. B.; Mattoussi, H.; Medintz, I. L., Delivering quantum dots into cells: strategies, progress and remaining issues. *Anal. Bioanal. Chem.* **2009**, *393* (4), 1091-105.
46. Nabiev, I.; Mitchell, S.; Davies, A.; Williams, Y.; Kelleher, D.; Moore, R.; Gun'ko, Y. K.; Byrne, S.; Rakovich, Y. P.; Donegan, J. F.; Sukhanova, A.; Conroy, J.; Cottell, D.; Gaponik, N.; Rogach, A.; Volkov, Y., Nonfunctionalized nanocrystals can exploit a cell's active transport machinery delivering them to specific nuclear and cytoplasmic compartments. *Nano Lett.* **2007**, *7* (11), 3452-61.
47. Jaiswal, J. K.; Mattoussi, H.; Mauro, J. M.; Simon, S. M., Long-term multiple color imaging of live cells using quantum dot bioconjugates. *Nat. Biotechnol.* **2003**, *21* (1), 47-51.
48. Derfus, A. M.; Chan, W. C.; Bhatia, S. N., Intracellular delivery of quantum dots for live cell labeling and organelle tracking. *Advanced Materials* **2004**, *16* (12), 961-966.

49. Dubertret, B.; Skourides, P.; Norris, D. J.; Noireaux, V.; Brivanlou, A. H.; Libchaber, A., In vivo imaging of quantum dots encapsulated in phospholipid micelles. *Science* **2002**, *298* (5599), 1759-1762.
50. Medintz, I. L.; Pons, T.; Delehanty, J. B.; Susumu, K.; Brunel, F. M.; Dawson, P. E.; Mattoussi, H., Intracellular delivery of quantum dot⁺ protein cargos mediated by cell penetrating peptides. *Bioconjugate Chemistry* **2008**, *19* (9), 1785-1795.
51. Lei, Y.; Tang, H.; Yao, L.; Yu, R.; Feng, M.; Zou, B., Applications of mesenchymal stem cells labeled with Tat peptide conjugated quantum dots to cell tracking in mouse body. *Bioconjugate Chemistry* **2007**, *19* (2), 421-427.
52. Hoshino, A.; Fujioka, K.; Oku, T.; Nakamura, S.; Suga, M.; Yamaguchi, Y.; Suzuki, K.; Yasuhara, M.; Yamamoto, K., Quantum dots targeted to the assigned organelle in living cells. *Microbiology and immunology* **2004**, *48* (12), 985-994.
53. Gao, X.; Cui, Y.; Levenson, R. M.; Chung, L. W.; Nie, S., In vivo cancer targeting and imaging with semiconductor quantum dots. *Nature biotechnology* **2004**, *22* (8), 969-976.
54. Cai, W.; Chen, X., Preparation of peptide-conjugated quantum dots for tumor vasculature-targeted imaging. *Nature protocols* **2008**, *3* (1), 89-96.
55. Yum, K.; Na, S.; Xiang, Y.; Wang, N.; Yu, M.-F., Mechanochemical Delivery and Dynamic Tracking of Fluorescent Quantum Dots in the Cytoplasm and Nucleus of Living Cells. *Nano Lett.* **2009**, *9* (5), 2193-2198.
56. Goldman, E. R.; Balighian, E. D.; Mattoussi, H.; Kuno, M. K.; Mauro, J. M.; Tran, P. T.; Anderson, G. P., Avidin: A Natural Bridge for Quantum Dot-Antibody Conjugates. *J. Am. Chem. Soc.* **2002**, *124* (22), 6378-6382.
57. Jing, C.; Cornish, V. W., A Fluorogenic TMP-Tag for High Signal-to-Background Intracellular Live Cell Imaging. *ACS Chem. Biol.* **2013**, *8* (8), 1704-1712.

58. Xu, J.; Teslaa, T.; Wu, T. H.; Chiou, P. Y.; Teitell, M. A.; Weiss, S., Nanoblade delivery and incorporation of quantum dot conjugates into tubulin networks in live cells. *Nano Lett.* **2012**, *12* (11), 5669-72.

Chapter IV: Genetic targeting of cyanine dyes for photostable imaging

Introduction

Since the discovery of the first cyanine dye in 1856 by Greville Williams, the cyanine dyes have come a long way in their applications from photography to cell biology.¹ The immense commercial importance of cyanines for over a century stemmed from their ability to impart sensitivity of silver halide photographic plates in a region where they are not generally emissive.¹ Over the last few decades cyanines have found utility in inorganic semiconductor materials, optical disc recording, trapping solar energy, lasing, light harvesting systems, in photodynamic therapy, as membrane protein and DNA labels, and in superresolution microscopy on the account of their excellent photophysical properties.²⁻¹¹ Despite being among the oldest dye family, the development of cyanines tailored for a variety of biological applications remains an active research area.

The generic cyanine dyes consist of two nitrogen centers with one of the centers bearing a positive charge. Commonly employed nitrogen bearing systems are quinolone, indole, bezoxazole and benzothiazole.¹² The two ring centers are separated by a polymethine bridge containing an odd number of carbon atoms. This conjugated system for unsymmetrical cyanines exhibits a push-pull mechanism where the electrons delocalize from one side to the other and give rise to fluorescence. The dyes adopt all-trans geometry in their stable form and also undergo photoisomerization. The absorption and emission wavelengths of these dyes are a function of the number of carbon atoms in the polymethine system. In addition, the heterocyclic rings provide sites for derivatization of these dyes to change solubility, specificity and ease of conjugation.^{10, 13-16} The spectroscopic properties of Cy3 and Cy5 are summarized in Table 1.

Cyanines can form a variety of isomers through a rotation around the polymethine bridge.¹⁷ This structural property gives rise to one of the most interesting aspects in cyanine photophysics. As mentioned earlier, Cy3 and Cy5 exist in an all-trans configuration in the ground state. However, with sterically hindered thiacyanines containing bulky substituents in the polymethine chain, a solvent dependent equilibrium between the all-trans state and a mono-cis state has been observed.¹⁸ Rigidization of the methine chain, as in the case of Cy3B also inhibits the rotation.¹⁹ In an unhindered system, the cyanine dye goes to an all trans excited state upon light absorption. The singlet excited state depopulates through three competing pathways: fluorescence emission, internal conversion and a rotation around the C-C double bonds of the polymethine chain.^{20, 21} The efficiency of the photoisomerization depends on temperature, solvent viscosity and the presence of molecules that can create steric hindrance.²² The photoisomer is twisted and exhibits a very low quantum yield and deactivates rapidly to the ground state, in a mono-cis or an all-trans form with a branching ratio of 1:2 (trans:cis).²³ From the mono-cis form in the ground state, the photoisomer rapidly back isomerizes into an all trans state.

Cyanines are very sensitive to solvent polarity and a small Stokes shift and bathochromic shifts are observed as solvent polarity decreases.²⁴ Cyanines are also very sensitive to the presence of biomolecules in their vicinity. The attachment of a biomolecule to Cy3 or Cy5 can dramatically reduce the efficiency of photoisomerization thus leading to a higher quantum yield. For instance Cy3 covalently conjugated to immunoglobulin G shows a fivefold increase in the fluorescence lifetime and a bathochromic shift.²⁵ Similarly, the amino acid used to conjugate the Cy3 to a helicase protein can affect the quantum yield.²⁶ Cy3 conjugated to DNA also shows variations in photophysical properties. These variations depend on the linker used for attachment,

DNA sequence and the secondary structure.²⁷ As opposed to Cy3, Cy5 does not show drastic differences in the presence of biomolecules. For instance Cy3 conjugated to the beta subunit of F1-ATPase shows an eightfold enhancement in quantum yield whereas Cy5 bound to the gamma subunit of the same protein does not show any fluorescence enhancement.²⁸ The phenomenon of photoisomerization forms the basis of single molecule measurements such as Protein Induced Fluorescence Enhancement (PIFE) and STochastic Optical Reconstruction Microscopy (STORM).^{9, 29} Other dye families such as rhodamines, bodipy, oxazines and coumarins are quenched by nucleobases, in particular by guanine due to its high electron donating ability.³⁰ The cyanines, Cy3 and Cy5 however, are not quenched by the nucleobases due to their low electron accepting ability.³¹ Instead, these dyes show an enhancement in their fluorescence quantum yield in the presence of nucleobases due to stacking interactions that affect the isomerization aspect of the dyes.³²

Another very interesting property exhibited by cyanine dyes is aggregation that leads to marked changes in their absorption properties.³³ A hypsochromic shift is observed upon the dimerization of cyanines in aqueous solutions with a reduction in the main absorption band. At higher concentrations, a bathochromic shift known as the J band appears due to the formation of higher order aggregates.³⁴ The stacking of the dye molecules can be parallel (H aggregates) or head-to-tail (J aggregates).^{5, 35} The aggregates often have longer excited singlet state lifetimes but smaller fluorescence quantum yields. Thiocarbocyanines exhibit a tendency to aggregate that is proportional to the length of the polymethine chain.³⁶ Some dicarbocyanine dyes also dimerize in the minor groove of the DNA at alternating A-T sequences. These aggregates propagate by a cooperative end to end binding as the DNA structure prevents the dye molecules from stacking on the dimer.^{3, 37}

The cyanine dyes were initially developed to stain silver halide plates used in photography. For these reasons, aqueous solubility was not a requirement on these dyes. However, as their utility for labeling lipids and the possibility of labeling proteins was established owing to their excellent photophysical properties, water solubility became a key issue. In this regard, the development of Cy3 and Cy5 with sulfonate groups was a big step towards their use in cell biology. In addition to the sulfonate modification, other modifications have been targeted for site specific labeling of proteins. The NHS ester and maleimide derivatives of Cy3 and Cy5 are commercially available and tend to be the conjugates of choice for protein labeling.¹³⁻¹⁵

One of the main utilities of Cy3 and Cy5 as a dye pair has been in the area of single molecule FRET or single molecule PIFE experiments. The excellent FRET energy efficiency of the dye pair makes them a powerful tool for measuring distance based interactions of proteins and DNA.³⁸ In these experiments however, the photon demand is very high due to the single molecule observation aspects. Therefore, making these dyes efficient such that fluorescence becomes the most efficient pathway for deactivation from the excited singlet state, is of utmost importance. In this regard, extensive research has been done on the dye pair with a variety of redox agents and triplet state quenchers (TSQ) that we covered in detail in chapter 2.⁷ More recently, redox compounds and TSQs have been conjugated to Cy3 and Cy5 to obtain over a 100 fold enhanced photostability at a single molecule level.³⁹ While the photostability enhancement was established, a big unmet need is the genetic targeting of these dyes while preserving the photostability. In this regard, we developed approaches to screen for scFvs that could bind Cy3 and Cy5. Further, we developed methods to impart higher photostability to these dye-scFv complexes. In this chapter we will be discussing the screening method development and the preliminary results that indeed prove that these scFvs enhance the

dye photostability upon binding, thus solving two problems with one probe: genetic targeting and photostability enhancement.

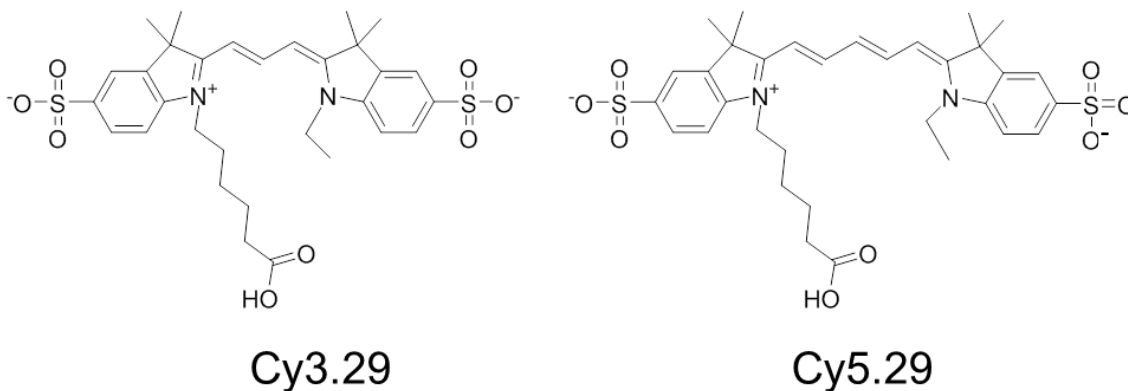


Figure 1. Structures of Cy3.29 and Cy5.29, the dyes used for screening the scFv library in this study.

Dye	ϵ ($M^{-1}cm^{-1}$)	λ_{max}^{abs} (nm)	λ_{max}^{em} (nm)	ϕ_F	τ (ns)
Cy3.29	150,000	560	575	0.09	0.16
Cy5.29	250,000	650	667	0.20	0.98

Table 1. Spectroscopic properties of Cy3.29 ad Cy5.29 the dyes used in this study. The extinction coefficients and quantum yields are reported in water while the fluorescence state lifetimes are reported in ethanol.^{12, 40}

Results

Screening of Cy3 and Cy5 binding clones

A yeast display library of scFvs in the pPNL6 vector with a diversity of 10^9 clones was utilized to screen for binders of Cy3 and Cy5.^{41, 42} The library was labeled at saturating concentrations of Cy3 and Cy5 (2 μ M) for the first round and at a 50nM dye concentration for the subsequent rounds of sorting using flow cytometry. For Cy3 binding clones, the cells were excited at 532 nm and the emission signal was collected at 585 nm with a 35 nm bandpass filter. For the Cy5 binding clones, a 639 nm laser was used and emission signal was collected at 685 nm with a 35 nm bandpass filter. 0.1% of the brightest clones were collected in every round. For the fourth round of sorting, the clones were labeled with an anti-myc antibody conjugated to Alexa 488. Clones that were positive for both Cy5 (or Cy3) and myc were selected from the fourth round.

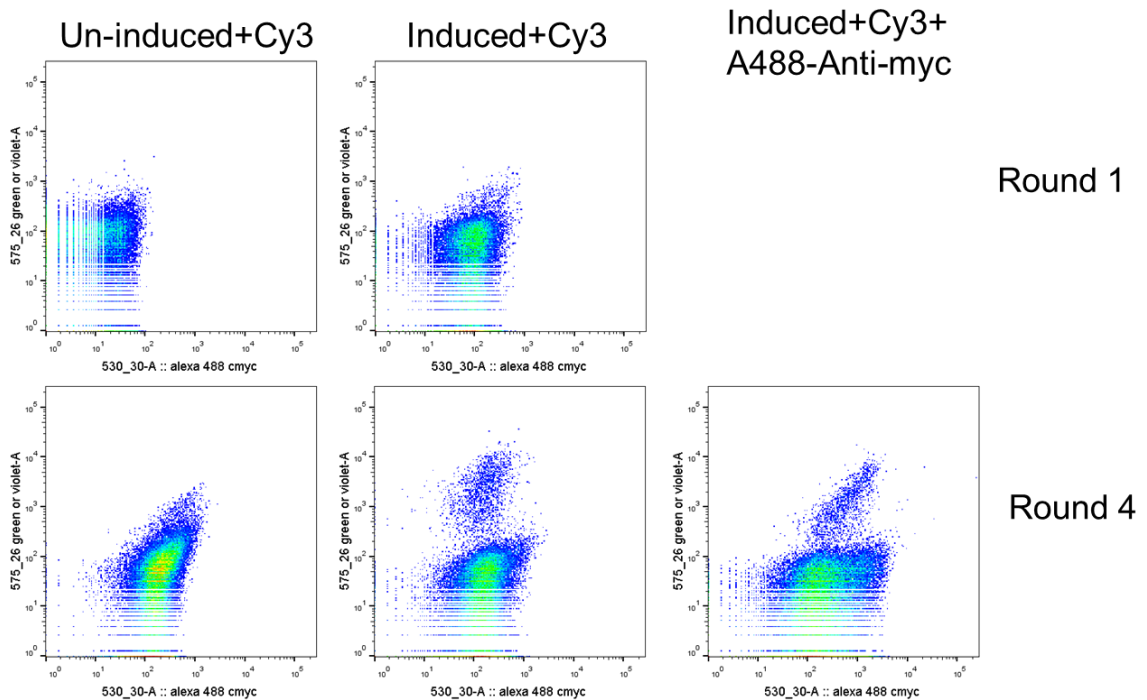


Figure 2. Progression of Cy3 binding clones between 4 rounds of sorting. For each round the top 0.1% cells were collected and induced for the next

round. The y axis shows the emission at 575/25 with 532nm excitation and the x axis shows an emission at 530/30 with 488nm excitation.

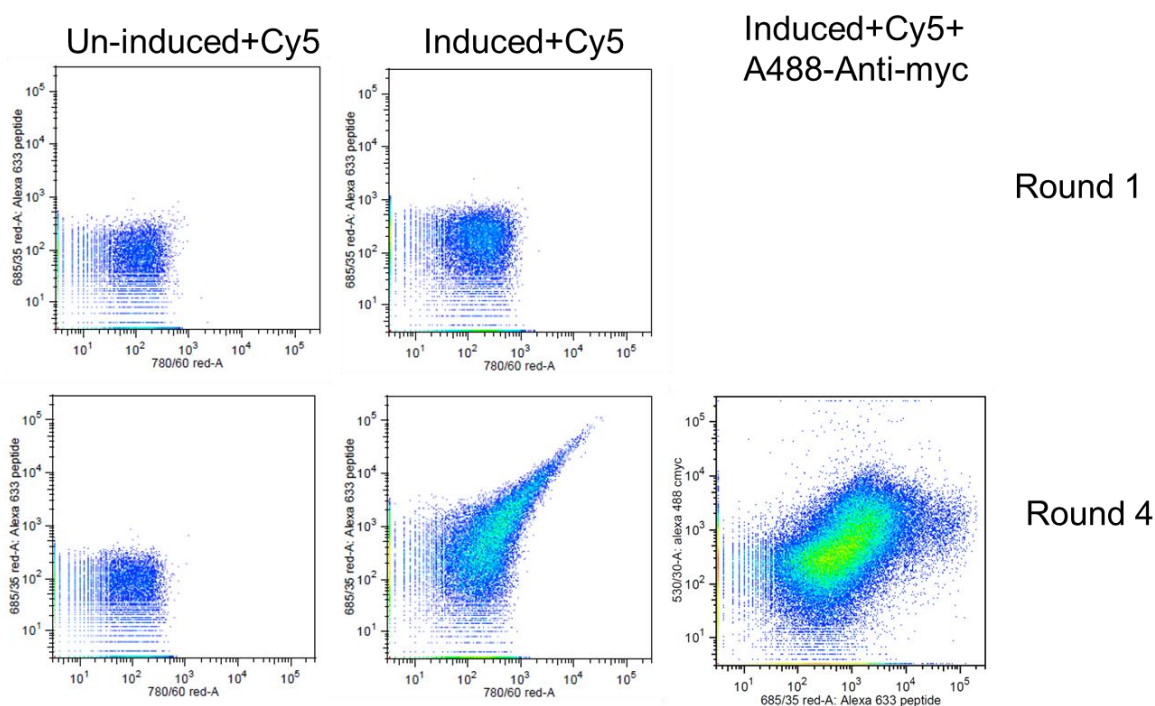


Figure 3. Progression of Cy5 binding clones between 4 rounds of sorting. For each round the top 0.1% cells were collected and induced for the next round. For the Un-induced and induced columns the y axis shows the emission at 685/35 nm and the x axis shows an emission at 780/60 nm with 635nm excitation. For the Induced control with anti-myc antibody, the y axis shows emission at 530/30 nm using a 488nm excitation and the x axis shows emission at 685/35 nm using a 635nm excitation.

The progression of Cy3 and Cy5 binding clones between four rounds is shown in Figures 2 and 3 respectively. While the screening method is time consuming, there are only two critical parameters to optimize. In order to obtain clones with a desired affinity, the dye labeling concentration should be set to this concentration after the first round of sorting. Additionally, the un-induced cells should be tested using this concentration of dye to ensure that there is no significant background signal. We performed a dose response with both Cy3 and Cy5 dyes with un-induced cells prior to sorting and did not

observe any background up to 5 μ M dye concentrations. However, this concentration varies from dye to dye and should be tested before screening.

Fluorescence spectroscopy of Cy3 and Cy5 binding yeast clones

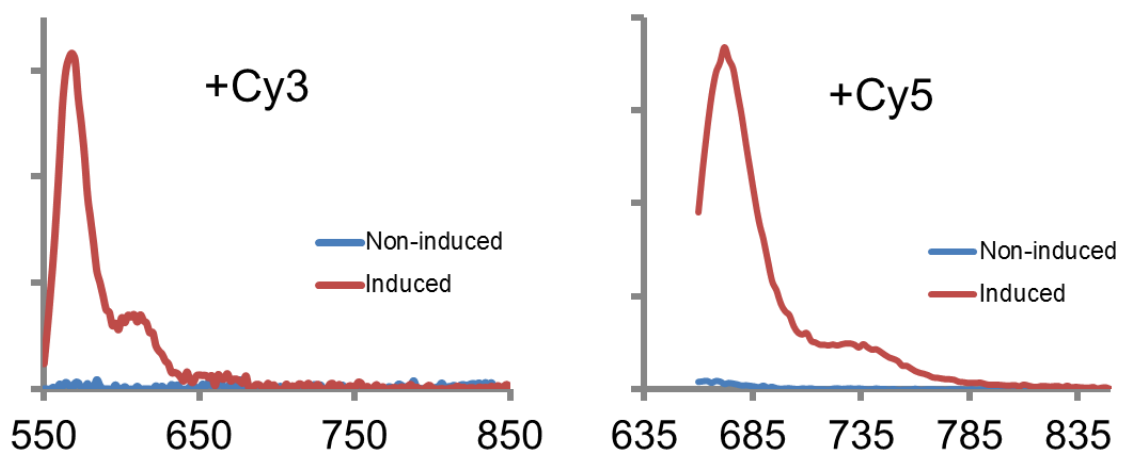


Figure 4. Emission spectra of yeast cell clones expressing clone PEPCy3 and PEPCy5 in the presence of 1 μ M Cy3 and Cy5 respectively. The cells were washed three times after incubation with the dye and the spectra were recorded in a 96 well format in a plate reader.

For the Cy5 binding clone, we obtained a library of 10^7 diversity by mutagenizing the clone DNA. We screened this library by biasing for enhanced photostability using the BleachSort approach that we discussed in chapter 2. We were able to obtain peptides that showed up to 8 fold photostability enhancement of Cy5. For the initially obtained Cy3 binding peptide we saw a threefold enhancement in photostability. We therefore named these peptides as Photostability Enhancing Peptides (PEP) for cy3 and Cy5, PEPCy3 and PEPCy5 respectively.

The selected dye binding clones were characterized spectrally on the JAR200 yeast cell surface. 10^7 cells were taken up in 1mL PBS (pH 7.4) and incubated with 500nM Cy3 or Cy5 for 1 hour at 4°C. As a control, un-induced cells that were not expressing the proteins on their surface were also incubated with the dye similarly. The

cells were washed three times and re-suspended in PBS. Fluorescence emission spectra were acquired in a 96 well plate using a Tecan infinite M1000 plate reader and are shown in Figure 4. Interestingly, the dyes binding to the proteins did not cause any significant red shift in the emission spectrum. Further, PEPCy3 expressing cells were labeled with Cy5 and PEPCy5 expressing cells were labeled with Cy3 to check for cross reactivity and the cells were imaged using an epi-fluorescence microscope. We see from the micrographs in Figure 5 that there is no cross labeling of dyes with these proteins. One may think that a protein pocket large enough to bind Cy5 may also bind Cy3. However, we see from the images that each protein pocket is specific to its own cognate dye.

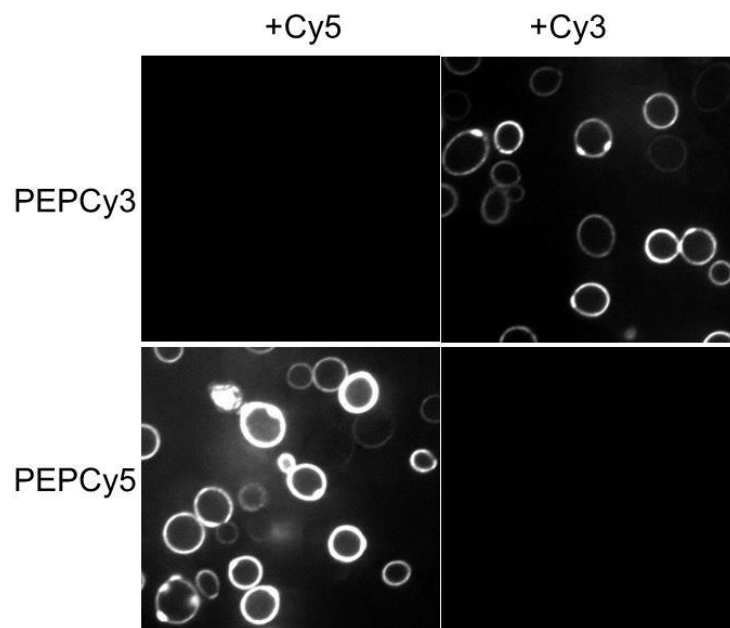


Figure 5. Fluorescence micrographs showing PEPCy3 and PEPCy5 expressing JAR200 yeast cells labeled with the respective dyes. As a control, cells expressing the protein dL5 were labeled with the dyes using the same protocol. These cells do not show any fluorescence signal corresponding to Cy3 or Cy5.

Following the characterization of the scFv-dye complexes on the yeast cell surface, we aimed at characterizing them in solution. For this, we attempted to purify the proteins using a pET21a vector for obtaining biotinylated proteins. The purified protein for Cy5 binding peptide was highly unstable and precipitated from even high salt buffers. Therefore, we performed equilibrium measurements on the surface of JAR200 yeast cells. The K_d obtained for PEPCy5 is 1.02nM as shown in Figure 6. For PEPCy3 we could not obtain a K_d on the cell surface and instead, used bio layer interferometry to measure it for purified protein-Cy3 complex.⁴³ We measured the K_d of this complex to be 2.1nM as shown in Figure 7. This also explains the inability to observe this K_d on the cell surface due to detection limit issues of the plate reader and the lower brightness of Cy3 compared to Cy5.

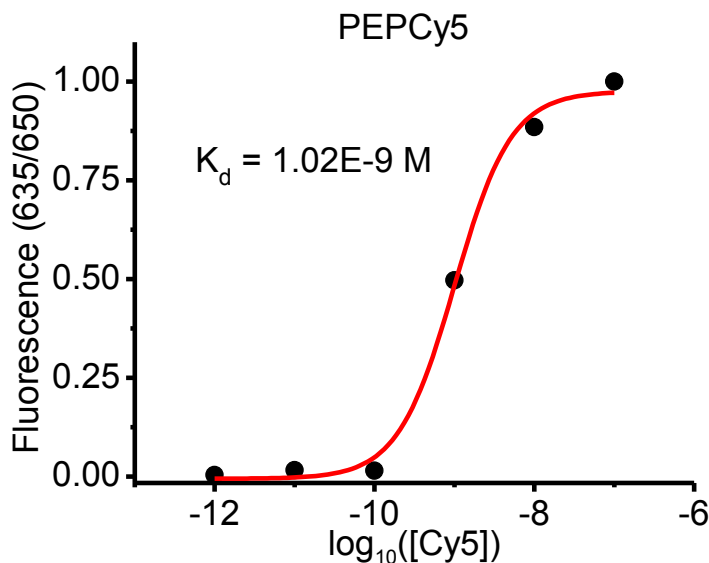


Figure 6. Cell surface K_d measurement for PEPCy5. 10^6 JAR200 cells were incubated with varying concentrations of Cy5 for 2 hours, followed by three washes with PBS (pH 7.4). The black dots are experimentally obtained points after subtraction of the signal from un-induced cells incubated with the respective dye concentrations. The red curve is the fit using a ligand depletion method.

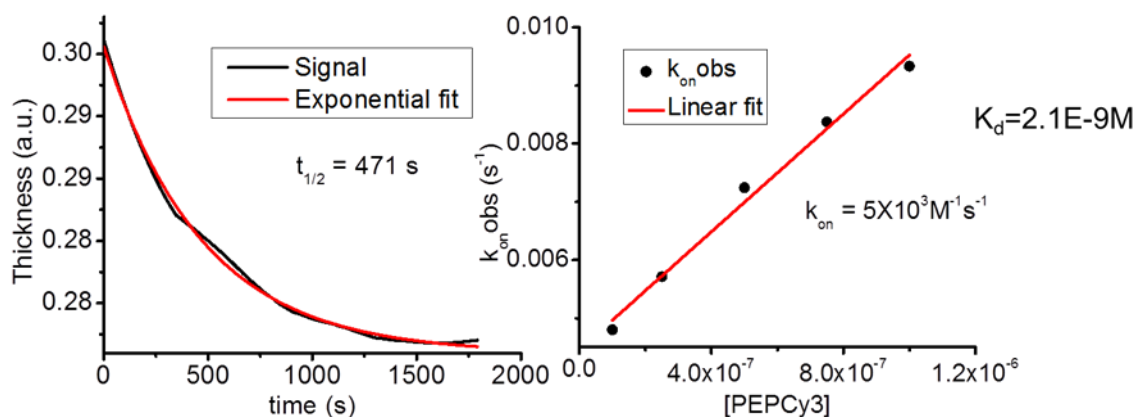


Figure 7. Off rate and on rate measurements of PEPCy3-Cy3 complex using bio-layer interferometry. The K_d was calculated using a ratio of the off and on rate.

Targeting other Cy3 and Cy5 derivatives

We were interested in testing whether PEPCy3 and PEPCy5 were capable of binding Cy3 and Cy5 with other functional groups and pH sensing capabilities. For this, we obtained four derivatives of the dye Cy3: Cy3pHSA, Cy3pHS, Cy3pHSSA and Cy3-COOH. The structures of these dyes are shown in Figure 8. Cy3pH dye series are pH sensitive with pKa values ranging from 6.6-7.8. The pKa values increased as the sulfonate (S) groups on the phenyl rings of Cy3 were replaced by sulfonamides (SA). PEPCy3 not only bound to the pH sensitive Cy3 molecules, but it also showed a pH dependent behavior on the yeast cell surface. Interestingly, we observe a peak at 650nm for the bis-Sulfonate derivative that is pH independent. Nevertheless, the peak at 567nm can be used to monitor pH and it opens the possibility for use of these peptides as pH sensors in the cell. The non sulfonated Cy3 free acid derivative also bound PEPCy3 and interestingly showed a slight pH response in the protein pocket. These results are shown in Figure 9. While more careful measurements need to be performed to understand the basis of this pH sensitivity of the Cy3 free acid, this experiment proves that the protein is

not affected by the charge on the Cy3 molecule and is solely dependent on the structure of the polymethine bearing part of the dye while being independent of the tail.

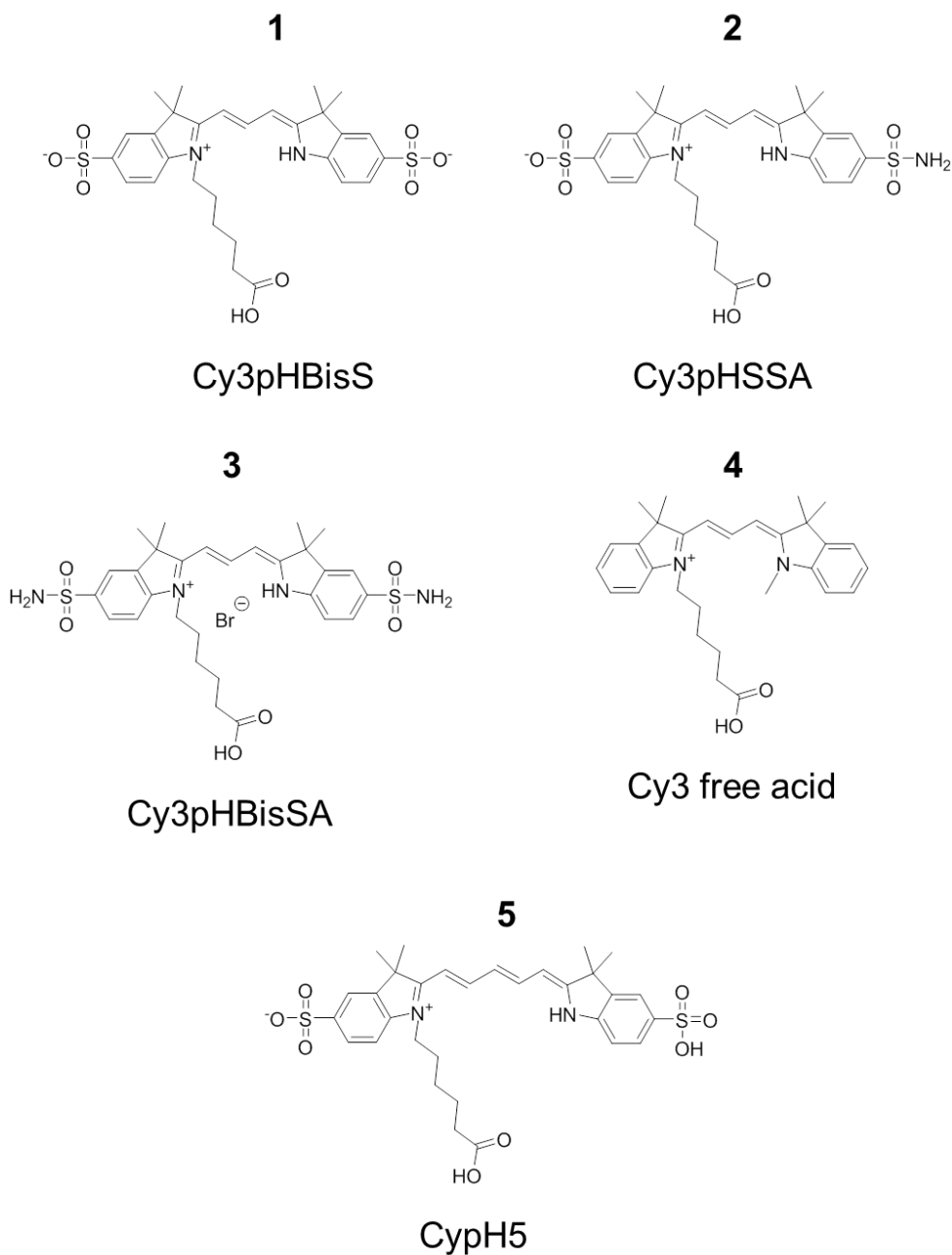


Figure 8. Structures of the Cy3 and Cy5 derivatives used in this study for testing binding to PEPCy3 and PEPCy5. Dyes provided by Brigitte Schmidt (MBIC).

A pH sensitive Cy5 derivative, CypH5 was used to test binding with PEPCy5. The peptide binds the dye and shows pH sensitivity in the pH4-8 range as seen in Figure 9. For both PEPCy3 and PEPCy5 these findings are significant since they indicate that the protein binding pocket does not affect the pH sensitivity of these dyes. Of course, a crystal structure of these complexes will clarify the dynamics of these complexes and inform us more about the pH sensitivity of these fluoromolecules.

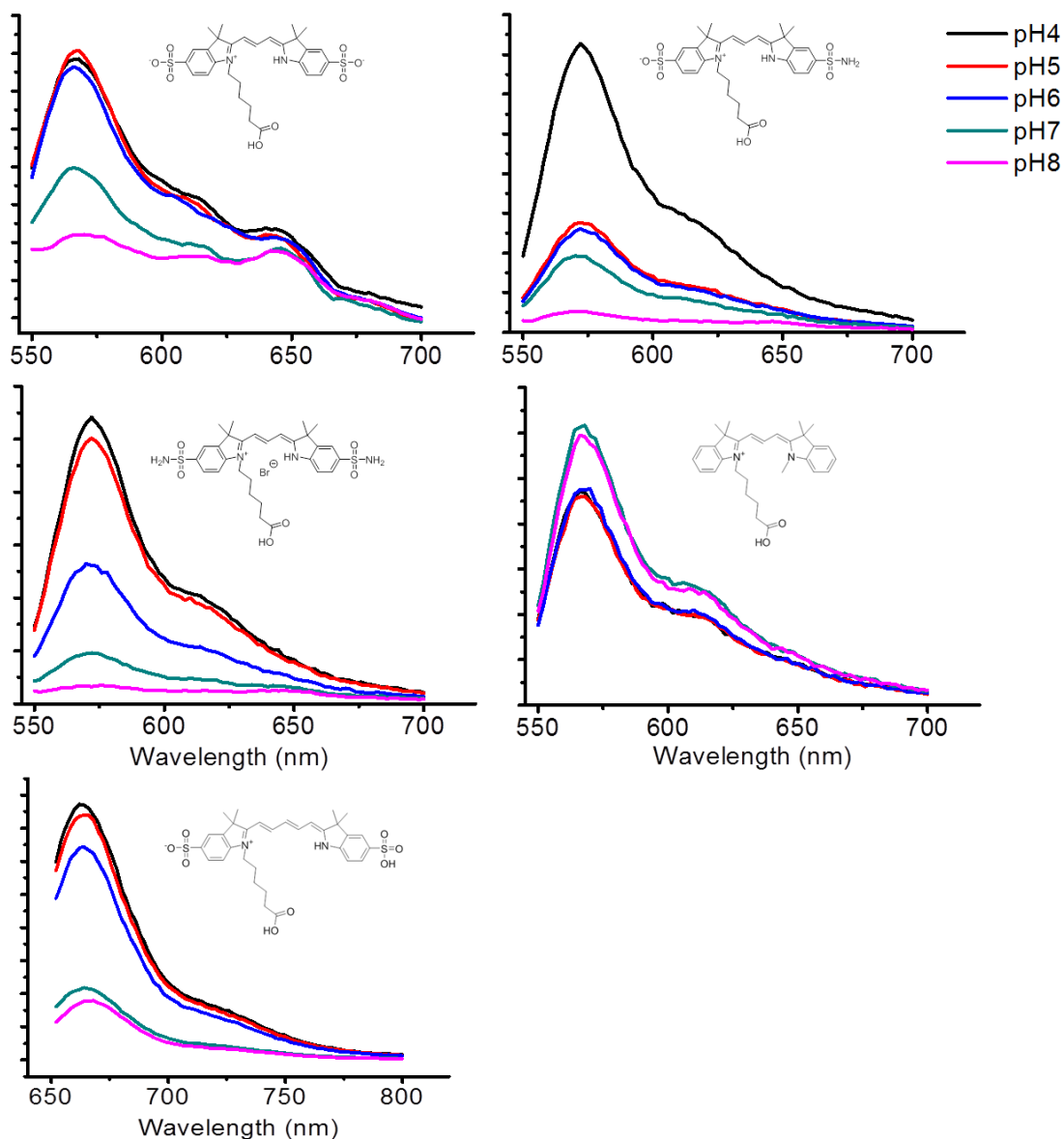


Figure 9. Emission spectra of yeast cell clones expressing clone PEPCy3 and PEPCy5 bound to various Cy3 and Cy5 dyes shown in Figure 6. The PEPCy3 expressing cells were excited at 532 nm with emission collected from 545 to 700 nm. For PEPCy5 expressing cells, excitation at 635 nm was used and emission signal was collected from 650 to 800 nm.

Mammalian cell studies using PEPCy3 and PEPCy5

After establishing the binding and equilibrium properties, we were interested in finding out what domain of the proteins was responsible for binding the dye. For this, we expressed the individual heavy and light domains with a 6-His tag in a yeast secretion vector (pPNL9) and tested their ability to bind dye on Ni-NTA beads.⁴⁴ We found that the heavy unit of PEPCy3 and the light unit of PEPCy5 were the units responsible for binding the respective dyes. Next, we imaged these proteins on the mammalian cell surface. For this, PEPCy3 and PEPCy5 were expressed in HEK293 cells as an Ig (K) signal peptide-PEP-CD80 fusion to provide plasma membrane targeting (Transfected cells provided by Ming Zhang, Waggoner Lab).

PEPCy3 expressing cells were incubated with 100nM Cy3 in the imaging media for 30 mins at 37°C. This was followed by washing the cells 2x and replacing the imaging media with dye-free medium. The cells looked healthy and were imaged on an epifluorescence microscope using a 532nm laser source. We can see very clearly from Figure 10 that the cells that are transfected are labeled with Cy3 and exhibit a very intense signal whereas the nearby non-transfected cells do not show any signal. This demonstrates that the PEPCy3 binding to Cy3 is a very specific interaction and can be used in various applications such as live cell imaging and flow cytometry.

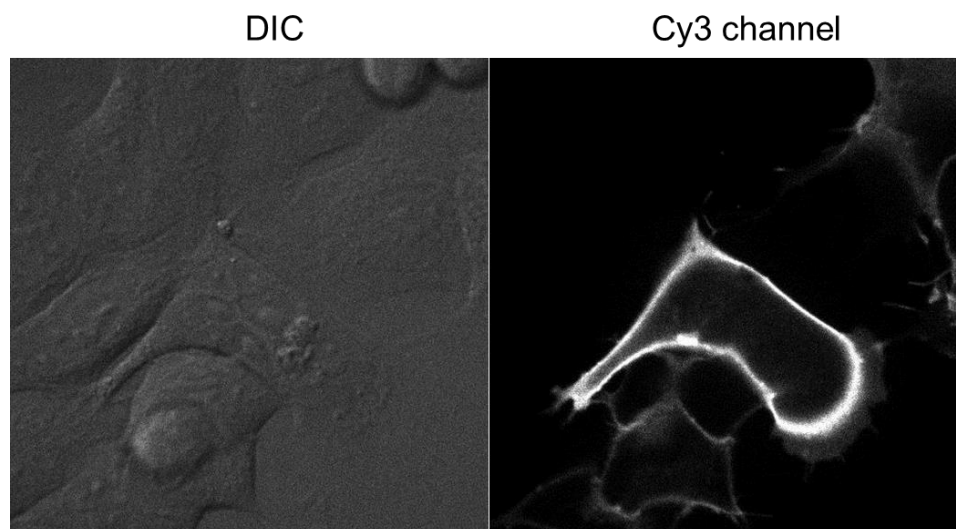


Figure 10. HEK293 cells transfected with the PEPCy3 plasmid on the cell surface labeled with 50nM Cy3 and imaged using an epi-fluorescence setup. The non-transfected cells in the vicinity of the transfected cells show no binding to the dye.

PEPCy5 expressing cells were labeled with 100 nM Cy5 using a similar protocol as used for the PEPCy3 cells. The cells were healthy and were also imaged using the epi-fluorescence setup but this time, with a 639nm laser excitation source. Again, we can see from Figure 11 that only the cells that have the PEPCy5 expression, bind the dye and the adjoining non-transfected cells do not show any signal from the dye. Having these two dyes expressed on the cell surface, now gives us the ability to perform two-color measurements on the cell surface. Additionally, for interacting proteins, we can potentially use the FRET between Cy3 and Cy5 to measure the distance between two interacting proteins on the cell surface.

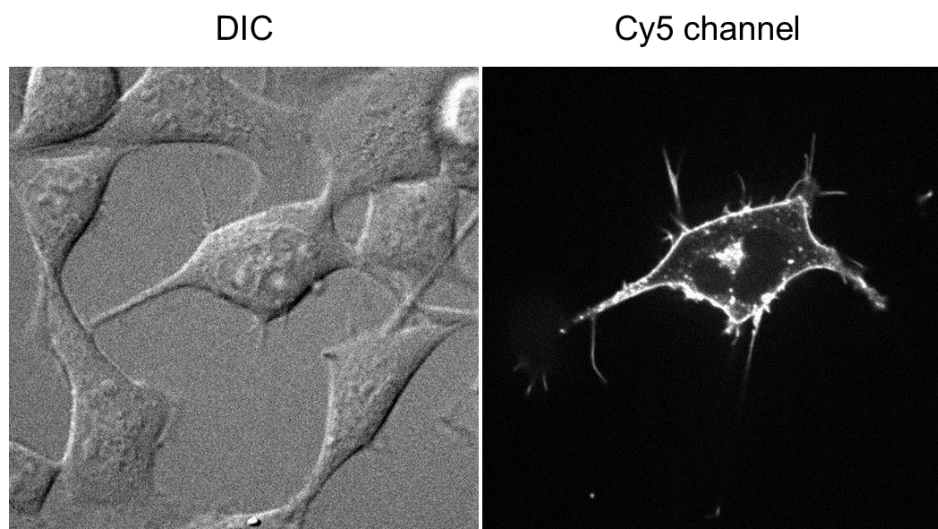


Figure 11. HEK293 cells transfected with the PEPCy5 plasmid on the cell surface labeled with 100nM Cy5 and imaged using an epi-fluorescence setup. The un-transfected cells in the vicinity of the transfected cells show no binding to the dye. We also notice some intracellular labeling due to dye uptake.

Live cell single molecule imaging using PEPCy3 and PEPCy5

As discussed earlier, the dyes Cy3 and Cy5 hold a very critical place in single molecule microscopy. Therefore, we wanted to study PEPCy3 and PEPCy5 complexes on the cell surface at a single molecule level. For this, we used the HEK293 cells expressing the PEPs and labeled the PEPCy3 expressing cells with 10pM dye for 10 mins and the PEPCy5 expressing cells with 50pM dye for 10 mins. The dye containing medium was replaced with warm dye free medium before imaging. Images were obtained on a TIRF microscope using the illumination and acquisition parameters for the respective dyes (materials and methods). The exposure times used for these measurements were 100ms. The proteins were sufficiently slow-diffusing to observe their motion on the cell surface using an EMCCD camera. We collected 1000 frames worth of data for each case and could use these tracks for single particle tracking. A maximum intensity projection of the first 5 frames is shown in Figure 12.

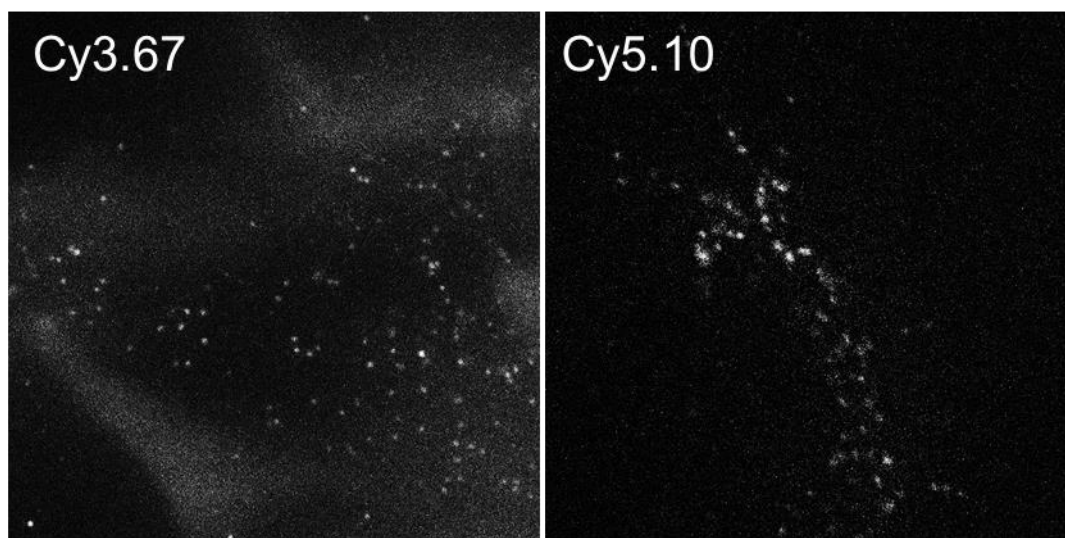


Figure 12. SM images of PEPCy3 and PEPCy5 on the HEK293 cell surface. The dyes appear at the bottom of the cells and not in adjacent cell-free regions.

The SPT algorithm used for tracking PEPCy3 and PEPCy5 molecules on HEK293 cell surface was similar to the one used in chapter 3 for tracking QDs. The molecules were bright and at least threefold over the background for PEPCy3 and fourfold over the background for PEPCy5.

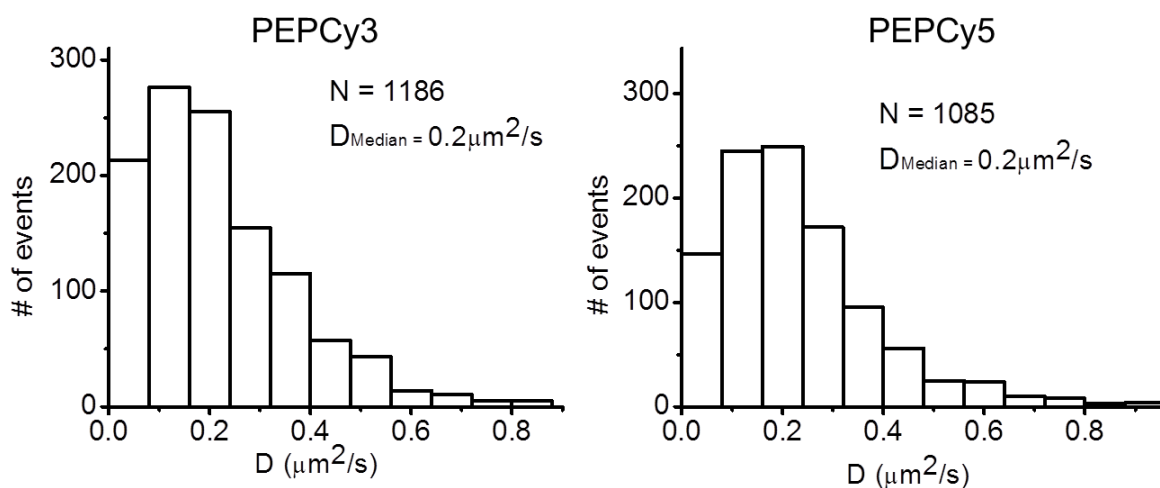


Figure 13. Diffusion coefficient for PEPCy3 and PEPCy5 expressed on the surface of HEK293 cells. Over 1000 tracks were used to obtain the diffusion coefficient from the MSD analyses.

MSD analyses were performed on the single tracks and diffusion coefficients for these two complexes on the cell surface were calculated to be $0.2 \mu\text{m}^2/\text{s}$, as shown in Figure 13. Therefore, we have proven the utility of the Cy3 and Cy5 binding peptides in single molecule imaging on the cell surface.

Photostability enhancement of Cy3 and Cy5 bound to PEPs

The principal motivation behind screening for Cy3 and Cy5 binding peptides was the encapsulation hypothesis for photostability enhancement. We asked how photostable these clones were at a single molecule level. Ensemble measurements with these probes were challenging since we did not see a significant difference in the brightness upon the dye binding to the protein on the cell surface. Therefore we compared biotinylated Cy3 and Cy5 analogues that were pre-complexed with streptavidin in a 1:1 ratio to the single PEP complexes on the HEK cell surface.

It is challenging to extract the total number of photons emitted from a rapidly moving single molecule diffusing in solution, therefore, we used another parameter; the number of fluorophores observed/ frame to quantify photostability. The idea here being that for a comparable number of molecules in the first frame, faster bleaching species will lose the molecules rapidly and the number of molecules/ frame will go down rapidly. The streptavidin-Biotin-Cy3 and Cy5 dyes were immobilized on a Biotin-PEG decorated glass surface. They were illuminated with the same excitation flux and the acquisition settings were kept constant for the live cell imaging and the in vitro imaging. We can see from Figure 14 that for PEPCy3 the number of molecules per frame decreases exponentially as a function of time. This exponential decay has a half-life of 27 s as compared to Biotin-Cy3 bound to streptavidin that shows a half-life of 10 s. It should be noted that the Cy3 binding peptide was not mutagenized further or screened with a BleachSort method. This is because the mutagenesis was not successful several times

and we could not obtain a diverse library using this clone. For PEPCy5, which was screened using the BleachSort method, we find the same exponential decay with a half-life of 43 s compared to a half-life of 5 s for Biotin-Cy5 bound to streptavidin, as shown in Figure 15. While these results are somewhat less quantitative than photon emitted before photobleaching measurements that can be performed with purified proteins, they give us an idea of the photostability of these complexes under real time live cell imaging conditions.

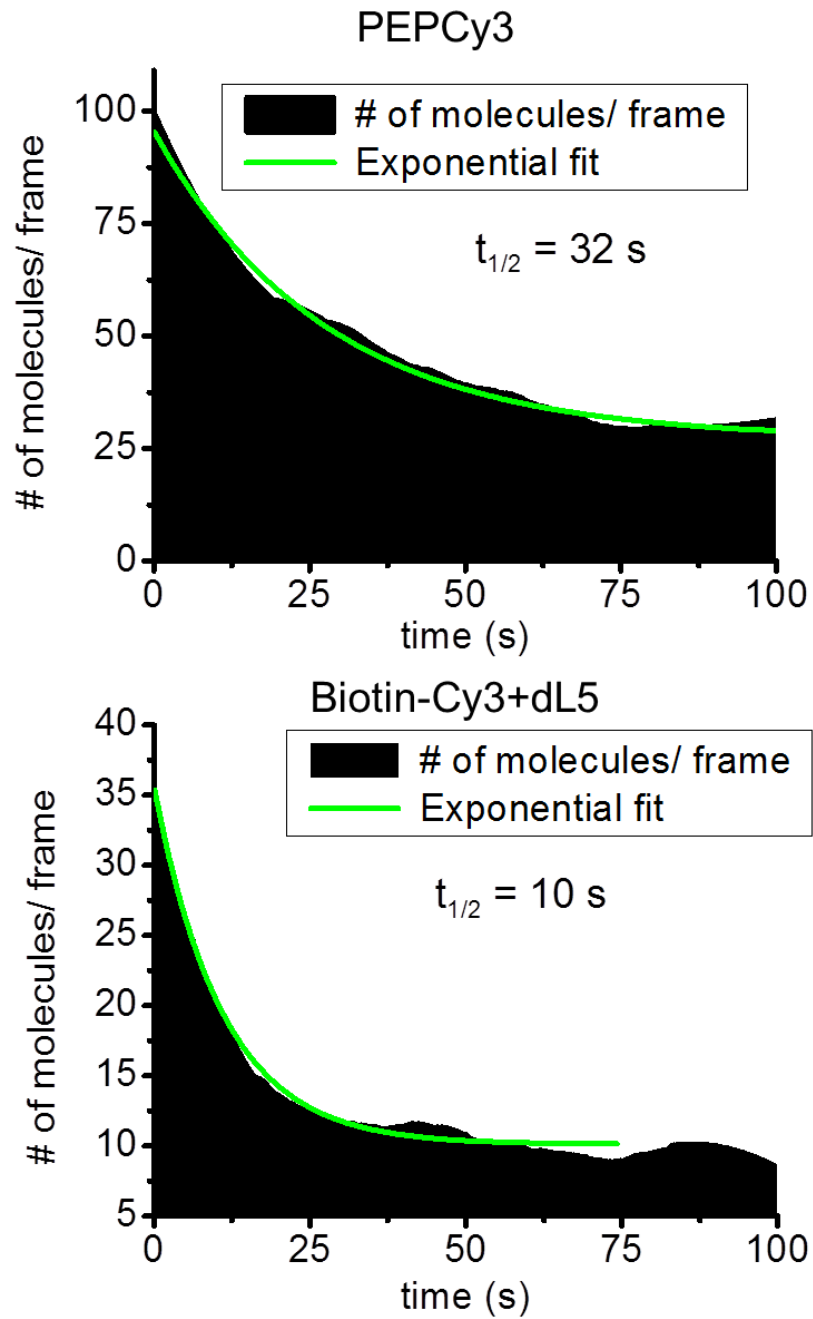


Figure 14. Number of molecules per frame for PEPCy3 on the HEK293 cell surface and Biotin-Cy3 bound to streptavidin on a PEG decorated glass surface.

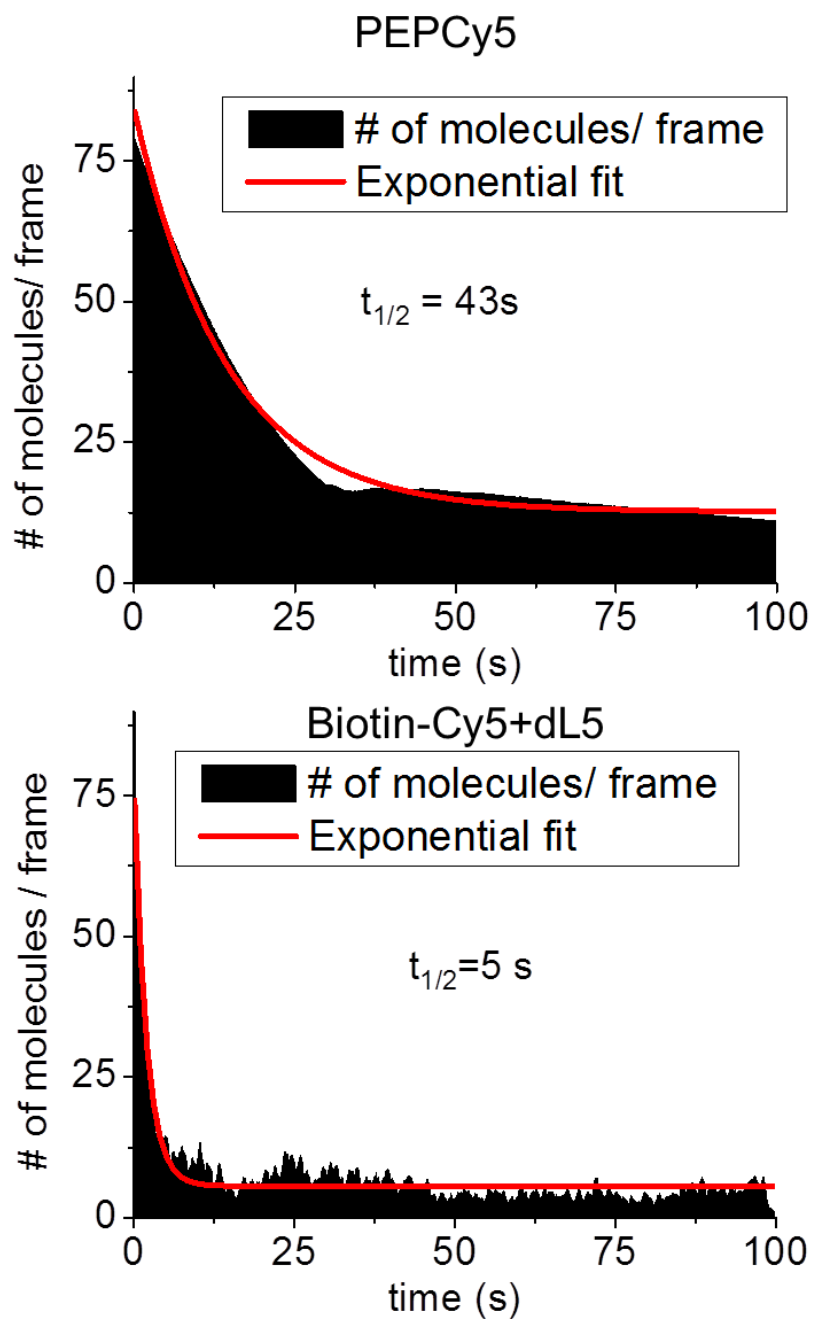


Figure 15. Number of molecules per frame for PEPCy5 on the HEK293 cell surface and Biotin-Cy5 bound to streptavidin on a PEG decorated glass surface.

PEP	MW (kDa)	Binding domain	K_d (nM)	$\lambda_{\max}^{\text{abs}}$ (nm)	$\lambda_{\max}^{\text{em}}$ (nm)	PS ^a (fold)
Cy3	14.7	V _H	2.10 ^b	560	575	3
Cy5	11.5	V _L	1.02 ^c	650	667	8

^a : Fold photostability (PS) enhancement compared to biotin conjugates of Cy3.29 and Cy5.29 in the presence of dL5, a non-cognate protein

^b : Measured with purified protein using bio-layer interferometry

^c : Measured on JAR200 cell surface using a fluorescence plate reader

Table 2. Physical and spectroscopic properties of Cy3.29 and Cy5.29 the dyes used in this study. The extinction coefficients and quantum yields are reported in water while the fluorescence state lifetimes are reported in ethanol

Discussion

Cyanines have undergone several breakthroughs in their development from the discovery over a hundred and fifty years ago. Improving solubility, functionalization to enable bio-conjugation and photostability enhancement have been the three major improvements that enabled live cell single molecule imaging. However, there is no single approach available until now that addresses the genetic targeting of Cy3 and Cy5 while enhancing their photostability. We have reported in this chapter, a first of its kind approach that not only targets the dyes to proteins of interest but also enhances their photostability. The properties of these tags are summarized in table 2. We have used these constructs for imaging on the yeast and mammalian cell surfaces at ensemble and single molecule levels. The small size of these tags is an added advantage and may be suitable for fusing to proteins of interest without any perturbations. The labeling approach using these tags is much simpler than dye conjugated antibodies and does not require rigorous washing. Finally, it can be extended to Cy3 and Cy5 derivatives for pH sensing measurements as well.

While we have established the labeling technology and its utility in cell imaging applications, several aspects of the PEP-Dye binding need to be investigated. For this we are trying to optimize the protein with additional tags such as the glutathione S-transferase (GST) to make the proteins more soluble in vitro. Bio-layer interferometry measurements need to be performed on these purified proteins to obtain K_d values in vitro. The purified proteins will also enable the comparison of these complexes with Cy3 and Cy5 in properties such as molecular brightness and photons absorbed before photobleaching. Finally, from an applications standpoint, testing of protein binding to the Redox and TSQ conjugated photostable Cyanine dyes will be very important. If these

proteins bind the dyes, it may be the most photostable organic dye based genetically targeted probe yet reported.

Materials and methods

Flow cytometry protocols

For flow cytometry the a library of JAR200 cells with a diversity of 10^9 was grown in 500 mL growth media (20g Dextrose, 5g Casamino acids, 1.7g Yeast nitrogen base, 5.3g Ammonium sulfate, 7.4g Sodium citrate, 2.2g Citric acid per liter at pH 4) at 30° C for 24 hours. The cells were spun down and transferred to induction medium and were induced in 35 mL of SG/R-CAA (1g Dextrose, 20g Raffinose, 20g Galactose, 5g Casamino acids, 1.7g Yeast nitrogen base, 5.3g Ammonium sulfate, 60mg Uracil per liter at pH 7.4) at 20° C for 72-96 hours. As a control experiment, un-induced cells were incubated with Cy3 and Cy5 concentrations ranging from 10nM to 5 μ M to test the background. No background was observed with 3x washes with PBS up to 2 μ M dye concentration for both Cy3 and Cy5. For the first round of FACS, 10^{10} cells were incubated with 1 μ M dyes in PBS (pH7.4) supplemented with EDTA for 2 hours at 4 °C. The cells were washed 3x with PBS and sorted using a FACSDiva cell sorter (BD Biosciences). The top 0.1% brightest cells were collected, cultured and induced using the same protocol as above for subsequent rounds. For rounds 2 through 4, the dye concentration for incubation was reduced to 50nM and cells were sorted with the same thresholds. After the fourth round of screening, cells positive for Cy3 and a myc tag were cloned on SD-CAA plates and used for downstream experiments. From the initial Cy5 binding clone, a library was created by random mutagenesis. This library was screened again with the BleachSort technique to yield the clone PEPCy5. No BleachSort was performed for the PEPCy3 clone.

Spectroscopy measurements

Cell surface spectra were acquired on the JAR200 cells expressing PEPCy3 and PEPCy5. The clones were grown and induced as above and incubated with 500nM Cy3

or Cy5 for 1 hour at 4°C. The cells were washed 3x with PBS+EDTA and resuspended in 500µL of PBS (pH7.4). A 250µL aliquot of cells was transferred to a 96-well, flat bottom transparent plate (Greiner, Cellstar) and fluorescence was measured from these cells using a Tecan infinite M1000 plate reader using respective excitation and emission parameters for Cy3 and Cy5. Another 100µL of the labeled cells were plated on glass bottom dishes coated with Concanavalin A. The cells were allowed to adhere to the surface by incubating for 20 mins. The dish was washed to remove any non-adherent cells and was filled with 2mL of PBS (pH7.4). Imaging was performed on a Nikon Ti Eclipse inverted epi-fluorescence microscope using solid state laser illumination at 532nm (PEPCy3) and 639nm (PEPCy5) and appropriate emission filter sets.

Single molecule mammalian imaging

The genes required for making trans-membrane constructs of PEPCy3 and PEPCy5 were assembled via PCR using overlapping primers, with the Ig(kappa) signal sequence and PEP (Heavy chain domain for Cy3 and Light chain domain for Cy5) fused to nucleotides encoding residues 237 to 306 of murine CD80. The resulting open reading frame was cloned into pEGFP-N1 (Clontech) between native NheI and XmaI sites to produce plasmids pOIU0367HN and pOIU0510LN, respectively. HEK293 cells at post-thaw passage 5 were transfected using TransIT LT1 (Mirus Bio LLC, Madison WI) in accordance with manufacturer-supplied protocols for transfection in a 6-well tray format. PEP-expressing cells were used for imaging two to four days post-transfection. Stable clones were isolated via FACS after two weeks of constant selection with G-418 (Research Products International Corp., Mount Prospect IL) at a concentration of 500 µg/mL. Cells were imaged using the setup described above for epi-fluorescence. For single molecule imaging the same microscope was used in a total internal reflection mode. Single particle tracking and mean squared displacement analyses were

performed using particle tracking code written in Matlab. For MSD analyses, no attempts were made to reconnect broken trajectories.

Proteins sequences

Peptide sequence of the binding domain of the PEPCy3 and PEPCy5 proteins are as follows:

PEPCY3

EVQLVESGGDLVQPGRSLRLSCTASGFPPFDYAITWFRQAPGKGLEWVGFIRSKPFG
GTTEYAASVRGRFTISRDDSKSIAYLQMNSLKAGDTAVYYCTRFSPFHNDRGVYSRDD
AFDIWGQGTMTVSSGILGS

PEPCy5

EIVLTQSPATLSLSPGDRATLSCRTSQSVSHHLAWYQQKPGQAPRLLIYGASNRATGIP
DRFSGSGSGTDFTLTISRLEPEDFAVYYCQQSPAFGQGTKVEIKSGIL

Initial clone selected prior to BleachSort for binding Cy5 was named M13. The alignment of **M13** with PEPCy5 is as follows:

QVQLQQSGPGLVKPSQTLSTCVISGDSVSSSSAAWNWIRQSPARGLEWLGRTYYRA
QVQLQQSGPGLVKPSQTLSHLCHLRGQCLKQQCCLELGQAVPARGLEWLGRTYYRA
KWYHDYVLSAKSRITINPDTSKNQFSLQLSSVTPEDTAVYYCARTPGYSIGWPYFFDQ
KWYHDYVLSAKSRITINPDTSKNQFPLQLSSVTPEDTAVYYCARTPGYSIGWPYFFDQ
WGQGTLVTVSSGILGSGGGGSGGGGSGGGGSEIVLTQSPATLSLSPGDRATLSCRAS
WGQGTLVTVSSGILGSGGGGSGGGGSGGGGSEIVLTQSPATLSLSPGDRATLSCRTS
QSVSHHLAWYQQKPGQAPRLLIYGASNRATGIPDRFSGSGSGTDFTLTISRLEPEDFAV
QSVSHHLAWYQQKPGQAPRLLIYGASNRATGIPDRFSGSGSGTDFTLTISRLEPEDFAV
YYCQQSPAFGQGTKVEIKSGIL

YYCQQSPAFGQGTKVEIKSGIL

Bibliography

1. Doja, M. Q., The Cyanine Dyes. *Chemical Reviews* **1932**, 11 (3), 273-321.
2. Ehret, A.; Stuhl, L.; Spitler, M., Spectral sensitization of TiO₂ nanocrystalline electrodes with aggregated cyanine dyes. *The Journal of Physical Chemistry B* **2001**, 105 (41), 9960-9965.
3. Hannah, K. C.; Armitage, B. A., DNA-templated assembly of helical cyanine dye aggregates: a supramolecular chain polymerization. *Accounts of chemical research* **2004**, 37 (11), 845-853.
4. Ishchenko, A. A., Laser media based on polymethine dyes. *Quantum Electronics* **1994**, 24 (6), 471-492.
5. Mishra, A.; Behera, R. K.; Behera, P. K.; Mishra, B. K.; Behera, G. B., Cyanines during the 1990s: a review. *Chemical Reviews* **2000**, 100 (6), 1973-2012.
6. Pass, H. I., Photodynamic therapy in oncology: mechanisms and clinical use. *Journal of the National Cancer Institute* **1993**, 85 (6), 443-456.
7. Rasnik, I.; McKinney, S. A.; Ha, T., Nonblinking and long-lasting single-molecule fluorescence imaging. *Nature methods* **2006**, 3 (11).
8. Roy, R.; Hohng, S.; Ha, T., A practical guide to single-molecule FRET. *Nature methods* **2008**, 5 (6), 507-516.
9. Rust, M. J.; Bates, M.; Zhuang, X., Sub-diffraction-limit imaging by stochastic optical reconstruction microscopy (STORM). *Nature methods* **2006**, 3 (10), 793-796.
10. Waggoner, A., Optical probes of membrane potential. *The Journal of membrane biology* **1976**, 27 (1), 317-334.

11. Wang, M.; Silva, G. L.; Armitage, B. A., DNA-templated formation of a helical cyanine dye J-aggregate. *Journal of the American Chemical Society* **2000**, *122* (41), 9977-9986.
12. Levitus, M.; Ranjit, S., Cyanine dyes in biophysical research: the photophysics of polymethine fluorescent dyes in biomolecular environments. *Quarterly reviews of biophysics* **2011**, *44* (01), 123-151.
13. Mujumdar, R. B.; Ernst, L. A.; Mujumdar, S. R.; Waggoner, A. S., Cyanine dye labeling reagents containing isothiocyanate groups. *Cytometry* **1989**, *10* (1), 11-19.
14. Mujumdar, S. R.; Mujumdar, R. B.; Grant, C. M.; Waggoner, A. S., Cyanine-labeling reagents: sulfobenzindocyanine succinimidyl esters. *Bioconjugate chemistry* **1996**, *7* (3), 356-362.
15. Southwick, P. L.; Ernst, L. A.; Tauriello, E. W.; Parker, S. R.; Mujumdar, R. B.; Mujumdar, S. R.; Clever, H. A.; Waggoner, A. S., Cyanine dye labeling reagents—carboxymethylindocyanine succinimidyl esters. *Cytometry* **1990**, *11* (3), 418-430.
16. Waggoner, A. S., Cyanine dyes as labeling reagents for detection of biological and other materials by luminescence methods. Google Patents: 1997.
17. Kolesnikov, A.; Mikhailenko, F., The conformations of polymethine dyes. *Russian Chemical Reviews* **1987**, *56* (3), 275.
18. Khimenko, V.; Chibisov, A. K.; GÄ¶rner, H., Effects of alkyl substituents in the polymethine chain on the photoprocesses in thiocarbocyanine dyes. *The Journal of Physical Chemistry A* **1997**, *101* (39), 7304-7310.
19. Mujumdar, R. B.; Waggoner, A. S., Rigidized trimethine cyanine dyes. Google Patents: 2000.

20. Momicchioli, F.; Baraldi, I.; Berthier, G., Theoretical study of trans-cis photoisomerism in polymethine cyanines. *Chemical physics* **1988**, 123 (1), 103-112.
21. Dempster, D.; Morrow, T.; Rankin, R.; Thompson, G., Photochemical characteristics of cyanine dyes. Part 1. 3,3'-diethyloxadicarbocyanine iodide and 3,3'-diethylthiadicarbocyanine iodide. *J. Chem. Soc., Faraday Trans. 2* **1972**, 68, 1479-1496.
22. Chibisov, A., Triplet states of cyanine dyes and reactions of electron transfer with their participation. *Journal of Photochemistry* **1977**, 6 (3), 199-214.
23. Chibisov, A.; Zakharova, G.; Gärner, H.; Sogulyaev, Y. A.; Mushkalo, I.; Tolmachev, A., Photorelaxation processes in covalently linked indocarbocyanine and thiocarbocyanine dyes. *The Journal of Physical Chemistry* **1995**, 99 (3), 886-893.
24. Yu, A.; Tolbert, C. A.; Farrow, D. A.; Jonas, D. M., Solvatochromism and solvation dynamics of structurally related cyanine dyes. *The Journal of Physical Chemistry A* **2002**, 106 (41), 9407-9419.
25. Brismar, H.; Trepte, O.; Ulfhake, B., Spectra and fluorescence lifetimes of lissamine rhodamine, tetramethylrhodamine isothiocyanate, texas red, and cyanine 3.18 fluorophores: influences of some environmental factors recorded with a confocal laser scanning microscope. *Journal of Histochemistry & Cytochemistry* **1995**, 43 (7), 699-707.
26. Rasnik, I.; Myong, S.; Cheng, W.; Lohman, T. M.; Ha, T., DNA-binding orientation and domain conformation of the E. coli rep helicase monomer bound to a partial duplex junction: single-molecule studies of fluorescently labeled enzymes. *Journal of molecular biology* **2004**, 336 (2), 395-408.

27. Sanborn, M. E.; Connolly, B. K.; Gurunathan, K.; Levitus, M., Fluorescence properties and photophysics of the sulfoindocyanine Cy3 linked covalently to DNA. *The Journal of Physical Chemistry B* **2007**, *111* (37), 11064-11074.
28. Yasuda, R.; Masaike, T.; Adachi, K.; Noji, H.; Itoh, H.; Kinosita, K., The ATP-waiting conformation of rotating F1-ATPase revealed by single-pair fluorescence resonance energy transfer. *Proceedings of the National Academy of Sciences* **2003**, *100* (16), 9314-9318.
29. Hwang, H.; Kim, H.; Myong, S., Protein induced fluorescence enhancement as a single molecule assay with short distance sensitivity. *Proceedings of the National Academy of Sciences* **2011**, *108* (18), 7414-7418.
30. Seidel, C. A.; Schulz, A.; Sauer, M. H., Nucleobase-specific quenching of fluorescent dyes. 1. Nucleobase one-electron redox potentials and their correlation with static and dynamic quenching efficiencies. *The Journal of Physical Chemistry* **1996**, *100* (13), 5541-5553.
31. Torimura, M.; Kurata, S.; Yamada, K.; Yokomaku, T.; Kamagata, Y.; Kanagawa, T.; Kurane, R., Fluorescence-quenching phenomenon by photoinduced electron transfer between a fluorescent dye and a nucleotide base. *Analytical Sciences* **2001**, *17* (1), 155-160.
32. Harvey, B. J.; Levitus, M., Nucleobase-specific enhancement of Cy3 fluorescence. *Journal of fluorescence* **2009**, *19* (3), 443-448.
33. Herz, A., Aggregation of sensitizing dyes in solution and their adsorption onto silver halides. *Advances in Colloid and Interface Science* **1977**, *8* (4), 237-298.
34. Jelley, E. E., Spectral absorption and fluorescence of dyes in the molecular state. *Nature* **1936**, *138* (3502), 1009-1010.

35. Harrison, W. J.; Mateer, D. L.; Tiddy, G. J., Liquid-crystalline J-aggregates formed by aqueous ionic cyanine dyes. *The Journal of Physical Chemistry* **1996**, *100* (6), 2310-2321.
36. West, W.; Pearce, S., The dimeric state of cyanine dyes. *The Journal of Physical Chemistry* **1965**, *69* (6), 1894-1903.
37. Armitage, B. A., Cyanine dye-DNA interactions: intercalation, groove binding, and aggregation. In *DNA binders and related subjects*, Springer: 2005; pp 55-76.
38. Toprak, E.; Selvin, P. R., New fluorescent tools for watching nanometer-scale conformational changes of single molecules. *Annu. Rev. Biophys. Biomol. Struct.* **2007**, *36*, 349-369.
39. Altman, R. B.; Terry, D. S.; Zhou, Z.; Zheng, Q.; Geggier, P.; Kolster, R. A.; Zhao, Y.; Javitch, J. A.; Warren, J. D.; Blanchard, S. C., Cyanine fluorophore derivatives with enhanced photostability. *Nature methods* **2012**, *9* (1), 68-71.
40. Mujumdar, R. B.; Ernst, L. A.; Mujumdar, S. R.; Lewis, C. J.; Waggoner, A. S., Cyanine dye labeling reagents: Sulfoindocyanine succinimidyl esters. *Bioconjugate chemistry* **1993**, *4* (2), 105-111.
41. Chao, G.; Lau, W. L.; Hackel, B. J.; Sazinsky, S. L.; Lippow, S. M.; Wittrup, K. D., Isolating and engineering human antibodies using yeast surface display. *Nature protocols* **2006**, *1* (2), 755-768.
42. Feldhaus, M. J.; Siegel, R. W.; Opresko, L. K.; Coleman, J. R.; Feldhaus, J. M. W.; Yeung, Y. A.; Cochran, J. R.; Heinzelman, P.; Colby, D.; Swers, J., Flow-cytometric isolation of human antibodies from a nonimmune *Saccharomyces cerevisiae* surface display library. *Nature biotechnology* **2003**, *21* (2), 163-170.
43. Concepcion, J.; Witte, K.; Wartchow, C.; Choo, S.; Yao, D.; Persson, H.; Wei, J.; Li, P.; Heidecker, B.; Ma, W., Label-free detection of biomolecular interactions

using bilayer interferometry for kinetic characterization. *Combinatorial chemistry & high throughput screening* **2009**, 12 (8), 791-800.

44. Feldhaus, M.; Siegel, R., Flow cytometric screening of yeast surface display libraries. In *Flow Cytometry Protocols*, Springer: 2004; pp 311-332.

Thesis summary

In this thesis I focused on the photochemical properties of fluorogen activating peptides and two other methodologies to achieve photostable live cell imaging using quantum dots and cyanine dyes. The FAP-fluorogen technology, on account of its non-covalent binding has some excellent photochemical aspects to offer. The fast off rate complexes that exchange on the order of photobleaching rates are really useful for superresolution imaging. Quantum dot imaging using fluorogen haptens opens yet another pathway for genetically targeting commercially available streptavidin conjugated quantum dots without any need for synthetic steps. Finally, the discovery of Cy3 and Cy3 binding peptides that enhance photostability through encapsulation are a unique addition to the limited number of genetically targeted fluorophores available for live cell imaging. Finally, the methods developed for selectively screening for highly photostable fluorogen and fluorophore binders exploiting encapsulation and exchange can go a long way and can be applied to a variety of small molecules.

Future directions

Superresolution microscopy using MG exchangers

One of the main applications of FAPs that can exchange is in superresolution microscopy methods that use stochastic blinking. The FAPs that have been isolated using the sorting methods developed, should be purified and studied in detail in vitro to characterize their on and off rates at a single molecule level. These can be further optimized for expression in mammalian and bacterial cells to perform superresolution microscopy of mammalian cell structures and bacterial proteins.

Intracellular targeting of quantum dots

Fluorogenic haptens can be utilized to perform intracellular labeling of proteins inside the cell. Further optimization using a variety of peptide tags can be performed to target QDs into cells expressing FAPs. In addition, methods such as electroporation should also be tested for their efficiency in delivering QDs inside the cells. Finally, the mechanisms of uptake of the QDs need to be understood in more detail. Eventually, once the QDs are targeted inside the cells, superresolution imaging can be performed on structures such as actin filaments on the account of excellent photophysical properties that the QDs offer.

In vitro characterization of PEPCy3 and PEPCy5

The proteins PEPCy3 and PEPCy5 need to be further optimized for purified protein expression. Using glutathione S transferase tag on them may make them more soluble, thus making it easier for protein purification. Once these proteins can be obtained in good yields, one can obtain their K_d values using bio-layer interferometry. Fluorescence polarization may be another useful technique that may be used to measure the equilibrium properties of these peptides. Further, their molecular brightness can be determined using single molecule methods such as fluorescence correlation spectroscopy. Accounting all these unknowns that can be obtained for these peptides, it is pertinent to invest an effort in the direction of the optimization of these proteins for purification purposes.

Live cell imaging using PEPCy3 and PEPCy5

Since the PEPCy3 and PEPCy5 proteins also bind pH sensitive derivatives of Cy3 and Cy5, they can be used in cells to measure pH. For this, a careful characterization of the pKa values of these complexes needs to be done. Further, depending on the pKa changes, we can selectively utilize these probes for intracellular or extracellular labeling.

Finally, it remains to be seen if these PEP tags can bind the ultra-photostable Cy3 and Cy5 derivatives synthesized by the Blanchard lab. If that be the case indeed, these probes may be the most photostable, genetically targeted Cy3 and Cy5 tags known till date. Additionally, owing to the good FRET overlap between Cy3 and Cy5 these probes can also be used to study protein interactions on the cell surface such as dimerization and oligomerization. For the case of PEPCy3 it also remains to be seen if it can show enhancements in the presence of bigger proteins, in which case we can use the probes for smPIFE measurements.